Dissertation zur Erlangung des Doktorgrades
der Fakultät für Chemie und Pharmazie
der Ludwig-Maximilians-Universität München

In silico Investigations towards Homochirality

in the Context of the Origin of Life

Symmetry Breaking by Consecutive Amplification

&

Atmospheric Modelling of a Reaction Network in a Prebiotic Context

&

System Validation for a Soai Autocatalysis

Laura Huber

aus

Mannheim, Deutschland

2023

Eidesstattliche Erklärung

Diese Dissertation wurde im Sinne von § 7 der Promotionsordnung vom 28. November 2011 von Herrn Prof. Dr. Oliver Trapp betreut.

Eidesstattliche Versicherung

Diese Dissertation wurde eigenständig und ohne unerlaubte Hilfe erarbeitet.

München, den 22.05.2023

....

(Laura Huber)

Dissertation eingereicht am   25.05.2023

1. Gutachterin/ 1. Gutachter: Prof. Dr. Oliver Trapp

2. Gutachterin/ 2. Gutachter   Prof. Dr. Anja Hoffmann-Röder

Mündliche Prüfung am   14.07.2023

Publications

Paper Publications

Parts of this work have already been published in peer-reviewed journals:

Huber, L., Trapp, O. (2022). Symmetry breaking by consecutive amplification: Efficient paths to homochirality. *Origins of Life and Evolution of Biospheres*, *52*(1), 75-91.

Parts of this work are currently being prepared for publication:

Huber, L., Trapp, O. (2023). The tipping point in the atmosphere of a planet: a large-scale *in silico* simulation. *In preparation.*

During the period of this work the following papers were published or prepared with my contribution:

Betzenbichler, G., Huber, L., Kräh, S., Morkos, M. L. K., Siegle, A. F., Trapp, O. (2022). Chiral stationary phases and applications in gas chromatography. *Chirality*, *34*(5), 732-759.

Fuks, E., Huber, L., Schinkel, T., Trapp, O. (2020). Investigation of Straightforward, Photoinduced Alkylations of Electron-Rich Heterocompounds with Electron-Deficient Alkyl Bromides in the Sole Presence of 2, 6-Lutidine. *European Journal of Organic Chemistry*, *2020*(39), 6192-6198.

Bechtel, M., Ebeling, M., Huber, L., Trapp, O. (2023). The Emergence of Organocatalysis in the Origin of Life: Discovery, Applications and Molecular Evolution. *Accounts of Chemical Research. Submitted.*

Book Chapter

Huber, L., Trapp, O. (2022). First Steps of Prebiotic Chemistry Catalyzed by Minerals and Metals. In *Prebiotic Chemistry and Life's Origin* (pp. 77-123).

Outreach

Special exhibition "Simple, Complex, Alive" / "Simpel, Komplex, Lebendig" (09/2022-01/2023) about the Origin of Life on Earth; collaboration on texts and exhibition pieces.

Acknowledgements

I would like to take this opportunity to thank all the people who supported and accompanied me during my doctorate and contributed to this work.

First and foremost, I would like to thank my doctoral supervisor *Prof. Dr. Oliver Trapp* to work on these topics under his supervision. *Oliver*, your infectiously motivating way of encouraging and challenging me these last couple of years inspired and formed my way of thinking and working. Thank you so much for giving me space and trust to grow and learn in so many areas.

I would like to express my sincere thanks to *Prof. Dr. Anja Hoffmann-Röder* for taking on the secondary review, as well as to *Prof. Dr. Christian Ochsenfeld,* PD *Dr. Armin Ofial*, *Prof. Dr. Konstantin Karaghiosoff* and *Prof. Dr. Silvia Markic* for participating in my examination committee.

Furthermore, I would like to thank all the staff of the Ludwig-Maximilians-University of Munich, especially the analytics departments and the employees of our working group, who make the research operation possible in the first place. *Brigitte*, thank you for starting our laboratory week with your joyful "Happy Monday!" and *Carrie*, thank you for discussing analytics, life, yoga, and our shared love for classical concerts.

Heike, a big thank you for your support, our literary exchange, our walks and talks and the dear Ringelnatz and photography encouragement.

Claudia, a heartfelt thank you for your support and the great hand-flattering hedgehog that accompanied me throughout the writing of this thesis.

For the introduction to the analytical equipment and the insightful discussions, I want to thank *Max L. and Alex.*

I would also like to thank *Constanze*, *Simone, Max B.* and *Jan* for their very careful and elaborate proofreading of this thesis.

I would like to thank the entire TRAPP working group for the great time we spent together, which went far beyond the lab routine and enriched me by many friends. Thanks to my lab team in F3.004 *Elina*, *Kai*, *Conny* and *Maren* for the music quiz, the team spirit, *Elina* for being on fire-extinguisher-standby-duty and *Kai* as camera and sound man. I would especially like to thank my lab-box partner *Elina* for our online art evenings and matinees and the never-ending scientific and personal conversations, that developed into a close friendship.

wholehearted thank you goes to *Lea* for your friendship and coaching in any situation and for teaching me la dolce vita.

A very big thank you goes to *Konstantin* and *Hannah* for being my home away from home and that you prove to me that I am never alone. *Mama*, *Papa*, thank you for making me believe through your love, support, and confidence in me that I can achieve anything I set my mind to.

Equipped with their five senses,
humans explore the universe around them
and call the adventure Science.

Edwin P. Hubble

Table of Contents

Abbreviations

°C	degree Celsius
c	concentration
Cat	catalyst
CIP	Cahn–Ingold–Prelog (nomenclature)
CPL	circular polarized light
CPU	central processing unit
DAIB	(−)-(dimethylamino)isoborneol
DFT	density functional theory
DHPLC	dynamic high-performance liquid chromatography
DNA	deoxyribonucleic acid
$\Delta G^{\ddagger}$	Gibbs activation energy
$\Delta H^{\ddagger}$	activation enthalpy
$\Delta S^{\ddagger}$	activation entropy
Δt	difference between two points in time, time period (delta t)
ee	enantiomeric excess
e.g.	for example (Latin: *exempli gratia*)
ELT	Extremely Large Telescope
Eq.	equivalent
Eqn.	equation
Eqs.	equations
et al.	and others (Latin: *et alii*)
FaPy	formamidopyrimidine
g_0	sea-level (only for Earth)/ground-level value of the acceleration of gravity $g_0 = 9.80665 \text{ m/s}^2$
Ga	billion years (*Gigaannum*)
Gt	gigatonnes
GOE	great oxidation event

h	hour
h	Planck constant ($h = 6.626 \cdot 10^{-34}$ J·s)
H	geopotential height used as argument for all tables up to 86,000 km
H_b	geopotential height values (See Appendix Table 69)
HPLC	high-performance liquid chromatography
HRMS	high-resolution mass spectrometry
i.a.	among other things (Latin: *inter alia*)
i.e.	that is (Latin: *id est*)
k	reaction rate constant
k_B	Boltzmann constant ($k_B = 1.381 \cdot 10^{-23}$ J·K^{-1})
κ	transmission coefficient
km	kilometre
JWST	James Webb Space Telescope
LHB	late heavy bombardment
LUCA	last universal common ancestor
$L_{M,b}$	molecular-scale Temperature Gradient; $L_{M,b} = \frac{dT_M}{dH}$ (See Appendix Table 69)
mM	millimolar: 1mM = 0.001 M
M	molar, mol/L
M_g	mean molecular weight of a mixture of gases; $M_g = \frac{\Sigma[n_i \cdot M_i]}{\Sigma n_i}$
M_0	mean molecular weight value of the gas mixture at sea-level
M_i	defined molecular weight of the ith gas species
MISS	microbially induced sedimentary structures
Myr	million years
n_i	number density of the ith gas species
NLE	non-linear effects
ODE	ordinary differential equation
OoL	Origin of Life

OOM	Order of Magnitude
P	total pressure
P*	chiral product
P$_0$	pressure values defined at sea-level for P_b with $b = 0$; $P_\mathrm{b} = 01325.0 \ \mathrm{N/m^2}$
P$_\mathrm{b}$	pressure values defined for $b = 1$ through $b = 6$ are obtained from the appropriate member of the pair equations (45) and (46) for the case $H = H_\mathrm{b+1}$
PVED	parity-violating energy difference
r	reaction rate
R*	universal gas constant (R* = 8.314 J·K^{-1}·mol^{-1})
(*R*)	rectus–stereo descriptor for chiral sp^3 centre; after the Cahn–Ingold–Prelog (CIP) priority convention
RNA	ribonucleic acid
RNA.exe	reaction network analysis tool
s	second(s)
(*S*)	sinister–stereo descriptor for chiral sp^3 centre; after the CIP priority convention
SDE	self-disproportion of enantiomers
SIPF	salt induced peptide formation
σ^2	variance (denoted as sigma-squared)
SMK	single molecule kinetics
SMS	square-macrocycle-square
SMSB	spontaneous mirror symmetry breaking
t	time
T	temperature
T$_\mathrm{M,b}$	molecular-scale temperature
TMS	trimethylsilyl group
UV	ultraviolet

Vis   visible

ρ total density

Minerals

Cinnabar   HgS

Montmorillonite $(Na,Ca)_{0.33}(Al,Mg)_2Si_4O_{10}(OH)_2$

Quartz SiO_2

Siderite $FeCO_3$

Zircon $Zr[SiO_4]$

Kurzzusammenfassung

Die Zukunft der industriellen und chemischen Wertschöpfung wird wahrscheinlich datenbasiert sein. Ein elementarer Baustein dafür sind kontinuierlich weiterentwickelte Werkzeuge, um Erkenntnisse über komplexe Reaktionsnetzwerke zu gewinnen. Diese Arbeit gibt Einblicke in das Design und die Anwendung von zwei reaktionskinetischen Programmen und zeigt deren vielfältige Anwendungsmöglichkeiten von der Autokatalyse bis hin zu präbiotischen Reaktionsnetzwerken auf.

Der erste Kontext, in dem das entwickelte Programm zur Analyse von Reaktionsnetzwerken angewendet wurde, war ein „Origin of Life"−Projekt (Projekt zur Entstehung des Lebens). Es gibt eine Vielzahl an Ansätzen, um den Ursprung der Homochiralität als ein Schlüsselelement dieses Forschungsbereichs zu ergründen, daher ist für die Durchführbarkeit eine explizite Modellentwicklung entscheidend. In dieser Dissertation wurde für das erste Thema (Kapitel 3) ein cheminformatischer Ansatz gewählt, um Symmetriebrechungen auf molekularer Ebene zu beobachten. Dies ist insbesondere deshalb interessant, weil das von uns entwickelte Tool *SMK.exe* für eine Vielzahl unterschiedlicher chemischer Reaktionsnetzwerke angepasst werden kann.

Zunächst wurde ein Einblick in die Programmstruktur und -funktionalität gegeben. Eingabe- und Ausgabeanforderungen wurden diskutiert und die Validierung der Reproduzierbarkeit wurde gezeigt. Anschließend wurde diese effiziente Methode zur Untersuchung der Reaktionskinetik von Einzelmolekülen auf mehrere Modellsysteme angewandt, die sowohl autokatalytische Systeme als auch eine Kaskadenreaktion umfassen. Es wurden wichtige Implikationen für die Kombination von kinetischen Anforderungen in Richtung Symmetriebrechung auf molekularer Ebene gewonnen. Mittels einer statistischen Analyse und einer Langzeitsimulation konnte bestätigt werden, dass das System keine Verzerrung aufweist und die Bildung eines bevorzugten Enantiomers zufällig erfolgt.

Im zweiten Themenbereich (Kapitel 4) wurde die primordiale Atmosphäre eines Planeten mit einem weiterentwickelten Chemoinformatik-Tool (*RNA.exe*) untersucht. Basierend auf experimentellen Befunden wurde ein robustes Atmosphärenmodell entwickelt. Mit diesem Modell wurde eine groß angelegte *in silico* Katalyse durchgeführt, bei der wichtige organische Moleküle aus atmosphärischen Gasen gebildet wurden. Ein wichtiger Marker innerhalb des Systems für die CO_2-Fixierung und die Bildung der Bausteine des Lebens wurde identifiziert. Die entscheidende Rolle der H_2-Bildung und des H_2-Verbrauchs wurde aufgezeigt. Ein bemerkenswertes Ergebnis der Simulationen war, dass die Zeitspanne der gesamten CO_2-Fixierung relativ kurz gewesen sein muss - zwischen 20 und 100 Millionen

Jahren. Die allgemeine Bedeutung der Frage, ob ein Metallosilikatplanet, ähnlich der frühen Erde, die Entstehung von Leben ermöglichen kann, wurde diskutiert.

Der dritte Themenbereich war die Validierung des fortgeschrittenen Programms *RNA.exe* (Kapitel 5) anhand einer autokatalytischen Reaktion. Das Programm wurde anhand experimenteller kinetischer Daten zur SOAI-Reaktion validiert. Die Verfeinerungsmethode und die Genauigkeit der simulierten Sätze wurden aufgezeigt.

Abstract

The future of the improvements of industrial and chemical processes is likely to be data-based. An elementary implementation for this are continuously developed tools to gain insights into complex reaction networks. This work provides insights into the design and application of two reaction kinetic tools and exhibits the broad application potential thereof ranging from autocatalysis to prebiotic reaction networks.

The first context in which the developed program for reaction network analysis was applied to, was an Origin of Life project. Since the approaches to fathom the origin of homochirality are diverse, explicit model development is crucial. In this dissertation, a cheminformatics approach was chosen for the first topic (chapter 3) to observe symmetry breaking at the molecular level. This is particularly interesting because the tool *SMK.exe* we developed, can be adapted for a multitude of different chemical reaction networks.

First, an insight into the program structure and functionality was given. Input and output requirements were discussed as well as the validation of reproducibility. Then, this efficient method for studying the reaction kinetics of single molecules was applied to several model systems including both autocatalysis systems and a cascade reaction. Important implications for the combination of kinetic requirements towards symmetry breaking on a molecular level by statistical sampling were obtained. By means of a statistical analysis and a long-term simulation, it could be confirmed that the system has not exhibit any bias and that the formation of a preferred enantiomer is random.

In the second subject area (chapter 4) the primordial atmosphere of a planet was examined with a further developed cheminformatics tool (*RNA.exe*). Based on experimental findings, a robust atmospheric model was developed. With this model, a large-scale *in silico* catalysis was carried out in which important organic molecules were formed from atmospheric gases. A novel marker within the system for CO_2 fixation, building block formation and thus the Origin of Life was identified. The crucial role of H_2 formation and consumption was demonstrated. The general significance of whether any early Earth-like metallosilicate planet would be able to provide evidence of the emergence of life was discussed.

The third subject area was the validation of the advanced *RNA.exe* tool (chapter 5) in an autocatalytic setting. The program was validated using experimental kinetic data on the Soai reaction. The refinement method and the accuracy of the simulated sets were shown.

Chapter 1

Introduction

The Significance of Chirality

The question of the Origin of Life is one that concerns humankind since time immemorial. This topic is more relevant today than ever before, as inter- and trans-disciplinary research into the habitability of other planets drives space missions and satellite research, while the question of artificial life cuts across all areas of our daily lives.[1-5] Despite decades of intensive research, it has not yet been possible to answer this conundrum conclusively.

The almost exclusively selective occurrence of one enantiomer of the essential chiral biomolecular building blocks remains a research question to be answered. Almost all biologically relevant reactions are designed for L-amino acids, whereas sugars in nature mostly occur in their chiral D-form. Homochirality of molecules of life is of utmost importance because of their efficacy and biological function, but how it came about is still unclear.

Selected theories on how, when, and where simple chirality did emerge and lead to the Origin of Life (OoL) are shortly comprised in Figure 1.[6-10] The basic prerequisite is the occurrence of symmetry breaking, which in the further course must be stabilised, maintained and amplified by the mechanisms shown in order to finally obtain homochirality.
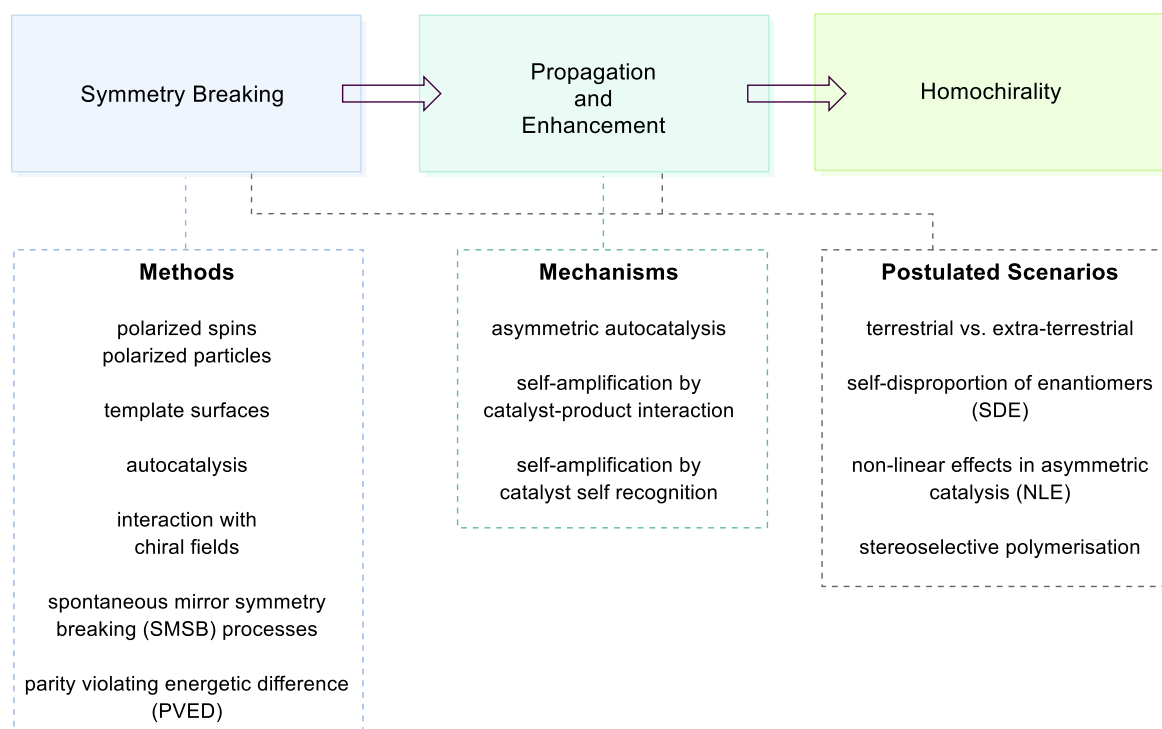
Figure 1: Hypotheses about the different pathways necessary to achieve symmetry breaking, propagation, amplification, and enhancement of chirality towards homochirality.

In order to fathom the Origin of Life, it must be clarified how one could arrive at the origin of homochirality starting from achiral molecules. One approach for solving this question is the SOAI reaction. From a small chiral imbalance in the reactants, a very high enantiomeric

excess *ee* is obtained by the smallest external influences, which makes the SOAI reaction the perfect model reaction for elucidating the origin of homochirality of biologically relevant molecules.

Stereochemistry is not only of essential interest in the context of the Origin of Life, but also for the specific production of pharmaceutically active substances along with pesticide synthesis via enantioselective catalysis. The selective synthesis of a specific enantiomer in the pharmaceutical sector is crucial, since enantiomers can often exhibit different, and in some cases, potentially harmful, physiological properties.[11,12]

Enantiomerically pure compounds are often produced by using enantioselective catalysts, the development of which has yielded remarkable results in recent decades and was rewarded with a Nobel Prize in chemistry 2001 for KNOWLES, NOYORI and SHARPLESS.[13-15]

Another approach to investigating the cause of homochirality, in addition to laboratory chemistry methods, is to use detailed analytical and kinetic observation and simulation methods to study reaction networks. How does one get to this initial symmetry breaking at the molecular level, which then needs to be efficiently amplified to achieve the desired effect at the macro level? *In silico* methods can help to cope with the large number of different scenarios that need to be tested or discarded in this context.

Chapter 2

Theoretical Background

2.1 Introduction to the "Origin of Life"

One of the most fundamental unsolved problems of our time has existed for centuries: understanding the OoL. In the chemical domain of interdisciplinary OoL research, one focus is on the prebiotic synthesis of cell components that are essential for the functions of metabolism, information transfer and cell division The unification of the subcomponents into a self-sufficient chemical system that can undergo some form of evolution is the subject of many international research efforts in this field and is as yet unachieved.[16]

The biggest obstacle in solving the OoL conundrum is the lack of contamination-free rock samples from the time period that is assumed for the emergence of life on the early Earth, i.e., the Hadean and early Archean (4.6 – 3.6 Ga ago). Therefore, the reconstruction of the exact reaction conditions of the early Earth, such as temperature, pressure, availability of inorganic reactants and the atmospheric composition is not feasible.[17]

There are different theories and approaches that can be taken to investigate this problem, e.g., the RNA-world first theory versus metabolism first theory and the diametrically opposed *top-down* or *bottom-up* approaches (see Chapter 2.1.5). It is not yet evident which theory best describes the correct scenario of abiogenesis, or whether a combination of approaches would be necessary to do so.

In addition to research into the Origin of Life on the early Earth, there is also the approach that life or important building blocks of life have reached the Earth through extraterrestrial material influx. The JAMES WEBB SPACE TELESCOPE (JWST) and the EXTREMELY LARGE TELESCOPE (ELT) are being used to help shed light on exoplanetary atmospheres and biosignatures using near- to mid-infrared measurements and optical spectrometers that could reveal parallels with the early Earth and where life may have originated.

2.1.1 What is Life?

The lack of a universally accepted definition of the phenomenon of "life" or the "degree of aliveness" is another issue in this research field.[18] So, before one can set out to explore the OoL, a definition of "life" as we know it is necessary. Natural sciences have so far failed to find a conclusive, satisfactory answer to the question "What is life?".[19] In 1961 OPARIN defined six characteristics according to which he classified living organisms as "alive" comprising the ability to exchange substances with the environment, the capacity of growth, reproduction (*population growth*), self-reproduction, movement, and the capacity of the system to be promoted into excited states.[20] The original statement that evolution being part of

a critical capacity of living objects to take part in was made by WADDINGTON in 1968.[21] Since then, extensive discussions within the literature exist about the information aspect being the key property of life.[22-24] A widely accepted specification of "life" is the NASA definition, which states that "*Life is a self-sustaining chemical system capable of DARWINIAN evolution*", and which takes into account the special characteristics of terrestrial life.[25]

A common denominator of all these definitions is, that they combine a set of chemical reactions of molecules consisting mainly of the elements carbon (C), hydrogen (H), nitrogen (N) and oxygen (O).

At least one of these properties need to be applicable for a system to be considered a prebiotically relevant reaction network model:

- being a thermodynamically open system[26]
- exhibiting a membrane
- entailing the use of gradients
- exhibit replication: the system is able to make (imperfect) copies of itself for information storage.

2.1.2 Early Earth's Environment

The OoL on the early Earth, whose age is dated to 4.54 billion years (Ga), is one of the most fundamental and interdisciplinary research questions of our time.[27-31] The age of our solar system is dated to 4.56 Ga (see Figure 2).[19,32] A collision of the early Earth with a protoplanet is supposed to have led to the formation of the moon 4.5 Ga ago ("moon-forming impact").[16,33,34,35]
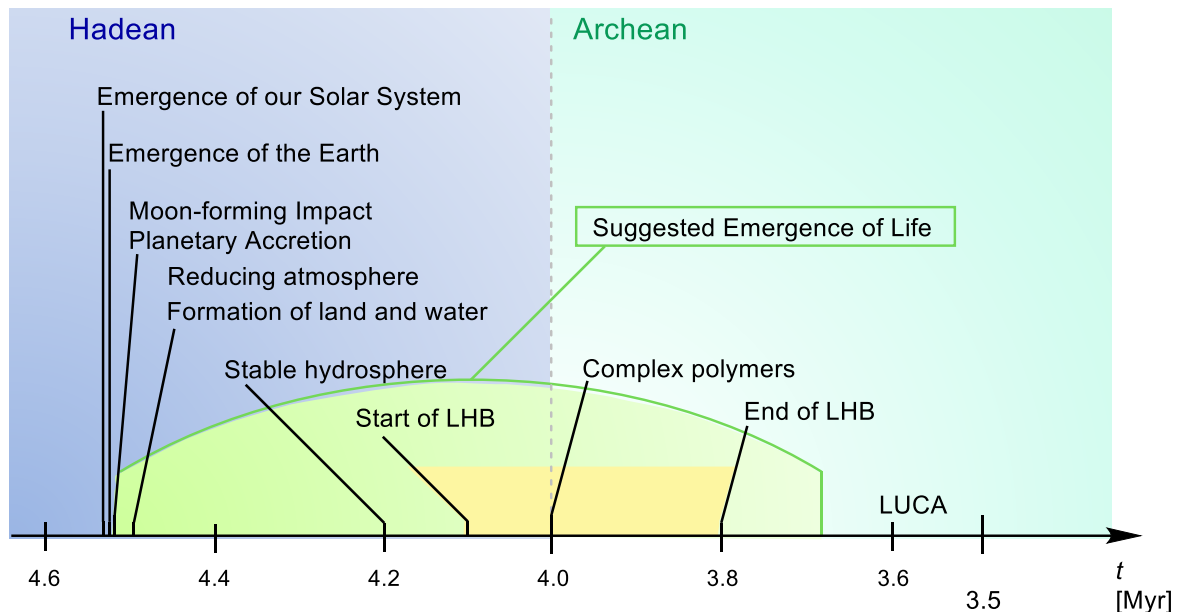
Figure 2: Timeline with postulated stages of development on the primordial Earth. Yellow: late heavy bombardment (LHB); last universal common ancestor (LUCA).

Subsequently, the cooling of the primordial Earth over a period of millions of years led to the formation of the early Earth's crust, thus fulfilling an important prerequisite for the existence of liquid water and subsequently of life.[36] The first presence of liquid water by studies of oxygen isotope ratios in zircons is dated to a period up to 4.4 - 4.3 Ga ago.[36-38] During the late heavy bombardment (LHB), increased meteorite impacts at around 3.9 Ga may have had a counterproductive effect on the emergence of life on Earth, possibly destroying organic material that had formed by then upon impact.[34-37]

The oldest evidence of terrestrial life are isotopically light graphite inclusions in zircons that are up to 4.1 Ga old.[39-42] However, it is debatable whether the isotope distribution could not have been the result of abiotic processes. As cause for the high $^{12}C/^{13}C$ isotope ratio, processes such as FISCHER-TROPSCH reactions, the disproportionation of siderite ($FeCO_3$) or the incorporation of meteoritic materials are conceivable.[42,43] The origin of biomolecules can be dated to 3.5 Ga ago, evidenced by ancient sedimentary rocks (stromatolites) formed as a result of the metabolic activity of microorganisms and by microbially induced sedimentary

structures (MISS).[19,44,45,46,47] Furthermore, photosynthetic activity occurring before 3.3 - 3.5 Ga can be assumed from the presence of certain microfossils.[48]

2.1.3 Early Earth's Atmosphere

The composition and oxidation state of early Earth's atmosphere remains a widely debated topic in prebiotic research.[49] Its composition is generally considered to consist predominantly of molecular carbon dioxide (CO_2), nitrogen (N_2), water (H_2O) and in some cases methane (CH_4).[50] Other substances discussed in the literature include carbon monoxide (CO), hydrogen sulphide (H_2S), sulphur dioxide (SO_2) and ammonia (NH_3).

Atmospheric chemists tend to suggest a neutral atmosphere, whereas some prebiotic chemists suspect highly reducing conditions with a high concentration of hydrogen (see Figure 3).[50-54] The free oxygen content in the atmosphere of the early Earth is considered to have been very low or non-existent. The percentage of free oxygen first increased significantly around 2.5 - 2.0 Ga ago, with a sudden increase in the Great Oxidation Event (GOE) or an increase lasting over a longer time span being discussed.[55-57]
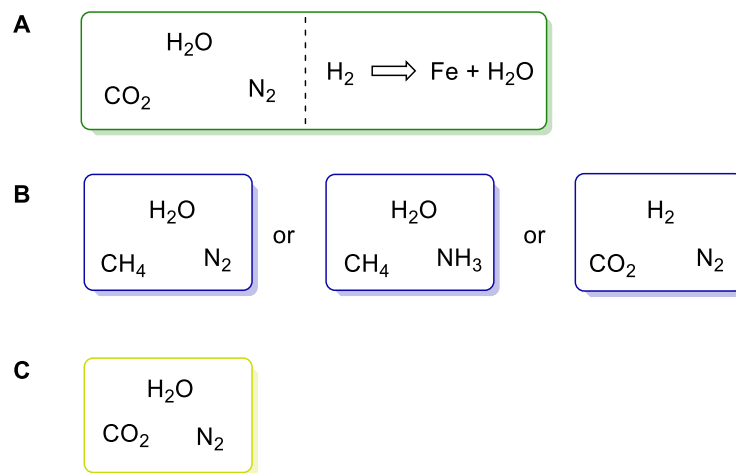
Figure 3: Different atmospheric scenarios for the early Earth. **A**: This thesis: neutral atmosphere with additional hydrogen; **B**: prebiotic chemists: strongly reducing atmosphere; **C**: atmospheric chemists: neutral atmosphere. Modified figure from reference [58].

The composition of the atmosphere of the primordial Earth could have therefore affected the radiation and particle flux on the surface.[59]

The pressure on early Earth is assumed to have been increased after the formation of the Moon and possibly a period of mass increase from chondritic material described as the "late veneer". The pressure then decreased in a still undetermined manner in the following millions of years.[60]

The temperature on the early Earth raises another unsolved scientific problem. The paradox of the weak, young sun refers to the contradiction between the 30% lower radiation output of the young sun and the absence of a corresponding colder climate at that time. Explanations are required for the existence of liquid water indicating temperatures above 0 °C. It is assumed that various greenhouse gases as well as melting due to meteorite impacts could have been responsible.[61-64]

HASHIMOTO et al. examined the composition of a mixed atmosphere of the early Earth towards the end of the accretion of planetesimals and calculated the thermodynamic equilibrium of a six-element system comprising the following elements: H, C, N, O, sulfur (S) and iron (Fe).[65] They postulated a very reducing atmosphere as a result of H_2O "collapsing" into oceans leaving considerable amounts of H_2 in the atmosphere.

If the time span for H_2 to remain in the atmosphere had been short, this could also indicate that it could only be significant if it reacted quickly, which again would fit the short time span over which life emerged.[66]

OPARIN (1924) and HALDANE (1929) independently of each other postulated the hypothesis that a reducing primordial atmosphere would be able to generate a large variety of molecules through a suitable energy source such as flashes of light or ultraviolet (UV) radiation.[27,67,68] These molecules would then form a "primordial soup" (OPARIN) and subsequently react with sunlight to form more complex molecules that would eventually lead to the first living organism. The seminal MILLER-UREY discharge experiment in 1953 (see Chapter 2.1.4) established the beginnings of the chemical discipline "prebiotic chemistry".[69] In 1956, MELVIN CALVIN introduced the concept of *chemical evolution* or *abiogenesis* for the "process of synthesis of biochemically essential molecules from the simplest building blocks (molecules and elements) under the hypothetical conditions of the primordial Earth", still one of the most sought-after prebiotic research topics.[70]

2.1.4 Scenarios, Frameworks, and Settings for the Emergence of Life

Let us first consider the plausible reaction conditions on the early Earth for prebiotic chemistry. The occurrence of prebiotic reactions can be dated to the late Hadean and early Archean (4.4 - 3.5 Ga), taking into account the evidence for the existence of liquid water.[71] The physical and chemical conditions prevailing on the early Earth during this period cannot be precisely determined due to the lack or scarcity of rock samples, which is why various scenarios are being discussed.[17,50,72] The redox state of early Earth's mantle has to be considered as well.[73]

Energy sources considered for the early Earth include solar radiation (UV/Vis light as well as circularly polarised light (CPL)), thermal energy (from volcanism and hydrothermal eruptions), electrical discharges in the atmosphere, high-energy particles from radioactive decay, plate tectonics, and shock waves from planetesimal impacts. [74-81]

An exemplary selection of energy sources and prebiotic reaction conditions is depicted in Figure 4.
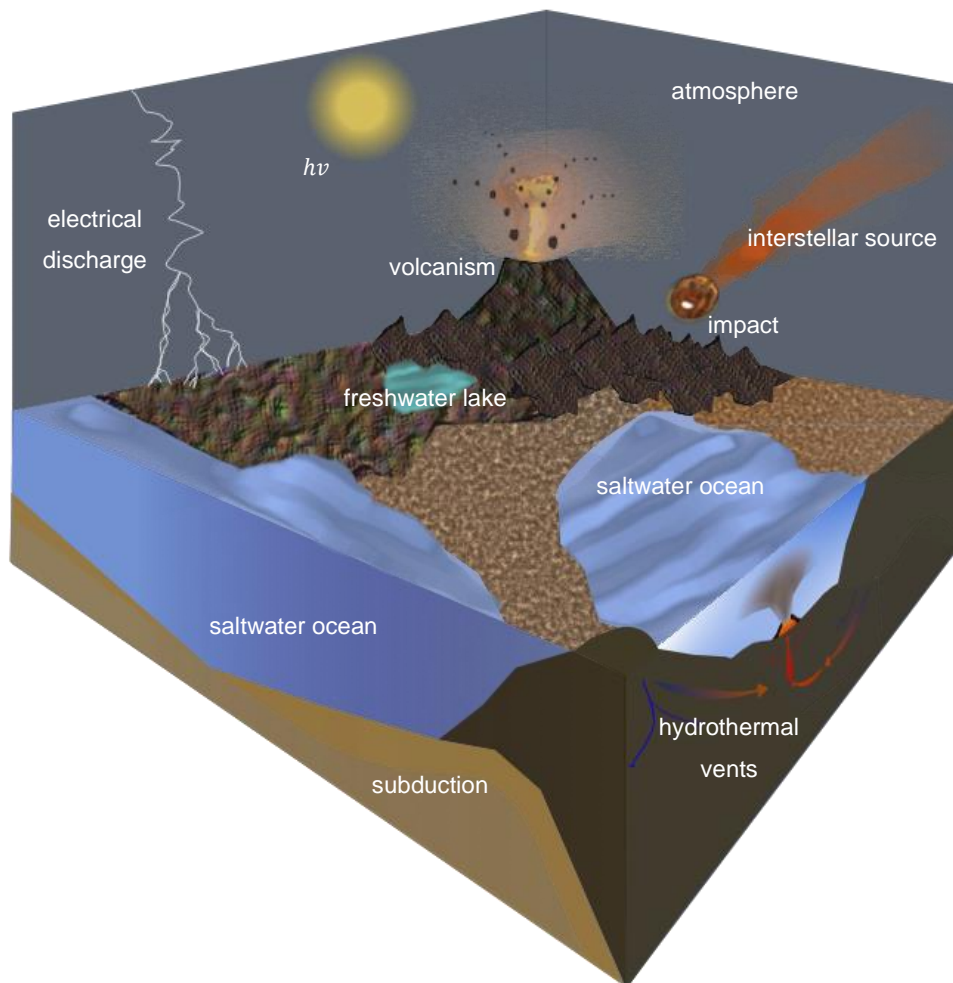
Figure 4: The figure exemplarily combines plausible scenarios of the conditions that may have been necessary for the emergence of life on the early Earth. The shown energy sources comprise electrical discharges, the young sun, vulcanism, subduction (mechanochemistry), hydrothermal systems and vents, interface chemistry. Saltwater and freshwater, early Earth surfaces and interfaces between the above are presented as conceivable reaction sites.

Among the most prominent scenarios of formation of life on the early Earth are DARWIN's warm little pond, the primordial soup, eutectic solutions and comet ponds.[82-89]

The primordial supply of material from meteorites and comets is another important factor in the debate about whether the origin of homochirality endogenously occurred on the early Earth.[90,91] Carbonaceous chondrites are often discussed as exogenous sources of *ee*s.[92]

The Murchison meteorite provides some clues to the origin of enantiomeric imbalance: not only does it exhibit a remarkable diversity of organic matter, but it contains some α-methyl amino acids with a preferential L-configuration of up to 15%, including isovaline, α-methyl isoleucine, α-methyl norvaline and α-methyl valine.[93-96] Since these molecules are unknown in terrestrial matter and are stable to chemical racemisation due to α-methylation, contamination during sampling on Earth can be almost completely ruled out.

2.1.5 Frameworks: *top-down* versus *bottom-up*

There are two conceptual frameworks to approach the questions embedded in the OoL research: the "*top-down*" approach examines complex, chemical constituents (biomolecules) that are active in modern organisms and may have played a role on early Earth.

Within this approach, prebiotic syntheses of biomolecules such as amino acids, sugars, nucleobases, nucleophiles and nucleotides need to be developed.

The substance class of amino acids has been detected on meteorites and in prebiotically plausible experiments, which makes them a widely accepted "given" on the early Earth.[69,96,97-101] Synthetically, they are easily available via the STRECKER synthesis starting from aldehydes, hydrogen cyanide (HCN) and NH_3.[102,103] A more selective approach was discovered by POWNER which proceeds via α-aminonitriles as activated derivatives and takes place at neutral pH.[111] To obtain peptides in a prebiotic scenario, several challenges must be overcome. Their formation in aqueous environment is thermodynamically unfavourable, as a condensation reaction is required for peptide bond formation.[104] Several approaches have been proposed in the literature via polyphosphates, cyanamides, imidazoles and nucleotides.[105,106] The salt induced peptide formation (SIPF) enabled polymerisation to short peptides on metal surfaces or using metal catalysts in concentrated aqueous salt solutions.[107-110] Although a first selection of α-amino acids was achieved to date only short oligomers have been formed and selective incorporation of the 20 proteinogenic monomers has not yet been achieved, although the foundations have been laid for a breakthrough in this area.[111] Priority coupling of the biotic L-enantiomer is also a research goal still to be achieved in this field.

The next important class of biomolecules are sugars. One of the milestone reactions in organic chemistry is still relevant today: the FORMOSE reaction by ALEXANDER BUTLEROW,

which yields a complex mixture of aldoses and ketoses.[112] However, this process does not yet allow direct control of the selectivity towards a desired sugar, but often leads to a vast and therefore analytically challenging mixture of sugars or even ultimately to a water-insoluble tar. In addition to the lack of selectivity, the polarity reversal of formaldehyde under prebiotically plausible conditions poses a problem for this approach. For the formation of nucleotides in the further course towards the building blocks of life, a selection, e.g., towards ribose and glyceraldehyde, is crucial. The selective formation of glycolaldehyde and glyceraldehyde via formaldehyde was achieved by SUTHERLAND using a KILIANI-FISCHER type photoredox reaction of HCN with H_2S as a reducing agent.[113]

As the second component of nucleosides, pyrimidines are required. These have already been detected on meteorites and in electrical discharge experiments, underlying their prebiotic plausibility.[92,114]

While the formation of pyrimidine RNA nucleosides was realised by SUTHERLAND, a synthesis of canonical purine RNA nucleosides was achieved by CARELL via the condensation of formamidopyrimidine (FaPy) intermediates with D-ribose.[115,116] The corresponding purine and pyrimidine DNA nucleosides were obtained with high regio- and stereoselectivity by TRAPP.[117] The next logical step towards life is phosphorylation to enable polymerisation to RNA/DNA strands. Important results have been achieved here by the groups of KRISHNA-MURTHY and TRAPP.[118, 119]

While the prebiotically plausible syntheses of all the building blocks are a crucial part of understanding the Origin of Life, this great leap can only be overcome if these approaches are studied in a connected way, as is currently done in the systems chemistry approach (see below).[120 -122]

In contrast, in the *top-down* approach, complexity of the biomolecule system is intended to be reduced to the point where cells and models are as primitive as possible. Features include capabilities such as genetic coding, metabolism, and the maintenance of chemical homeostasis. But even a simplified synthetic bacterium is already highly complex.[123] Instead of starting from bacteria, one solution might be to study the genome analysis of the last universal common ancestor (LUCA).[124]

The opposite, the *"bottom-up"* approach, examines which chemical or structural components of modern life may have been present on the early Earth or may have arisen through abiotic processes. This approach assumes a small number of reactive, organic molecules. Plausible reaction conditions such as the composition of the atmosphere and the early Earth's mantle must be considered. Challenges can be the analytical complexity of the

resulting product mixtures, but one of the potentials within this method is to discover by chance a novel pathway within the prebiotic but non-biological (by-)products.

One of the best known and still relevant experiments in this concept is certainly the famous MILLER-UREY discharge experiment.[69,97] Starting from a reducing atmosphere of CH_4, H_2, NH_3 and H_2O, this gas mixture was confined, subjected to electrical discharges and the resulting condensed product mixture analysed.[69,97,125] In these early experiments, a mixture of amino acids, hydroxy acids, short aliphatic acids, urea and amines could already be obtained, and modern modified approaches of MILLER-UREY type experiments were even able to extend the product spectrum.[100,114,126,127]

Another remarkable approach starting from small compounds and gases in the prebiotic *bottom-up* approach is the WÄCHTERSHÄUSER chemistry in volcanic hydrothermal systems.[128] Carbon fixation starting from the C_1-compounds CO_2, CO, COS and HCN in the presence of volcanic gases and iron, cobalt and nickel salts was able to provide amino acids, hydroxy acids and their cyanide derivatives.

The *bottom-up* approach partially provides the basis for the present work (see Chapter 4).

2.1.6 Systems Chemistry

In contrast to the simplification approaches discussed above, *systems chemistry* is a relatively recent multivariate approach to the study of a complex system to explain the out-of-equilibrium state of life.[129-131] Dynamical molecular networks are considered, with many possible intermediate stages towards biological molecules being explored. These intermediate states must be temporarily stable, for example through a kinetic energy barrier, to have the possibility to evolve to higher complexity. However, to keep the system far from equilibrium, the main prerequisite of life, a constant energy output is required, e.g., through autocatalytic cycles. Another criterion that must be considered in this context is the irreversibility of the process at the expense of the dissipated energy. This work is partially set in the systems chemistry concept by studying chemical networks that comprise different levels of complexity.

2.2 Origin of Homochirality

The study of the emergence of homochirality is a fascinating, interdisciplinary research topic that amongst other things seeks to uncover the unique importance and reason for the prevalence of L-amino acids and D-sugars on our planet.[132] Consequently, the enhancement of chirality is essential and requires asymmetric autocatalysis and positive non-linear effects.[133]

Since the accidental discovery of molecular chirality by PASTEUR and the definition of the term "chirality" by Lord CALVIN, enormous progress has been made in synthetic and analytical chemistry.[134-137] At that time, stereochemistry as a link between optical activity and molecular structure was, however, not yet known.

Although our modern technologies and capabilities allow us to delve deeper into previously unexplored scientific problems, there are still numerous major research questions that remain unanswered:

How did a racemic prebiotic mixture lead to such an excess of enantiomers as we have in our present homochiral world? And how did such an initial preference for one enantiomer come about: by random coincidence or as a result of a primordial template? After the question of the first deviation of the enantiomeric ratio, the next question then arises, namely how could this deviation not only be maintained but be amplified in such a way that we were able to achieve today's excess ratio? An important question in this context is: how do you prove or disprove a random event?

2.2.1 Non-linear Effects

Non-linear effects (NLE) are defined as the phenomenon that a discrepancy occurs between the ee of the catalyst ee_{aux} used and the ee of the products $ee_{product}$ and no direct proportionality between the two prevails.[138] A positive non-linear effect exists when the ee of the product is higher than that of the catalyst used, while it is called a negative non-linear effect when the ee of the product is lower. Although they are rarely observed, they have been intensively studied in recent decades.[139-141,147,149]

In 1953 FRANK published a purely mathematic treatise in which a kinetic model was described that postulated the emergence of homochirality exclusively via chemical processes.[142] He assumed an autocatalytic system with an unlimited substrate pool in which product formation is either promoted or inhibited by a pre-existing product enantiomer. In this antagonism theory, the desired reactions are supported and undesired side reactions,

here the formation of the undesired enantiomeric product, are suppressed. The underlying concept was that minimal ees occurring briefly in a non-asymmetric reaction due to statistical fluctuation can nevertheless form ees through stereo-amplifying effects. He furthermore hypothesized that heterochiral dimers would lead to catalyst deactivation. Consequently, with an equimolar presence of D- and L-catalysts, both would be deactivated. This thought experiment was hitherto entirely theoretical in nature and did not relate to any known chemical reaction.

A few years later, HOREAU published the first experiments on discrepancies between the ee and the experimentally determined specific rotation value of chiral succinic acid derivatives in chloroform.[143] These deviations result from the formation of diastereomeric associates via hydrogen bonds.

The influence of these enantiomeric interactions on the yields and ees of a chemical reaction depending on whether enantiomerically pure substrates or the corresponding racemic mixtures were used was shown by WYNBERG and FERINGA in 1976.[144]

In 1986, KAGAN then described and quantified the non-linearity between the ee of a catalyst used and the product formed in the asymmetric oxidation and aldolisation reactions.[145] A few years after this first example of a negative NLE, SHARPLESS showed an example of a positive NLE in the epoxidation of geraniol, where the epoxide obtained had a higher ee than the ligand diethyl tartrate used.[146]

In further studies by KAGAN and AGAMI, in addition to quantifying NLEs, a mechanism model was developed in which a particular species, here a metallic complex **M**, with two chiral ligands **L** is linked in a dynamic system (Scheme 1).[145,147] Two homochiral dimer catalysts, thus monomeric building blocks of the same configuration, and one heterochiral dimer catalyst, of monomers of opposite configuration, are formed and operate simultaneously at a steady state, subsequently yielding the chiral product. These homo- and heterochiral dimers are diastereomeric to each other and thus exhibit different chemical properties.
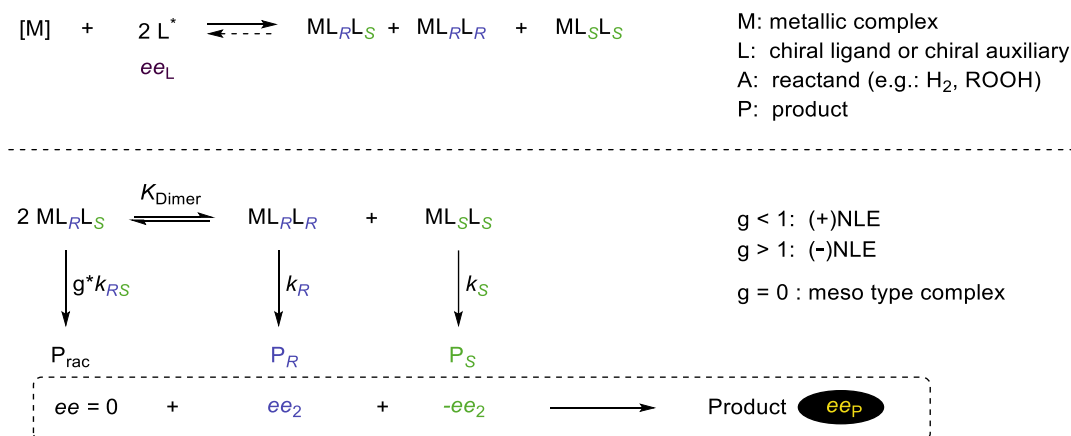
Scheme 1: ML₂-Model after KAGAN: A simplified presentation of the model to describe NLE and self-amplifying systems. The indices "2" refer to the values assigned to the products formed.[145]

The occurrence of an NLE is dependent on the relative catalyst concentration β (see equation 1) and the relative reactivity g (see equation 3):

$$\beta = \frac{[P_{rac}]}{[P_R]+[P_S]} \tag{1}$$

$$K = \frac{[P_{rac}]^2}{[P_R]^2[P_S]^2} \tag{2}$$

$$g = \frac{k_2'}{k_2} \tag{3}$$

If $\beta = 0$ or $g = 1$, no NLE occurs in the system, even if dimers were formed.

The enantioselective addition of organozinc compounds to aldehydes is probably one of the most thoroughly studied reactions with a positive NLE. As early as 1988, OGUNI et al. observed large NLEs in the enantioselective nucleophilic addition of diethylzinc to benzaldehyde using β-amino alcohols as catalysts.[148] This non-linearity can be explained with the dimerization of the chiral catalyst and the zinc organyl.

Both KAGAN and NOYORI investigated the quantification of NLE and proposed mechanisms to proceed via a dimeric species (see Scheme 2).[149,150] NOYORI used the chiral catalyst (2S)-(−)-exo-(dimethylamino)isoborneol (DAIB) and proposed a plausible reaction mechanism involving inactive dimer complexes, acting as a *reservoir*. Either homo- (*SS, RR*) or heterochiral (*SR*) dimers can be formed. The two hypotheses differ in nature regarding the catalytically active dimer unit: in NOYORI'S model, only the monomers are catalytically active, whereas in KAGAN'S, the dimers themselves act as active catalysts.

A

1/2 *SS*   1/2 *RR*

K_{homo} K_{homo}

catalytic cycle ← *S* + *R* → catalytic cycle

K_{hetero}

SR

B

1/2 *SS* + 1/2 *RR*

K_{dimer}

catalytic cycle ← *SR* → catalytic cycle

catalytic cycle
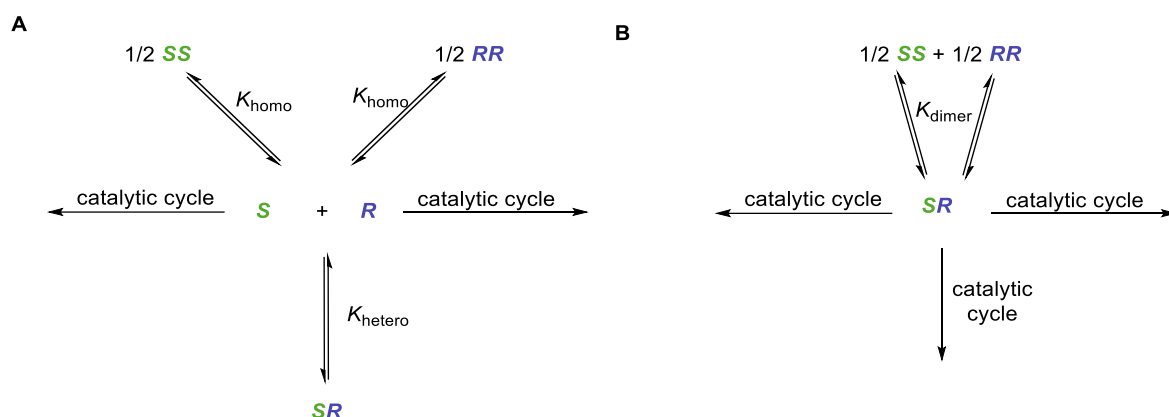
Scheme 2: Proposed mechanistic model for quantitatively investigate NLE in asymmetric alkylation reactions of aldehydes. A: NOYORI; B: KAGAN.[149]

FERINGAS investigations of positive and negative non-linear effects confirmed that these effects are due to formation of diastereomeric associations between chiral species in non-homochiral environments.[133]

The step from conventional asymmetric catalysis to asymmetric autocatalysis was achieved by SOAI in 1995 and still represents a singular reaction to this day, since in KAGAN's model the product did not yet serve as the catalyst.[186] Here, catalyst and product molecule must not only match in structure, but also in absolute configuration. This important reaction will be presented in more detail in chapter 2.2.3.1, examined in chapter 5 and is only put into context here.

BLACKMOND studied the NLE described with mathematical and kinetic models and high-lighted the impact kinetic investigations for the understanding of reaction mechanisms.[151,152]

2.2.2 Spontaneous Mirror Symmetry Breaking (SMSB)

Symmetry breaking is the imbalance between two enantiomeric molecules. There are many hypotheses for the emergence of homochiral life, most of them assume abiotic symmetry-breaking processes before the emergence of life. Only a few biotic scenarios postulate the emergence of life in a racemic environment with subsequent emergence of chirality.[153]

Spontaneous mirror symmetry breaking (SMSB) was first postulated in a theoretical model by FRANK IN 1953 and describes a process in which a physical system in a symmetric state spontaneously ends up in an asymmetric state.[142] The FRANK model is a model for non-equilibrium systems that are thought to be essential for the origin of the selected chirality of life and is based on reaction rate equations.

The following external influences have already been investigated as causes of symmetry breaking including CPL, parity violation, template surfaces such as chiral silica crystals, spontaneous symmetry breaking and spontaneous dissolution during crystallisation, asymmetric autocatalysis, which will be discussed in greater detail in Chapter 2.2.3, Chapter 3.2.2.1 and Chapter 5.[154-158]

CPL has been investigated as a cause of symmetry breaking because asymmetric molecules react differently when exposed to CPL due to circular dichroism.[81,159-161] This can lead to preferential synthesis or destruction and thus influence the enantiomeric ratio in the product.[162,163]

Crystallisation processes such as VIEDMA ripening or spontaneous resolution are among the random effects that allow for *ee*s to occur.[164,165]

One cause for symmetry breaking may be parity violating weak interactions. This phenomenon was first discovered in 1957 for the nuclear β-decay resulting in a small energy difference between two enantiomers, stabilizing one over the other.[166-168] This hypothesis was considered closely as a candidate for prebiotically plausible symmetry breaking when calculations indicated a preference of L-amino acids and D-sugars.[165,169-173] However, this relationship has not yet been experimentally proven, as the estimated energy differences based on the electromagnetic interaction are estimated to be very small, approximately between $10^{-14} - 10^{-13}$ J/mol, which would correspond to an *ee* value of about 10^{-15}%.[172,174,175] A parity-violating energy difference (PVED) between two enantiomers of a chiral molecule is caused by these weak interactions. While these parity violation effects are ubiquitous in biological systems, they have not yet been demonstrated for molecular systems despite great research efforts.[176-180]

2.2.3 Autocatalysis

An autocatalytic reaction is a form of catalysis reaction in which one of the products catalyses its own formation and no external catalyst is needed (see Scheme 3 A).[181] The expression goes back to WILHELM OSTWALD.[182] The presence of an exponential product-time curve, in the case of a very efficient system, and a positive correlation between initial product concentration and reaction rate indicate the presence of an autocatalytic system. In asymmetric autocatalysis, chiral induction of the chiral product enables enantioselective formation of the major product (Scheme 3 B).

A

P

A   +   B   autocatalysis   →   P

B

P*

A   +   B   asymmetric
autocatalysis   →   P*
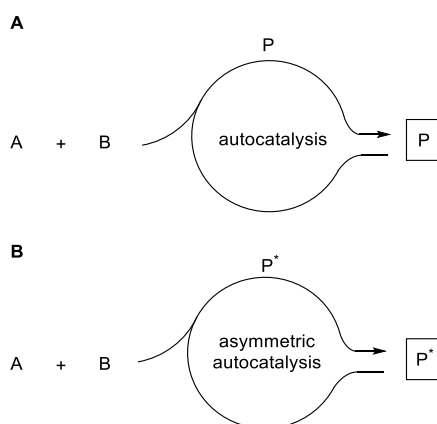
Scheme 3: Schematic concept of autocatalysis and asymmetric autocatalysis.

DANDA, WULFF and TRAPP found further examples of asymmetric, autoinductive behaviour with positive non-linear effects in the study of cyano hydrogenations, DIELS-ALDER reactions as well as hydrogenations respectively.[183-185]

Self-amplification of symmetry breaking due to catalyst-reaction product interaction and, in particular, asymmetric autocatalysis occurs in the SOAI reaction, which is one of the most interesting and exceptional examples.

2.2.3.1 The SOAI Reaction

The SOAI reaction represents a dynamic reaction system for chirality transfer. Here, the resulting chiral product catalyses the formation of further product molecules in a stereospecific manner. The combination of self-amplification and asymmetric autocatalysis in the alkylation reaction of pyrimidine carbaldehydes by diisopropylzinc to the corresponding alcohols represents a remarkable point in the research of homochirality. It was first described by KENSŌ SOAI and represents to date the only autocatalytic reaction with positive non-linear behaviour.[186,187]

The conversion of pyridine-3-carbaldehydes to the corresponding alcohols (see Scheme 4 A) was the first described system where the catalyst used was structurally identical to the reaction product 3-pyridyl alcohol. The product obtained, with an *ee* of 35% *ee*, was now used as an asymmetric autocatalyst in its own synthesis, thus closing the gap from asymmetric catalysis to asymmetric autocatalysis for the first time. The further developed system comprised a symmetrical pyrimidine unit instead of the pyridine ring in both the aldehyde and the alcohol (see Scheme 4 B).[186] Since a high enantioselectivity was observed for this system during asymmetric autocatalysis, experiments were carried out with a very low *ee*. After only four cycles, the *ee* was increased from an initial 2% *ee* to 88% *ee*. This was the first realisation of asymmetric autocatalysis with significant self-amplification of chirality and the first working example of Frank's antagonism theory.[142]
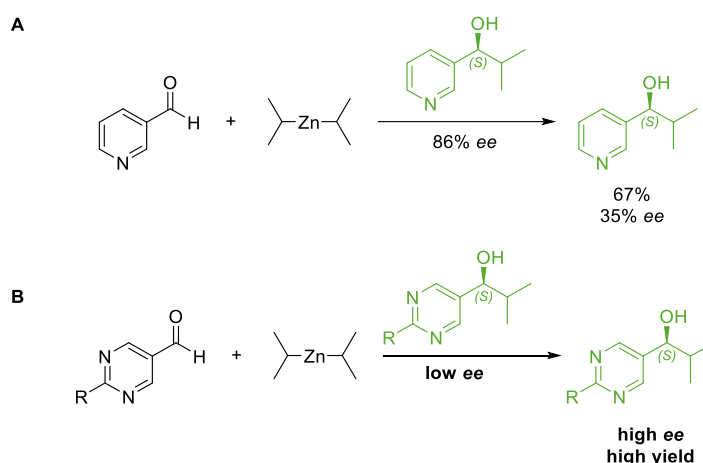
Scheme 4: SOAI's self-amplifying autocatalysis: A: Conversion of pyridine-3-carbaldehyde with diisopropylzinc (*i*Pr$_2$Zn); B: Conversion of substituted pyrimidine-5-carbaldehyde with *i*Pr$_2$Zn in the presence of a catalytic amount of pyrimidyl alcohol.[186,187] Modified scheme from reference [186]: Copyright Nature Publishing Group 1995.

Due to its singularity to date, the SOAI reaction has been intensively investigated and discussed.[188,189,190,191,192] Efforts to expand the substrate spectrum as well as test new chiral initiators provided new systems.[158,193-198] Sources of chiral initiators include cyclophanes, mandelic acid methyl ester, leucine, [5]-and [6]-helicenes, cinnabar, quartz and crystals of sodium chlorate or even the induction of chirality by isotopically labelled crypto chiral compounds and CPL was further tested.[199-213] Particularly interesting are observations of random spontaneous symmetry breaking, occurring even without the addition of a chiral additive.[214]

Numerous investigations have been undertaken to elucidate the mechanism and the kinetics of the SOAI reaction.[215-220]

BLACKMOND developed a microcalorimetry method that can be used to measure reaction rates and concentrations of reactants and products.[221] The measurement and determination of time-dependent reaction rates, the turnovers and concentrations of reactants and products is made possible by the time-resolved reaction profiles. For this purpose, this method records and evaluates heat flux profiles as a function of time. In the case of the SOAI reaction, a characteristic autocatalytic reaction profile is obtained. The determination of the rate law then enables statements about the mechanism. In 2003, BLACKMOND postulated the rate law in equation (4) for a system that assumes possible dimers as the catalytically active species.[222]

$$\text{r} = k[\text{aldehyde}]^2[(\text{alcohol-Zn-dimer})_{\text{active}}] \tag{4}$$

With this, agreement regarding the conversion and the *ee* of experimental and theoretical data could be shown by BLACKMOND and BROWN using KAGAN's systems of equations.[223] Later, by varying the initial concentrations and performing excess experiments, the reaction rates for aldehyde, alcohol, and zinc organyl were refined, leading to equation (5).

$$\text{r} = k[\text{aldehyde}]^{1.6}[\text{alcohol-Zn}] \tag{5}$$

For the aldehyde, the reaction order 1.6 was determined, which indicates that in the transition state, the addition of a free aldehyde molecule to a molecule containing another aldehyde molecule takes place. In this system, the alcohol occurs as a zinc alcoholate and enters the reaction law with the first order. The zinc organyl occurs in the zeroth order. This extended model includes tetrameric structures of the transition state of the active catalyst, which consists of alkoxide molecules that are mainly present as dimers in the ground state. Homo- and heterochiral dimers are formed in a statistically distributed manner. The selectivity of the system depends on the kinetic process in which the homochiral dimer forms the active catalyst.

ERCOLANI and SCHIAFFINO performed density functional theory (DFT) calculations for a postulated general reaction mechanism in which dimer catalysts serve as templates and that includes the BLACKMOND-BROWN dimer model.[224-226] The dimers subsequently form tetramers consisting of two aldehydes and two major product enantiomers (*AARR*). These tetrameric complexes are additionally coordinated by further zinc organyls, which are required for the incremental addition reactions. This gradual transfer of alkyl groups leads to the preferential formation of the more stable complexes ($stability(\mathbf{ARRR}) > stability(\mathbf{ARRS})$). The transfer of the alkyl group occurs in the tetrameric structure and the more stable complex is subsequently alkylated to an $all-\mathbf{RRRR}$ complex that disintegrates into two catalytically active dimers $\mathbf{RR}$ and thus enables a chirality transfer in the system. Their

quantum-mechanically derived predictions of chiral amplification or depletion are in agreement with the experimental data and also show that higher selectivities can be achieved at lower temperatures.[227] A preferential formation of highly active oligomeric catalyst complexes was postulated, whose stability decreases with increasing temperatures also should explain the shortened induction phase and the faster reaction rates at low temperatures. However, the significance of the postulated mechanism for the Soai reaction can only be considered to a limited extent, since it was a gas-phase DFT calculation and thus the comparison with a reaction taking place in toluene is only partially applicable.

DFT calculations for the Soai reaction in solution were carried out by Gridnev and Vorobiev considering homochiral tetrameric structures in concurrence to dimers, tetramers and oligomers.[228] Gridnev and Brown furthermore confirmed homo- and heterochiral dimers with a central $[ZnO]_2$ unit (see blue substructure in Scheme 5) that were also observed in NMR experiments.[229]

homochiral dimer   heterochiral dimer
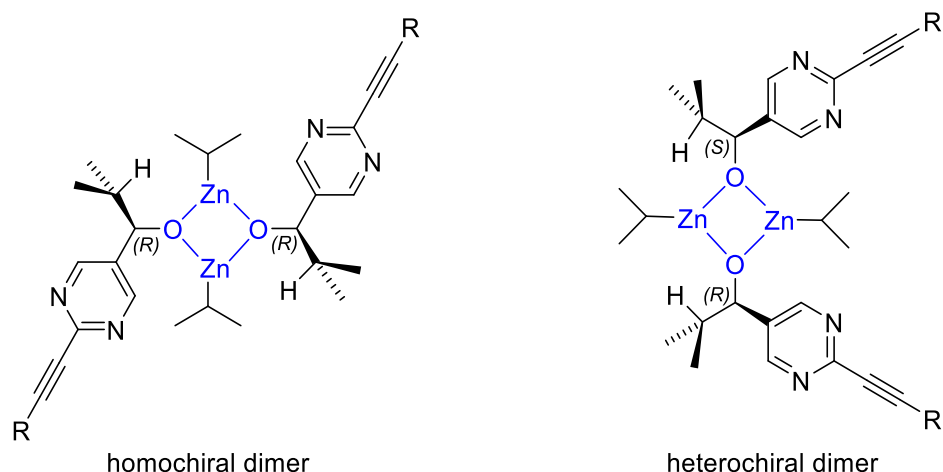
Scheme 5: Dimeric structures in the Soai reaction confirmed by DFT calculations and detected by NMR spectroscopy.[228,229]

Buhse presented a theoretical model similar to that of Ercolani and Schiaffino. The chiral products form a dimer and subsequently a trimer complex.[230] An aldehyde monomer attaches to the trimer and a closed-cage tetramer is formed from which the stereoselective alkyl addition takes place. They furthermore presented simplified kinetic models using non-linear differential equations to analyse chiral amplification in the Soai reaction investigating monomers and dimers as the catalytic species.[231-233]

Soai investigated crystallised component mixtures by X-ray structure analysis with the aim of identifying the most likely reaction-determining intermediate formed *in situ*, as indicated by previous findings.[234] Both tetrameric and oligomeric structures could be detected, including the square-macrocycle-square (SMS) conformation already discussed by Klankermayer et al. and the 12-membered macrocycle that had already been discussed by

BLACKMOND and BROWN.[223,235] Although these crystalline structures are not the active species in solution, they allow conclusions to be drawn about the mechanism of the SOAI reaction.

The TRAPP group investigated the prototype reaction (see Scheme 6) of 2-(*tert*-butylacetylene-1-yl)pyrimidyl-5-carbaldehyde with 2-propanol kinetically and thermodynamically and identified hemiacetalate complexes as transient catalysts by mass spectrometry.
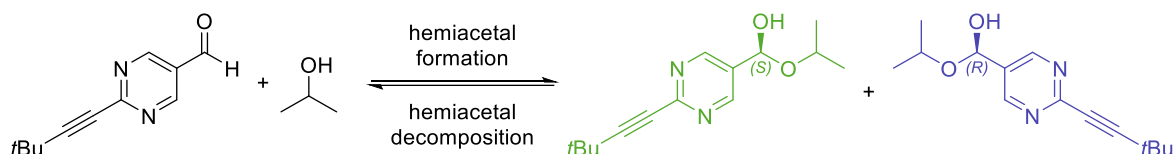
Scheme 6: Hemiacetal formation of 2-(*tert*-butylacetylene-1-yl)pyrimidyl-5-carbaldehyde with 2-propanol for the investigations conducted by TRAPP.

These hemiacetalate complexes are formed by reaction of aldehydes and the product alcoholate.[236] The formation of these homo- and heterodimers, which consist of two product alcohols and differ product-specifically in their formation equilibrium, removes the smaller enantiomer from the reaction and explains the NLE that occurs.

From dynamic HPLC (DHPLC) experiments, reaction rate constants were determined by direct methods on the basis of theoretical plate model. From the determined rate constants k_1, the thermodynamic parameters can be obtained by linear regression (see Figure 5) of the thermodynamic Gibbs free energies $\Delta G(T)$. $\Delta G(T)$ can be calculated by means of the Eyring equation (6) with R being the general gas constant ($R = 8.314$ J·K^{-1}·mol^{-1}), T the temperature, κ the transmission coefficient, k_B corresponds to the Boltzmann constant ($kB = 1.381 \cdot 10{-}23$ J·K^{-1}), h to the Planck constant ($h = 6.626 \cdot 10^{-34}$ J·s).

$$\Delta G^{\ddagger} = -\mathrm{R}T ln\left(\frac{k_1 h}{\kappa k_B T}\right) \tag{6}$$

After substituting the Gibbs-Helmholtz equation (7) into the Eyring equation and plotting ln(k/T) against T^{-1}, the activation parameters $\Delta H^{\ddagger}$ and can be obtained via the slope and $\Delta S^{\ddagger}$ via the intercept of the Eyring plots (ln(k/T) *vs.* 1/T).

$$\Delta G^{\ddagger} = \Delta H^{\ddagger} - T\Delta S^{\ddagger} \tag{7}$$
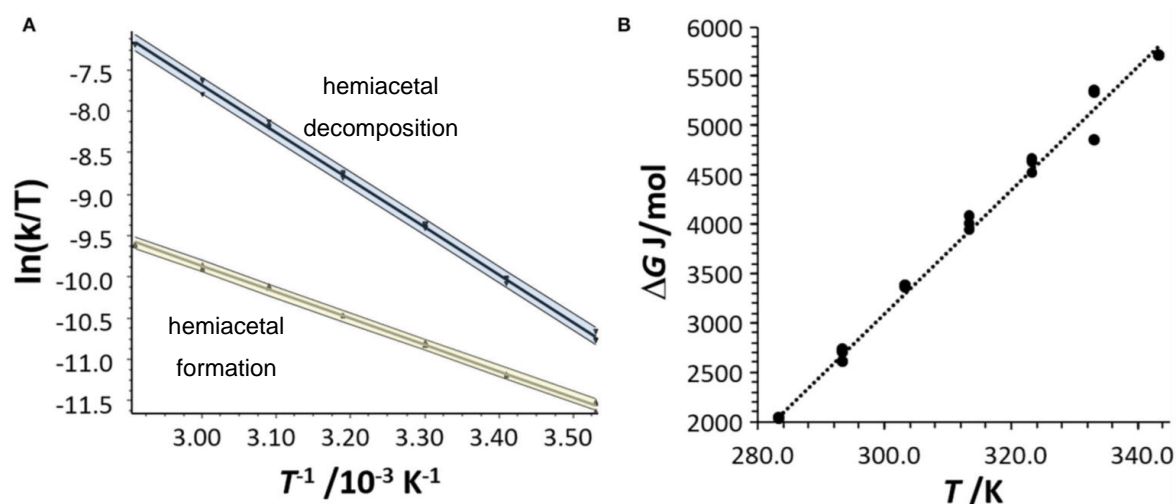
Figure 5: Determination of thermodynamic parameters by the TRAPP group. **A**: Eyring plot for the determination of the activation parameters ΔH^+ and ΔS^+ of the hemiacetal formation (yellow data points) and the hemiacetal decomposition (blue data points) from DHPLC experiment. Upper and lower curves represent error bands of the linear regression with level of confidence of 95%. **B**: Determination of the thermodynamic parameters ΔH^+ and ΔS^+ by plotting the Gibbs free energy ΔG as a function of T. Reproduced from reference [220]: John Wiley & Sons, Copyright © 2020. Copyright by Creative Commons Attribution 4.0 International License CC BY.

The thermodynamic parameters obtained from linear regression were ΔG^0 = 3 kJ mol^{-1}, ΔH^0 = 15.6 kJ mol^{-1} , and ΔS^0 = 62.5 J (K mol)$^{-1}$. The activation parameters for the hemiacetal formation were $\Delta H^+_{form} = 26.3 \pm 0.2$ kJ mol^{-1} and $\Delta S^+_{form} = -195 \pm 34$ kJ mol^{-1} and for the decomposition $\Delta H^+_{decomp} = 47.7 \pm 0.2$ kJ mol^{-1} and $\Delta S^+_{decomp} = -112 \pm 1$ J (K mol)$^{-1}$.[220]

The TRAPP group was able to present evidence that the previously observed hemiacetals play a crucial role in the chirality transfer (see Scheme 6 and Scheme 7).[185,220,237] These hemiacetals form from the aldehyde and the chiral alcohol product and are subject to interconversion.

Even though the reaction conditions of the known SOAI reaction systems are not prebiotically plausible, the implication that asymmetric catalysis could be able to convert an existing minute *ee* into homochirality is a promising step towards elucidating this problem for the early Earth.
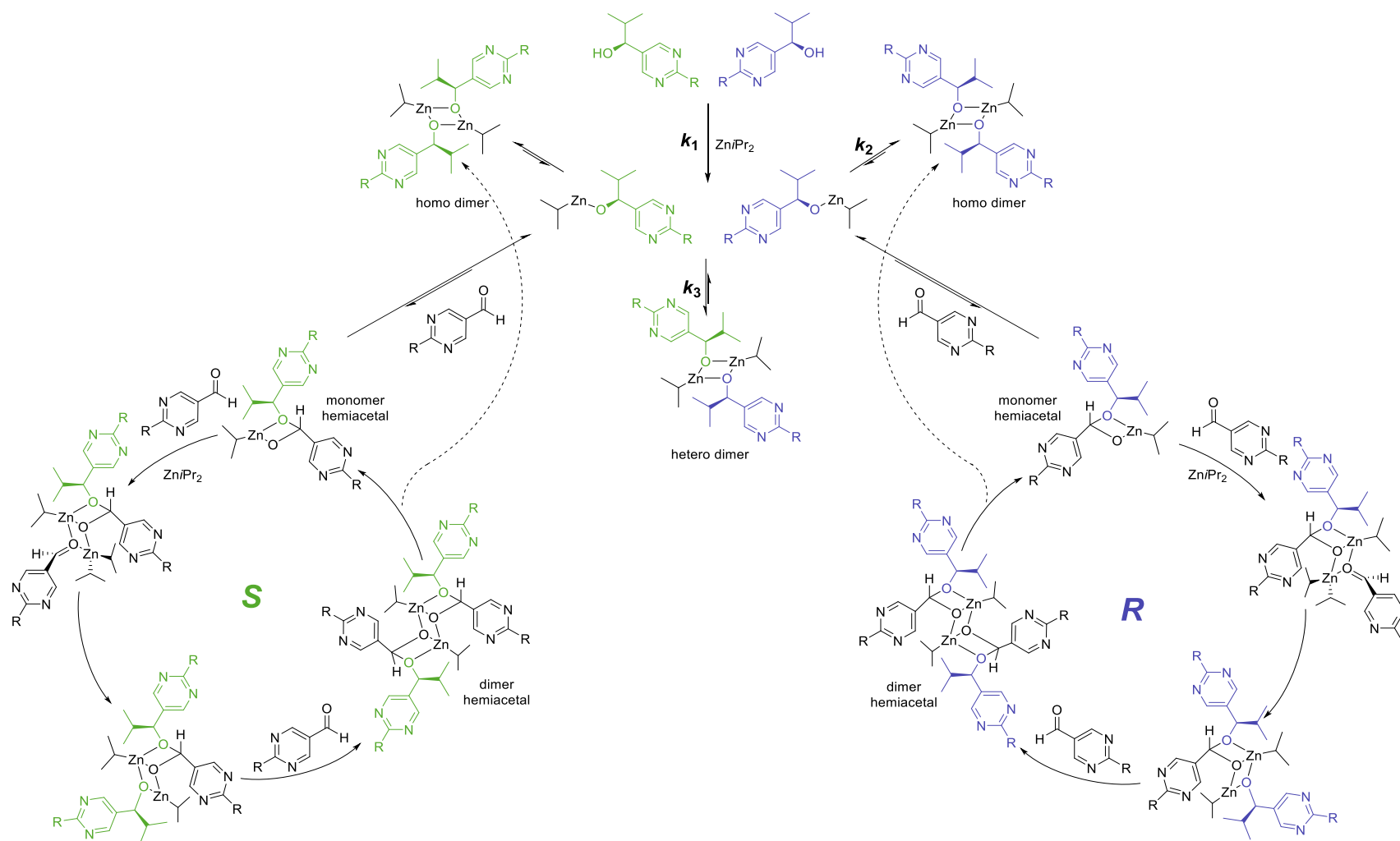
Scheme 7: Proposed mechanism of the SOAI reaction by TRAPP with the formation of the transient hemiacetal as the key intermediate. Structures were identified *in situ* by high-resolution mass spectrometry (HRMS) experiments.

2.3 Reaction Kinetics

For the elucidation of reaction mechanisms, reaction kinetics are especially important. If one can understand the implications of how the changes in conditions affect the reaction rate, the "black box" of a reaction can be better understood. Modern analytic methods now enable us to do so more detailed than ever before. This is important throughout the chemical field ranging from large scale industrial synthesis to environmental and atmospheric chemistry as well as drug discovery.[238]

The standard procedure for studying the kinetic properties of a system is to extract kinetic properties from experimental data, determine the rates of the reactions studied and, if simulations have been performed, compare the predicted results with those determined experimentally.

Rates of chemical reactions

In reaction kinetics, a sequence of elementary reactions within a reaction network are considered. The rate is expressed in terms of 1 mole of the reactants. The rates of change in concentration are normalised to the stoichiometric reaction coefficients, which are the number of moles of each compound occurring in the balanced chemical equation. Therefore, e.g., in the bimolecular reaction (Entry 2 in Table 1), the stoichiometric coefficients have to be considered.[239]

Chemical kinetics are the study of reaction rates of transformations of chemical compounds to form reaction products.[240] The rate of consumption of a reactant **R** at a given time is defined as $-\frac{d[R]}{dt}$ while the rate of formation of a product is $\frac{d[P]}{dt}$.

Rate laws and reaction orders

A general rate law r is given with the molar concentrations of the reactants **A**, **B** and **C**, the rate constant k_x, which is temperature dependent, but independent from the concentration of the reactants.

$$r = k_x[A]^l[B]^m[C]^n \ldots$$

Tables 1 and 2 contain universally applicable examples for rate determination and Chapter 2.2.3.1 shows exemplarily how the rate law can be obtained via microcalorimetry.[221]

First order reactions are reactions in which the exponents in the rate equation sum to unity. Prominent prebiotic examples are photodecompositions under UV light. Second order

reactions are bimolecular reactions, and the rate expression depends on the concentration of both reactants. This is the most ubiquitous form of in-solution reactions to be considered as higher order reactions are less likely to occur, based on impact theory. Third order reactions frequently occur in atmospheric chemistry, mostly for reactions comprising N_2 or O_2.[241]

The mathematical complexity for simulating kinetic profile increases significantly as soon as the reaction mechanism involves more than a few steps.

The most common method to examine kinetic properties is by double logarithmic plotting of the initial rates.[242]

Table 1: Kinetic equations for irreversible reactions of first, second and third order.

Reaction order	Reaction and molecularity	Substrate consumption	Product formation
First order	unimolecular $A \xrightarrow{k_1} B$	$\dfrac{d[A]}{dt} = -k_1 \cdot [A]$	$\dfrac{d[B]}{dt} = k_1 \cdot [A]$
Second order	bimolecular $2\,A \xrightarrow{k_1} B + C$	$\dfrac{d[A]}{dt} = -k_1 \cdot [A]^2$	$\dfrac{d[B]}{dt} = k_1 \cdot [A]^2$ $\dfrac{d[C]}{dt} = k_1 \cdot [A]^2$
	$A + B \xrightarrow{k_1} C$	$\dfrac{d[A]}{dt} = -k_1 \cdot [A] \cdot [B]$ $\dfrac{d[B]}{dt} = -k_1 \cdot [A] \cdot [B]$	$\dfrac{d[C]}{dt} = k_1 \cdot [A] \cdot [B]$
Third order	termolecular $2\,A + B \xrightarrow{k_1} C$	$\dfrac{d[A]}{dt} = -k_1 \cdot [A]^2 \cdot [B]$ $\dfrac{d[B]}{dt} = -k_1 \cdot [A]^2 \cdot [B]$	$\dfrac{d[C]}{dt} = k_1 \cdot [A]^2 \cdot [B]$
	$A + B + C \xrightarrow{k_1} D$	$\dfrac{d[A]}{dt} = -k_1 \cdot [A] \cdot [B] \cdot [C]$ $\dfrac{d[B]}{dt} = -k_1 \cdot [A] \cdot [B] \cdot [C]$ $\dfrac{d[C]}{dt} = -k_1 \cdot [A] \cdot [B] \cdot [C]$	$\dfrac{d[D]}{dt} = k_1 \cdot [A] \cdot [B] \cdot [C]$

Table 2: Kinetic equations for reversible reactions of first, second and third order.

Reaction order	Reaction and molecularity	Substrate consumption	Product formation
First order	unimolecular $A \underset{\text{-}k_1}{\overset{k_1}{\rightleftharpoons}} B$	$\frac{d[A]}{dt} = -k_1 \cdot [A] + k_{-1} \cdot [B]$	$\frac{d[B]}{dt} = k_1 \cdot [A] - k_{-1} \cdot [B]$
Second order	Bimolecular $2\,A \underset{\text{-}k_1}{\overset{k_1}{\rightleftharpoons}} B + C$	$\frac{d[A]}{dt} = -k_1 \cdot [A]^2 + k_{-1} \cdot [B] \cdot [C]$	$\frac{d[B]}{dt} = k_1 \cdot [A]^2 - k_{-1} \cdot [B] \cdot [C]$ $\frac{d[C]}{dt} = k_1 \cdot [A]^2 - k_{-1} \cdot [B] \cdot [C]$
	$A + B \underset{\text{-}k_1}{\overset{k_1}{\rightleftharpoons}} C$	$\frac{d[A]}{dt} = -k_1 \cdot [A] \cdot [B] + k_{-1} \cdot [C]$ $\frac{d[B]}{dt} = -k_1 \cdot [A] \cdot [B] + k_{-1} \cdot [C]$	$\frac{d[C]}{dt} = k_1 \cdot [A] \cdot [B] - k_{-1} \cdot [C]$
Third order	termolecular $2\,A + B \underset{\text{-}k_1}{\overset{k_1}{\rightleftharpoons}} C$	$\frac{d[A]}{dt} = -k_1 \cdot [A]^2 \cdot [B] + k_{-1} \cdot [C]$ $\frac{d[B]}{dt} = -k_1 \cdot [A]^2 \cdot [B] + k_{-1} \cdot [C]$	$\frac{d[C]}{dt} = k_1 \cdot [A]^2 \cdot [B] - k_{-1} \cdot [C]$
	$A + B + C \underset{\text{-}k_1}{\overset{k_1}{\rightleftharpoons}} D$	$\frac{d[A]}{dt} = -k_1 \cdot [A] \cdot [B] \cdot [C] + k_{-1} \cdot [D]$ $\frac{d[B]}{dt} = -k_1 \cdot [A] \cdot [B] \cdot [C] + k_{-1} \cdot [D]$ $\frac{d[C]}{dt} = -k_1 \cdot [A] \cdot [B] \cdot [C] + k_{-1} \cdot [D]$	$\frac{d[D]}{dt} = k_1 \cdot [A] \cdot [B] \cdot [C] - k_{-1} \cdot [D]$

Modern kinetic analyses and simulations

Stochastic kinetic simulations of molecular systems to analyse, for example biological cellular systems, were performed by GILLESPIE.[243] However, these systems contain only small populations of molecules, which leads to deviations from the expected reaction course when deterministic differential equations of classical chemical kinetics are used.

LENTE applied a theoretical approach to investigate a stochastic kinetic approach for chiral autocatalysis and showed that especially autocatalytic reaction systems of higher reaction order lead to symmetry breaking.[244,245]

PROSS et al. introduced the term *dynamic kinetic stability* when investigating a physico-chemical framework to bridge the gap between animate and inanimate systems, postulating that not traditional thermodynamic states but kinetic states determine the increase in complexity.[246]

BLACKMOND applied a reaction progress chemical analysis involving *in situ* measurements and data manipulation and graphical rate equations, indicating that this method provides valuable kinetic insights even with a minimal number of experiments.[247]

BURÉS presented a graphical method with which the reaction order of the catalyst can easily be determined from concentration data without the requirement of knowledge of the reaction rates, which might be beneficial for some reaction setups.[248,249] However, this variable time normalisation approach may miss detailed information that can be obtained directly from the kinetic profiles, as the focus of this method is on the overview of specific reaction properties.

LARROSA and BURÉS recently presented a very interesting new contribution including a machine learning approach for organic reaction mechanism classification. Their deep neural network model can be trained on kinetic data to then analyse the underlying mechanisms.[250]

Chapter 3

Investigation towards Symmetry

Breaking by Consecutive Amplification

3.1 Objective

Elucidating chiral symmetry breaking and the origin of homochirality is an important aspect of the study of the Origin of Life. The aim is to understand abiogenesis, which is based on increasing complexity starting from the primordial atmosphere to the first protocells, that can subsequently be modified by evolutionary mechanisms.

The goal of this work was to study systems that exhibit symmetry breaking in greater detail. For this purpose, a software program was developed to perform kinetic simulations at the molecular level in order to obtain effective single-molecule simulations.

The requirements for the developed tool are that a set of linked differential equations can be solved, and concentration curves can be generated; starting concentrations of the substrates and discrete values for reaction constants and reaction rates can be specified. A user interface with the respective interactive fields is best suited for this purpose.

Reaction scenarios that have already been well investigated experimentally were chosen to obtain the maximum knowledge gain from these symmetry breaking simulations. A prerequisite was that in these reaction scenarios two independent processes lead to the same reaction product. In these scenarios, one of the reaction channels is controlled by a stochastic process, while the other is controlled either by the reaction product or by an activator formed from the reaction product and another reactant. This constitutes the combination of a related stochastic process and an autocatalytic process.

As another mechanism, we wanted to investigate the hypothesis that kinetic acceleration in successive reactions by autocatalytic processes or reaction cascades is a possible way to enhance initial statistical imbalances in the formed product enantiomers.

3.2 Results and Discussion

3.2.1 The Single Molecule Kinetics Program (*SMK.exe* Program)

Parts of this section have already been published in *Origins of Life and Evolution of Biospheres*, *52*(1).[251]

3.2.1.1 Program Structure

The reaction network analysis tool *SMK.exe* was developed based on an adaptive fourth order Runge–Kutta algorithm, programmed in Pascal (Embarcadero Delphi XE 7), to solve a set of differential equations for single molecule reaction kinetics.

The main emphasis of the tool was to allow efficient single molecule simulations on a workstation computer within a reasonable timeframe. The program can be used on a normal desktop computer without interfering with other programs running at the same time. The program is employing a system of nonlinear differential equations. Figure 6 shows the structure of the algorithm for an exemplary reaction (A). This reaction equation is supplied to the program as input in differential equation form (B).

The software program allows the simulation of reaction profiles of a selected reaction network and enables the processing of large data sets with over one million kinetic profiles each. The reaction constant k is defined for 1 mol of molecules. This would require one array with addressable single molecules with $6.023 \cdot 10^{23}$ elements, presenting a computational challenge that would lead to long processing times. The *SMK.exe* program generates empty one-dimensional arrays of integers, that are deliberately truncated at $602\,214\,076$ elements, the size of which was chosen based on the size of the Avogadro number N_A and the resulting computability.

A   A   +   B $\xrightarrow{\quad k \quad}$ C

B $\dfrac{d[A]}{dt} = -k\,[A]\,[B]$ $\dfrac{d[B]}{dt} = -k\,[A]\,[B]$ $\dfrac{d[C]}{dt} = k\,[A]\,[B]$

C   **rate constant array**   **molecules arrays**

$k < 1 : N = \text{truncate}\,(10^{(1/\log(k))})$
$k > 1 : k\text{-fold iteration}$

D   **randomized rate constant array**   **randomized molecules arrays**
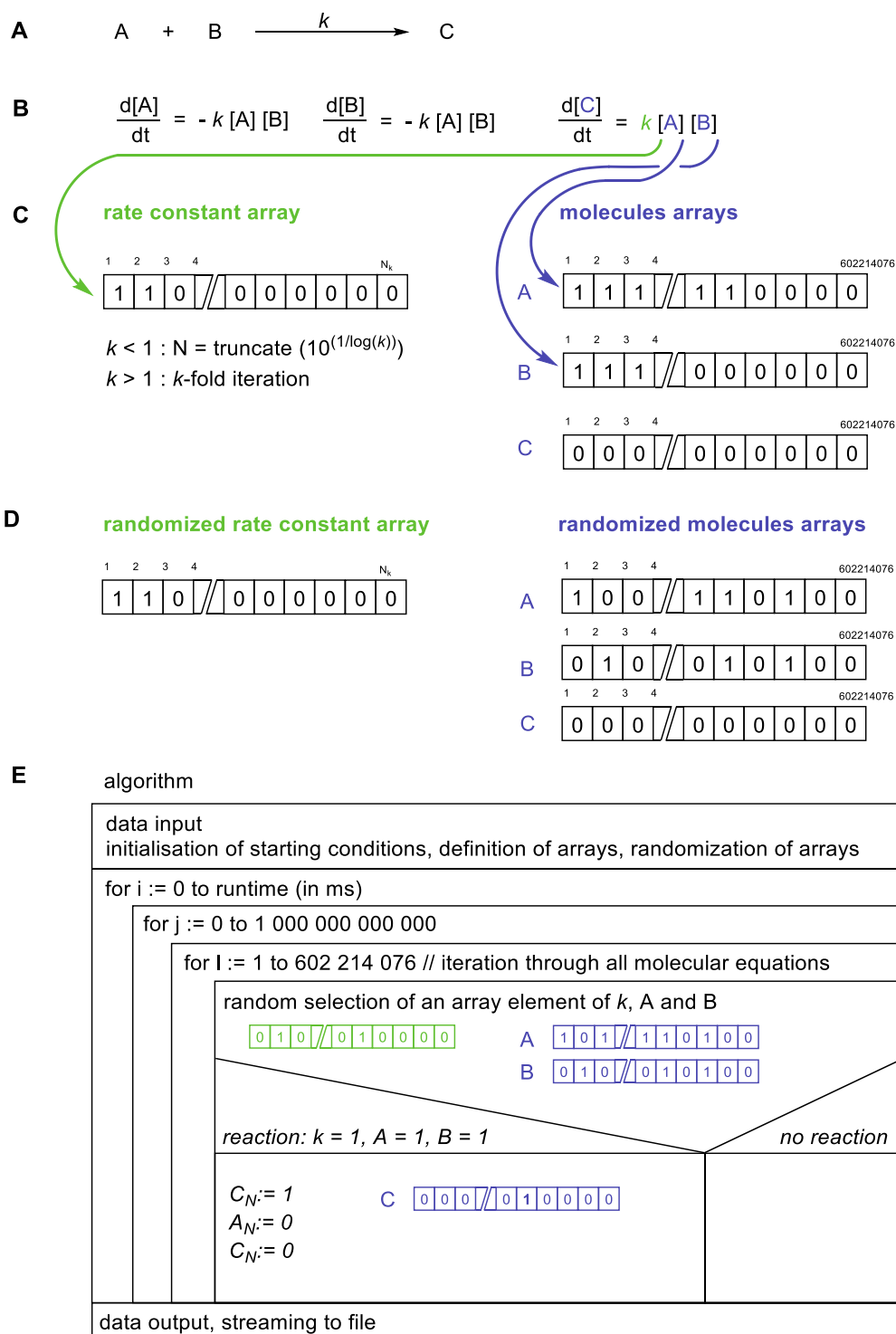
E   algorithm

Figure 6: Algorithm of the *SMK.exe* program. **A**: Example reaction equation for the simulation of a 2$^{\text{nd}}$ order irreversible reaction; **B**: Differential equations for reaction A; **C**: Binary rate constant array and molecule arrays corresponding to the reaction constant and substrates and products, respectively; **D**: Randomised rate constant array and randomised molecular arrays; **E**: Algorithm of the applied method within the *SMK.exe* program. Figure modified from reference: L. Huber and O. Trapp, Symmetry breaking by consecutive amplification: Efficient paths to homochirality. *Origins of Life and Evolution of Biospheres*, 2022, *52*(1-3), 75-91.[251] Copyright by Creative Commons Attribution 4.0 International License CC BY.

Prior to the simulation, the reaction rates of each reaction and the concentrations of the reactants and products are divided into two different types of arrays. One of these types of arrays is fixed at $N_A/10^{15} = 6.02214 \cdot 10^8$, the molecule arrays, the other type, the rate constant array has a flexible number of elements (see Figure 6: arrows from **B** to **C**). In the next step, both types of the described arrays are randomized (from **C** to **D**), and the algorithm performs a random selection of one array element of each array k, A and B. The intervals are set at $1.00 \cdot 10^{15}$ and each set is calculated $n = 602\,214\,076$ times, corresponding to the probability of a reaction kinetic in bulk material.
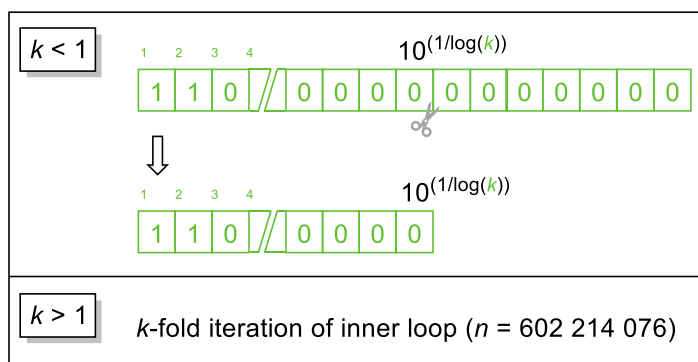
Figure 7: The algorithm performs different routines, depending on the size of the reaction rate constant k.

For reaction constant values smaller than one ($k < 1$), the number of elements in the reaction constant array is truncated at $10^{\left(\frac{1}{\log k}\right)}$ whereas for reaction constants k greater than one ($k > 1$), the program performs appropriate repetitions, e.g., for $k = 600$, 600 repetitions of the inner loop ($n = 602\,214\,076$ times) to calculate the kinetics.

During the simulation, statistical sampling is performed from the one-dimensional binary concentration arrays and binary reaction constant arrays. To shorten the computational time, the value is not selected directly, but the position in the array is randomly sampled and the value to be found in the array at this position is then selected.

If the combination of the randomly selected elements is $k = 1$, A = 1 and B = 1, then one product molecule is formed, and one randomly selected element of the product array(s) will be set from 0 to 1. A Boolean array was used as a filter to ensure the fastest way towards the product molecule array(s) (see Figure 8).
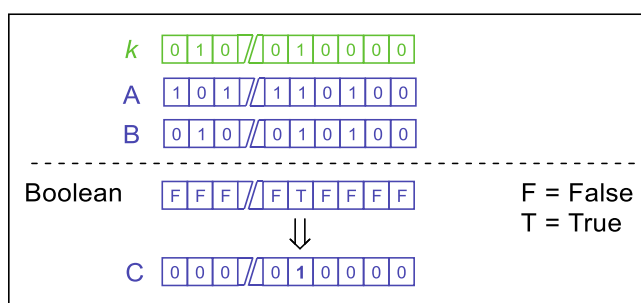
Figure 8: Visualization of the product formation step. Randomized rate constant array *k*, randomized molecule arrays of substrates A and B, Boolean array, and molecule array of the formed product C.

Any other combination (elements of k, A and/or B ≠ 1) corresponds to no reaction and no formation of a product molecule. The product molecule array(s) are successively filled with molecules.
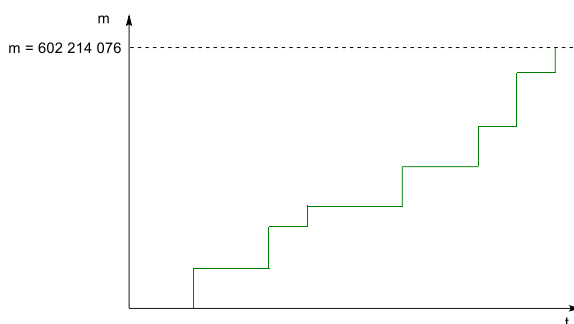
Figure 9: Arbitrary example of visualization of time-resolved product molecule formation.

The end of the simulation is reached when the product molecule array is full (if sum = 602 214 076). Then, the resulting simulated product concentration courses are generated and saved into the output file (see 3.2.1.3 Output), and the **ee** can be determined by subtracting the number of molecules of the minor product from the major product and subsequently dividing by the sum of the major and minor products ($ee = \frac{N_{major} - N_{minor}}{N_{major} + N_{minor}}$). The steps that were necessary to reach the full product molecule array correlate with the value of *k*.
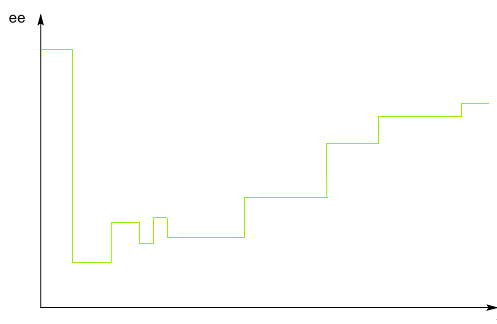
Figure 10: Arbitrary example of visualization of time-resolved **ee**.

3.2.1.2 Input

The initial inputs to the software are the starting concentrations of the substrates and the reaction rates. These can be discrete values, as well as variable ranges with upper and lower limits, together with the number of steps desired. If more than one variable is varied, a permutation of all possible combinations is calculated, resulting in several subsets of the simulation.

Figure 11: User interface of the *SMK.exe* program with input fields for differential equations, settings and parameter inputs such as rate constants, concentrations and an example of a reaction scenario.

The corresponding differential equations, the reaction rate constants k and the concentration of the reactants were chosen as input to the program for each set.

The "Create" button creates a .csv file, that saves all the input data for reproducibility and traceability of the simulations carried out. As soon as this file is saved, the "Calculate" button becomes active and the simulation can be run. The run times vary widely and depend on the set size, the desired increment of output data points and the capacity of the central processing unit (CPU) of the used computer, ranging from seconds to hundreds of minutes for the entire simulation.

The settings for data output allow simulations with very long simulated reaction times to be performed in a memory-saving manner by presenting the possibility to only save larger intermediate steps.

3.2.1.3 Output

In order to be a versatile tool, the *SMK.exe* program was designed to generate .csv documents as output files. One file contains the log of input parameters, the remaining are output .csv files: one for each parameter iteration set.

The data can then be exported to any program and the simulations of the generated concentration courses can then be plotted.

3.2.1.4 Reproducibility

To verify the reproducibility of the approach and algorithm described here, a feature to save and reassign the seed of the random number generator was implemented. A series of simulations were performed using the saved seed of the random number generator and identical starting parameters. These replicates gave the identical results for the reaction progress and *ee* values and confirmed the reproducibility of the method.

3.2.2 Simulated Scenarios

The kinetic data employed for the simulations are based on the experimentally studied kinetics of the SOAI reaction.[186] Different scenarios that are known to exhibit symmetry breaking were selected for investigation: several autocatalysis scenarios and one cascade reaction. The goal was to determine if and at what point an *ee* would occur in the system. For this purpose, combinations of different values for the reaction rate constant *k* were employed for each reaction mechanism.

The chosen reaction scenarios were designed to contain a defined substrate feedstock of 1 mol substrate and one single enantioselective catalyst molecule (**(R)-Cat** or **(S)-Cat**) to mimic kinetic effects at the molecular level.

3.2.2.1 Autocatalysis

Classical Autocatalysis

For a logical starting point, the program was used to simulate a classical autocatalysis reaction (see Scheme 8). In this scenario, reactants **A** and **B** initially react in a preceding stochastic reaction with a small reaction rate constant k_1 to form the enantiomers **(R)-C** or **(S)-C** at very low concentrations. The reactions to the enantiomers proceed with the same

probability. Next, the consecutive autocatalytic amplification follows with a much higher reaction rate constant k_2, where the products **(R)-C** or **(S)-C** catalyse the conversion of A and B to **(R)-C** or **(S)-C** and simultaneously control the selectivity. **(R)-C** catalyses only the formation of the product **(R)-C** and **(S)-C** the formation of **(S)-C**, respectively.
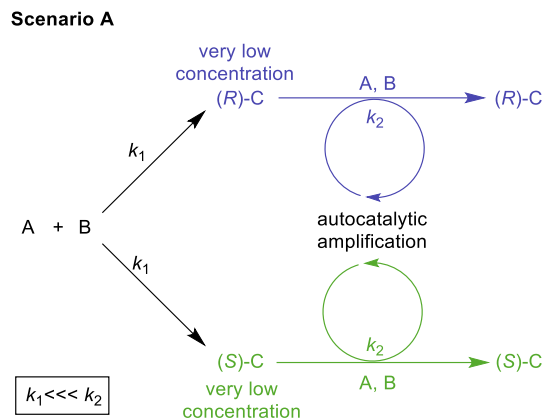
Scheme 8: Scenario A: schematic reaction mechanism of classical autocatalysis. Figure modified from reference: L. Huber and O. Trapp, Symmetry breaking by consecutive amplification: Efficient paths to homochirality. *Origins of Life and Evolution of Biospheres*, 2022, *52*(1-3), 75-91.[251] Copyright by Creative Commons Attribution 4.0 International License CC BY.

The following ODEs were used to simulate Scenario A (equations 8-11):

$$\frac{\mathrm{d}[A]}{\mathrm{d}t} = -2\,k_1[A][B] - k_2[A][B][(R)\text{-}C] - k_2[A][B][(S)\text{-}C] \tag{8}$$

$$\frac{\mathrm{d}[B]}{\mathrm{d}t} = -2\,k_1[A][B] - k_2[A][B][(R)\text{-}C] - k_2[A][B][(S)\text{-}C] \tag{9}$$

$$\frac{\mathrm{d}[(R)\text{-}C]}{\mathrm{d}t} = k_1[A][B] + k_2[A][B][(R)\text{-}C] \tag{10}$$

$$\frac{\mathrm{d}[(S)\text{-}C]}{\mathrm{d}t} = k_1[A][B] + k_2[A][B][(R)\text{-}C] \tag{11}$$

The change in concentrations over time of the substrates depend in each case on the initial second order stochastic reaction with reaction rate constant k_1 and the subsequent third order autocatalytic reaction with k_2. The respective parts of the differential equations (8) and (9) have a negative sign, as the substrates are used up in the reaction. The change in concentrations over time of product enantiomers **(R)-C** and **(S)-C** depends on the substrate concentrations and k_1 as well as the concentration of the product enantiomer formed, the substrates and k_2.

For the simplified reaction network shown in Scheme 8, a set of simulations was carried out. To observe the reaction progress at the molecular level, the initial concentration of the reactants was kept constant, and a permutation of the reaction rate constants was performed, the exact magnitudes of which are shown in Figure 12.
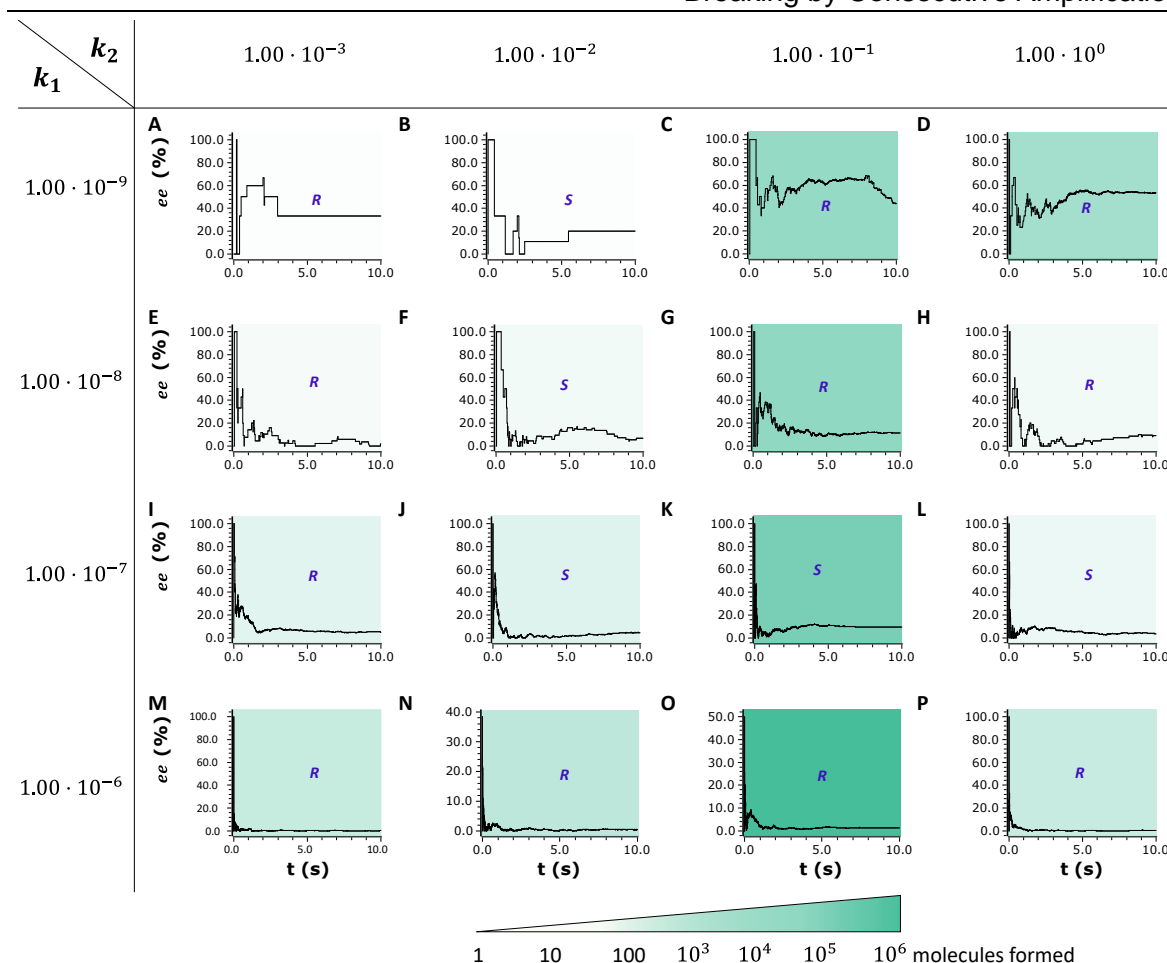
Figure 12: Scenario A: Results of the simulation with the *SMK.exe*-program: *ee* versus reaction time was plotted for each parameter subset; the respective stereo descriptor shows per plot which stereoisomer was formed predominantly after 10 s. The following reaction rate constants k_x were permuted: k_1: $1.00 \cdot 10^{-9}$ (**A** − **D**), $1.00 \cdot 10^{-8}$ (**E** − **H**), $1.00 \cdot 10^{-7}$ (**I** − **L**), $1.00 \cdot 10^{-6}$ (**M** − **P**), and k_2: $1.00 \cdot 10^{-3}$ (**A, E, I, M**), $1.00 \cdot 10^{-2}$ (**B, F, J, N**), $1.00 \cdot 10^{-1}$ (**C, G, K, O**), $1.00 \cdot 10^{0}$ (**D, H, L, P**). Figure according to L. Huber and O. Trapp, Symmetry breaking by consecutive amplification: Efficient paths to homochirality. *Origins of Life and Evolution of Biospheres*, 2022, *52*(1-3), 75-91.[251] Copyright by Creative Commons Attribution 4.0 International License CC BY.

We then determined the *ee* value of each system and indicated for each parameter subset the enantiomer that was predominantly formed after 10 seconds (s). Screening of the selected reaction parameters resulted in 16 subsets of total *ee* value courses, which were plotted against the simulated reaction time. The matrix of the different combinations of the selected reaction rate constants *k* provides information about favourable and unfavourable conditions in an autocatalytic system (see Figure 12).

The first four scenarios (Figure 12: Subsets A-D) show that when the stochastic process is very slow and the subsequent selective process is fast, there is an efficient amplification of an initially very small imbalance in the ratio of enantiomers. However, when the reaction

rates for the stochastic and selective processes converge, the resulting amplification and *ee* value converge to zero.

Here it is essential to note that the initial stochastic process is a bimolecular reaction of A and B, while the subsequent selective reaction is a trimolecular reaction in which the product molecules formed participate in the reaction as catalysts. As a result, the second process is less likely to occur, however, the product molecule acts as a catalyst, thus accelerating the reaction, and transferred to the molecular level, the probability of a successful reaction increases as the Gibbs activation energy $\Delta G^{\ddagger}$ is lowered. This is an important insight for experimental design and the proper selection of reactions, because an initially inefficient process that can trigger a selective and efficient process can lead to an amplification of the enantiomeric imbalance and thus to symmetry breaking.

Looking into the subset with the highest *ee* value of 53.3% *ee* after 10 s with predominantly (*R*)-enantiomer **(R)-C** reveals a total formation of 18202 (*R*)-enantiomers **(R)-C** and 5517 **(S)-C** (see Figure 13 D1; for detailed tables see Chapter 7.1 Appendix).
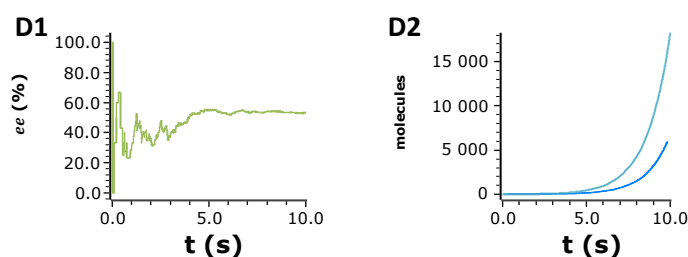
Figure 13: Enantiomeric excess and total number of molecules formed for Scenario A, reaction D: D1: *ee* versus reaction time; *ee* after 10 s: 53.5% *ee* with predominantly (*R*)-enantiomer; D2: number of molecules formed versus reaction time: major product (*R*)-enantiomer, light blue) and minor product ((*S*)-enantiomer, blue). Modified figure according to L. Huber and O. Trapp, Symmetry breaking by consecutive amplification: Efficient paths to homochirality. *Origins of Life and Evolution of Biospheres*, 2022, *52*(1-3), 75-91.[251] Copyright by Creative Commons Attribution 4.0 International License CC BY.

The initial stochastically induced formation of **(R)-C** occurs after 0.017 s with 100% *ee* for this single enantiomer molecule that was formed, and is already compensated after 0.019 s by the stochastic formation of **(S)-C**. After a total of 0.122 s another **(R)-C** enantiomer is formed, and rapid amplification can be observed after 0.212 s.

The first real amplification of the initial imbalance can be observed after 1s, leading to a rapid increase in the formation of **(R)-C** enantiomers. Since the total number of molecules formed is still relatively small within the first 4 s - after 2 s only 34 molecules of **(R)-C** and 16 **(S)-C** and after 5 s 446 **(R)-C** and 128 **(S)-C**) enantiomers are formed - any stochastic

formation of **(S)-C** enantiomers and their amplification causes major setbacks in terms of symmetry breaking.

This phenomenon of uneven gradual change in *ee* can also be observed for other scenarios, in particular for subgroups A and B of Scenario A and B, A-D of Scenario B and the entire Scenario C (see p. 46ff.). This becomes more robust as the number of molecules increases.

Another interesting result that can be observed, for example, in subsets E and P of scenario A is that an initial *ee* in favour of one of the enantiomers is lost and later reversed within the first 10 s of the simulated reaction. This shows that while an initial imbalance may form in a system, the important factor in the formation of the overall major product is the subsequent amplification of this initial imbalance and the timing of this amplification is therefore crucial.

Autocatalysis with heterochiral dimer formation

The second scenario (scenario B) comprises an autocatalytic reaction with heterochiral dimer formation. While scenarios B and C are comparable to the SOAI reaction, this scenario in particular is similar to scenario A, but with the addition of a subsequent equilibrium to form a heterochiral dimer. Since heterochiral dimers from an enantiomerically enriched mixture can have a positive effect on the ee of the main monomeric enantiomer, this phenomenon was investigated here. The dimer then efficiently removes the smaller enantiomer from the mixture of compounds formed and influences the *ee*.[145,252,253]

In scenario B, substrates **A** and **B** react in an initial stochastic reaction to either form the catalyst [**(R)-C**] or [**(S)-C**], which each subsequently catalyse the reaction to form more **(R)-C** or **(S)-C**, respectively (see Scheme 9). Subsequent heterochiral dimerization of the formed compounds was considered.
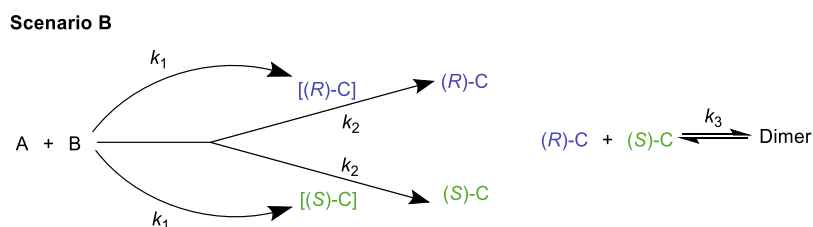
Scheme 9: Scenario B: autocatalytic reaction with heterochiral dimer formation. Modified scheme from reference: L. Huber and O. Trapp, Symmetry breaking by consecutive amplification: Efficient paths to homochirality. *Origins of Life and Evolution of Biospheres*, 2022, *52*(1-3), 75-91.[251] Copyright by Creative Commons Attribution 4.0 International License CC BY.

The ODEs used for the simulation are shown in the following equations 12-16:

$$\frac{d[A]}{dt} = -2k_1[A][B] - k_2[A][B][(R)\text{-C}] - k_2[A][B][(S)\text{-C}] \tag{12}$$

$$\frac{d[B]}{dt} = -2k_1[A][B] - k_2[A][B][(R)\text{-C}] - k_2[A][B][(S)\text{-C}] \tag{13}$$

$$\frac{d[(R)\text{-C}]}{dt} = k_1[A][B] + k_2[A][B][(R)\text{-C}] - k_3[(R)\text{-C}][(S)\text{-C}] \tag{14}$$

$$\frac{d[(S)\text{-C}]}{dt} = k_1[A][B] + k_2[A][B][(S)\text{-C}] - k_3[(R)\text{-C}][(S)\text{-C}] \tag{15}$$

$$\frac{d[\text{Dimer}]}{dt} = k_3[(R)\text{-C}][(S)\text{-C}] \tag{16}$$

The change in concentrations over time of the substrates depends on the initial second order stochastic reaction with reaction rate constant k_1 and the subsequent third order autocatalytic reactions for each enantiomer with k_2. The respective parts of the differential equations (12) and (13) have a negative sign, as the substrates **A** and **B** are used up in the reaction. The change in concentrations of product enantiomers **(R)-C** and **(S)-C** over time depends on the substrate concentrations for the initial second order stochastic reaction with reaction rate constant k_1 as well as on the substrate and the stereospecific product enantiomer concentrations for the subsequent third order autocatalytic reactions for each enantiomer with k_2. The change in concentrations of the dimer over time depends on both concentrations of the two product enantiomers and the reaction rate constant k_3.

In order to better compare the magnitude of the results with those of scenario A, the same reaction rates for the two consecutive reactions were chosen. The rate of formation of the heterochiral dimers to efficiently remove the racemate, was set at $k_3 = 1.00 \cdot 10^{-2}$.

The resulting concentration courses were evaluated and the *ee* values were plotted against the reaction time (see Figure 14). For the first four parameter sets (sets A-D), the step size looks different to sets E-P, as only a small number of total molecules were formed in these reactions. Therefore, the fluctuations in *ee* are also more pronounced. This phenomenon is already known from scenario A. In parameter sets I-L, significantly more molecules were formed in the first 10 s of the simulated reactions, but the *ee* values are significantly lower.
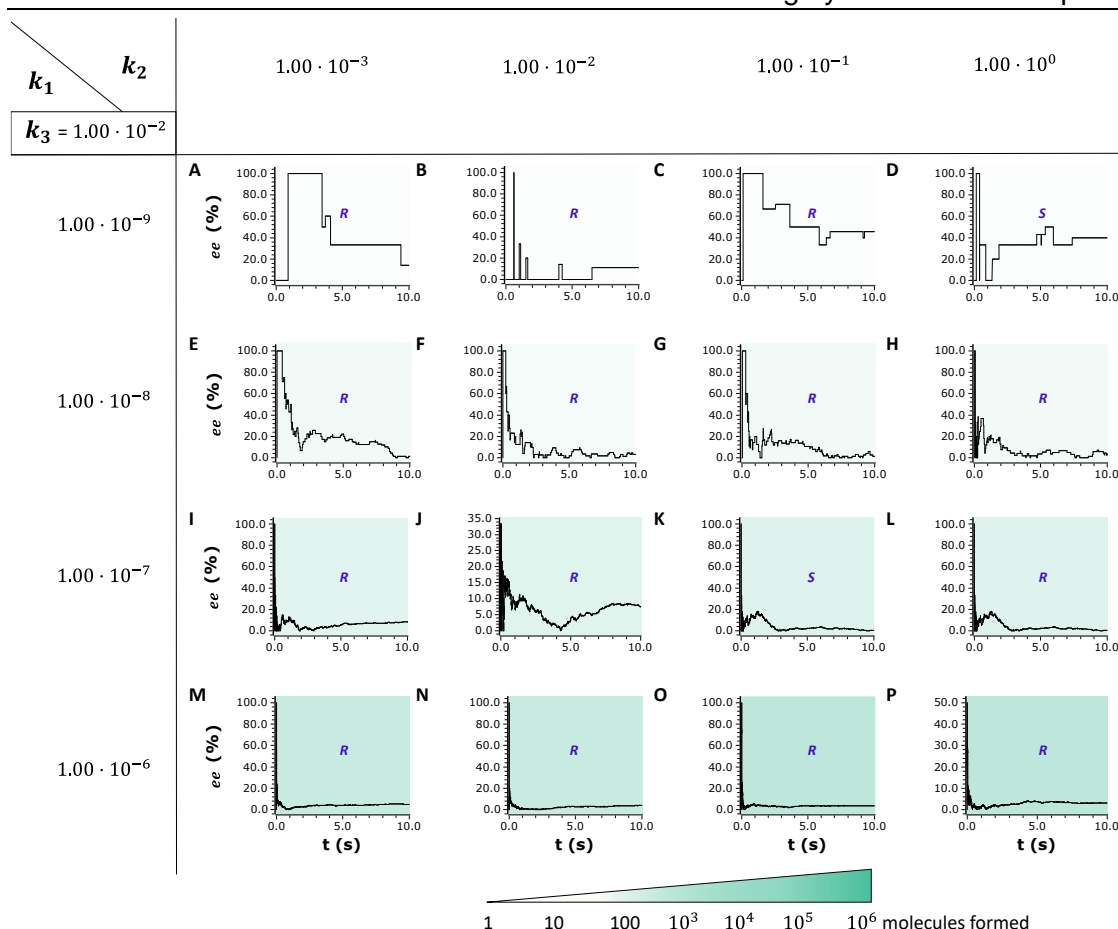
Figure 14: Scenario B: *ee* versus time courses for the simulations of scenario B with the *SMK.exe* tool. The respective stereo descriptor shows for each plot which stereoisomer was predominantly formed after 10 seconds. The following reaction rate constants k_x were permuted: k_1: $1.00 \cdot 10^{-9}$ (**A** − **D**), $1.00 \cdot 10^{-8}$ (**E** − **H**), $1.00 \cdot 10^{-7}$ (**I** − **L**), $1.00 \cdot 10^{-6}$ (**M** − **P**) , and k_2: $1.00 \cdot 10^{-3}$ (**A, E, I, M**), $1.00 \cdot 10^{-2}$ (**B, F, J, N**), $1.00 \cdot 10^{-1}$ (**C, G, K, O**), $1.00 \cdot 10^{0}$ (**D, H, L, P**) and k_3: $1.00 \cdot 10^{-2}$. Figure according to L. Huber and O. Trapp, Symmetry breaking by consecutive amplification: Efficient paths to homochirality. *Origins of Life and Evolution of Biospheres*, 2022, *52*(1-3), 75-91.[251] Copyright by Creative Commons Attribution 4.0 International License CC BY.

This scenario once again shows the strong dependence of the fluctuation of *ee* on the number of enantiomers formed. In this autocatalytic system, the dimerisation of (*R*)-**C** and (*S*)-**C** to the heterochiral dimer can be regarded as a corrective mechanism in which the minor enantiomer is removed from the reaction mixture and, ideally, the major enantiomer is relatively enriched compared to the minor enantiomer. This mechanism also leads to a considerable decrease in catalytic activity, which slows down autocatalytic amplification.

Autocatalysis with hemiacetal formation

The third reaction scenario (scenario C, see Scheme 10) involves substrates **A** and **B** reacting to form the enantiomers **(R)-C** or **(S)-C**, with the same probability, which is determined by the reaction rate constant k_1. **(R)-C** or **(S)-C** then react with substrate **A** giving the catalyst **(R)-D$_{cat}$** or **(S)-D$_{cat}$**, subsequently catalysing the formation of more **(R)-C** or **(S)-C** respectively.

A prominent example of such a scenario is the formation of hemiacetal from the product alcohol and the aldehyde to form the accelerating ligand for the zinc reagent in the S$_{OAI}$ reaction.
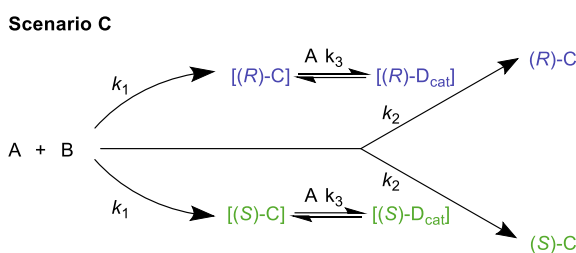
Scheme 10: Scenario C: Reaction scheme for hemiacetal model in the S$_{OAI}$ reaction. **A** and **B** react to from the either **(R)-C** or **(S)-C**. They subsequently react with **A** to form the catalyst **(R)-D$_{cat}$** or **(S)-D$_{cat}$**, respectively, catalysing the conversion of **A** and **B** to **(R)-C** or **(S)-C** and controlling the selectivity. **(R)-D$_{cat}$** catalyses only the formation of the product **(R)-C** and **(S)-D$_{cat}$** the formation of **(S)-C**. Modified scheme from reference: L. Huber and O. Trapp, Symmetry breaking by consecutive amplification: Efficient paths to homochirality. *Origins of Life and Evolution of Biospheres*, 2022, *52*(1-3), 75-91.[251] Copyright by Creative Commons Attribution 4.0 International License CC BY.

The ODEs used for the simulation are shown in the following equations 17-22:

$$\frac{d[A]}{dt} = -2k_1[A][B] - k_2[A][B][(R)\text{-}D_{cat}] - k_2[A][B][(S)\text{-}D_{cat}] -$$
$$k_3[A][(R)\text{-}C] + k_{-3}[(R)\text{-}D_{cat}] - k_3[A][(S)\text{-}C] + k_{-3}[(S)\text{-}D_{cat}] \tag{17}$$

$$\frac{d[B]}{dt} = -2k_1[A][B] - k_2[A][B][(R)\text{-}D] - k_2[A][B][(S)\text{-}D] \tag{18}$$

$$\frac{d[(R)\text{-}C]}{dt} = k_1[A][B] + k_2[A][B][(R)\text{-}D_{cat}] - k_3[A][(R)\text{-}C] + k_{-3}[(R)\text{-}D_{cat}] \tag{19}$$

$$\frac{d[(S)\text{-}C]}{dt} = k_1[A][B] + k_2[A][B][(S)\text{-}D_{cat}] - k_3[A][(S)\text{-}C] + k_{-3}[(S)\text{-}D_{cat}] \tag{20}$$

$$\frac{d[(R)\text{-}D_{cat}]}{dt} = k_3[A][(R)\text{-}C] - k_{-3}[(R)\text{-}D_{cat}] \tag{21}$$

$$\frac{d[(S)\text{-}D_{cat}]}{dt} = k_3[A][(S)\text{-}C] - k_{-3}[(S)\text{-}D_{cat}] \tag{22}$$

The change in concentrations over time of the substrate **A** depends on the initial second order stochastic reaction with reaction rate constant k_1, the subsequent third order autocatalytic reactions for each enantiomer with k_2 as well as the third order autocatalytic reactions for each enantiomer with k_3. The change in concentrations over time of the substrate **B** depends on the initial second order stochastic reaction with reaction rate constant k_1 and the subsequent third order autocatalytic reactions for each enantiomer with k_2. The respective parts of the differential equations (17) and (18) exhibit a negative sign, as the substrates **A** and **B** are used up in the reaction, as do parts of the differential equations where either the two enantiomers **(R)-C** and **(S)-C** are consumed in the conversion to the catalyst, and the catalysts themselves when catalysing the product enantiomer formation. The change in concentrations of product enantiomers **(R)-C** or **(S)-C** over time each depend on the substrate concentrations for the initial second order stochastic reaction with reaction rate constant k_1, the substrate and the stereospecific product enantiomer concentrations for the subsequent third order autocatalytic reactions with k_2, the second order consumption reaction with concentration of substrate **A** and stereospecific enantiomer concentration, either **(R)-C** or **(S)-C,** with k_3 as well as the first order back-reaction with stereospecific catalyst concentration and k_{-3}. The change in concentrations of the respective catalysts over time depend on the concentrations of the substrate **A** and stereospecific intermediate, either **(R)-C** or **(S)-C**, as well as the consumption of the respective catalyst concentration with k_{-3}.

These simulations exhibit parameter sets with remarkably high *ee* values (see Figure 15, e.g., reaction D: 61.1% *ee*) and, at the same time, yield a large number of molecules. For example, for subset D 8881 **(R)-C** and 2146 **(S)-C** enantiomers are formed (see Chapter 7.1.3 Appendix, Table 40). In contrast, the first two parameter sets (A, B) show large stepwise fluctuations of the *ee* values, which again is due to the fact that overall, only very few molecules are formed. In the case of the simulated reactions J-L and N-P, an excessively fast stochastic seeding process takes place and no significant *ee* value occurs.
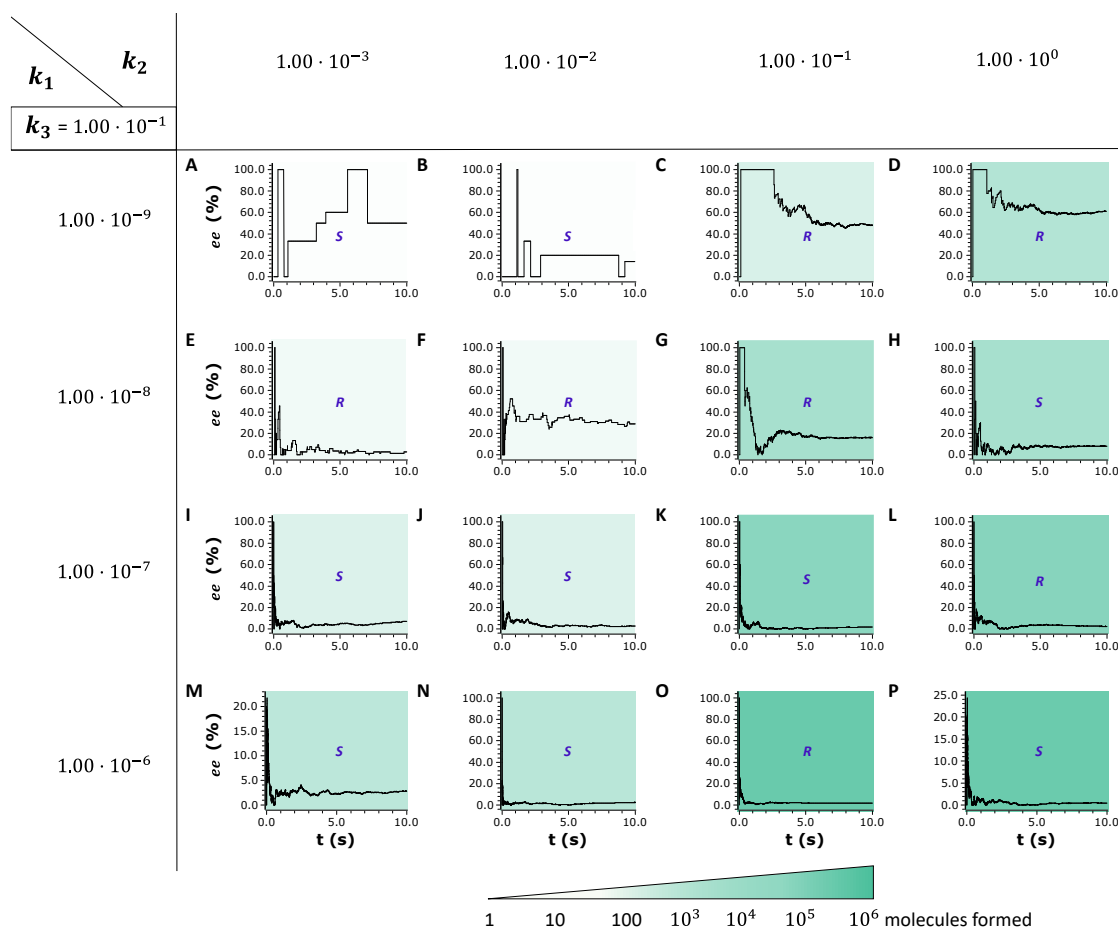
Figure 15: Scenario C: *ee* versus time courses for the simulations of scenario C with the *SMK.exe* tool. The respective stereo descriptor shows for each plot which stereoisomer was predominantly formed after 10 s. The following reaction rate constants k_x were permuted: k_1: $1.00 \cdot 10^{-9}$ (**A** − **D**), $1.00 \cdot 10^{-8}$ (**E** − **H**), $1.00 \cdot 10^{-7}$ (**I** − **L**), $1.00 \cdot 10^{-6}$ (**M** − **P**) , and k_2: $1.00 \cdot 10^{-3}$ (**A, E, I, M**), $1.00 \cdot 10^{-2}$ (**B, F, J, N**), $1.00 \cdot 10^{-1}$ (**C, G, K, O**), $1.00 \cdot 10^0$ (**D, H, L, P**) and k_3: $1.00 \cdot 10^{-1}$. Figure according to L. Huber and O. Trapp, Symmetry breaking by consecutive amplification: Efficient paths to homochirality. *Origins of Life and Evolution of Biospheres*, 2022, *52*(1-3), 75-91.[251] Copyright by Creative Commons Attribution 4.0 International License CC BY.

The selectivity in scenario C seems to be improved by the additional step of forming a transient catalyst, as the probability for the initial stochastic process is reduced when the reactant A is initially consumed to form the catalyst but is later released again to participate in the reaction. In addition, high concentration of substrate A at the beginning of the reaction ensures the breakthrough of one of the pre-catalysts, while this process slowly recedes into the background as the reaction proceeds. In particular, data set D (see Figure 15) shows a remarkable *ee* of 61.1% *ee*, which represents an excellent selectivity of this reaction cascade. In this context, it is interesting to highlight the connection with the case where inhibition of the homochiral products is observed. These effects can be reversed if the active catalyst is a more complex entity, such as an oligomer, or can even act as an allosteric modulator corresponding to the substrate-product adduct.[254,255]

Overall, scenario C represents an efficient system in which although the initial stochastic seeding reaction is slow, the subsequent amplification is fast. The efficiency in symmetry breaking might occur precisely because and not in spite of this discrepancy.

3.2.2.2 Cascade Reactions

The last reaction scenario investigated (scenario D, see Scheme 11) comprised a reaction cascade as broadly occurring in nature. First, reactants **A** and **B** react in a preceding reaction to form the respective catalyst **(R)-C_cat** and **(S)-C_cat** with the same probability determined by the reaction rate constant k_1. These catalysts subsequently each catalyse the conversion of the substrate molecules **D** and **E** to give either the product enantiomer **(R)-F** or **(S)-F**, respectively, and control the selectivity.
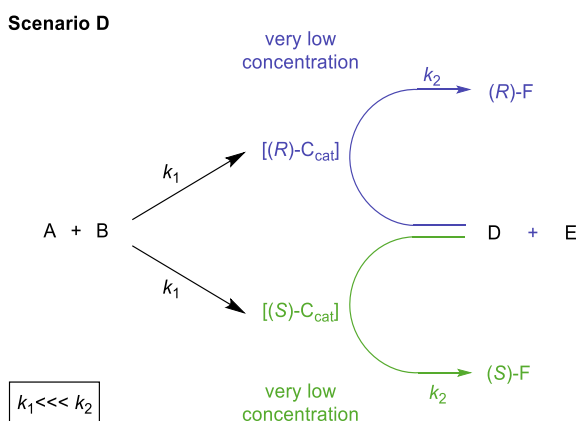
Scheme 11: Scenario D: Reaction scheme for a cascade reaction where **A** and **B** react to the enantiomers **(R)-C_cat** or **(S)-C_cat**. The reaction of D and E to give **(R)-F** and **(S)-F** is selectively catalysed by **(R)-C_cat** or **(S)-C_cat**, respectively. Modified scheme from reference: L. Huber and O. Trapp, Symmetry breaking by consecutive amplification: Efficient paths to homochirality. *Origins of Life and Evolution of Biospheres*, 2022, *52*(1-3), 75-91.[251] Copyright by Creative Commons Attribution 4.0 International License CC BY.

The ODEs used for the simulation are shown in the following equations 23-30:

$$\frac{d[A]}{dt} = -2k_1[A][B] \tag{23}$$

$$\frac{d[B]}{dt} = -2k_1[A][B] \tag{24}$$

$$\frac{d[(R)\text{-}C_{Cat}]}{dt} = k_1[A][B] \tag{25}$$

$$\frac{d[(S)\text{-}C_{Cat}]}{dt} = k_1[A][B] \tag{26}$$

$$\frac{d[D]}{dt} = -k_2[D][E][(R)\text{-}C_{Cat}] - k_2[D][E][(S)\text{-}C_{Cat}] \tag{27}$$

$$\frac{d[E]}{dt} = -k_2[D][E][(R)\text{-}C_{Cat}] - k_2[D][E][(S)\text{-}C_{Cat}] \tag{28}$$

$$\frac{d[(R)\text{-}F]}{dt} = k_2[D][E][(R)\text{-}C_{Cat}] \tag{29}$$

$$\frac{d[(S)\text{-}F]}{dt} = k_2[D][E][(S)\text{-}C_{Cat}] \tag{30}$$

The change in concentrations over time of the substrates **A** and **B** depend in each case on the initial second order stochastic reaction with reaction rate constant k_1. The respective parts of the differential equations (23) and (25) have a negative sign, as the substrates are used up in the reaction. The change in concentrations over time of the transient catalysts **(R)-C$_{cat}$** and **(S)-C$_{cat}$** depend in each case on the initial second order stochastic reaction with reaction rate constant k_1. The change in concentrations over time of the substrates **D** and **E** depend in each case on both third order reactions of substrates **D** and **E** with respective catalyst **(R)-C$_{cat}$** or **(S)-C$_{cat}$** for both catalysts with k_2. The respective parts of the differential equations (27) and (28) have a negative sign, as the substrates are used up in the reaction. The change in concentrations over time of product enantiomers **(R)-F** and **(S)-F** depend on the substrate concentrations **D** and **E**, the concentration of the stereospecific catalyst **(R)-C$_{cat}$** or **(S)-C$_{cat}$** and k_2.

For this scenario, only a low concentration in **A** and **B** (1 *mM*) was used as starting conditions to simulate a process that is triggered by only a few molecules and then enables another process by the product molecules acting as a catalyst. This leads, as discussed earlier, to a total of only a few molecules being formed within the simulated reaction time (10 s), which explains the wide step size of the *ee* versus time plots. The results of the simulations (see Figure 16) are thus drastically different from those of the autocatalytic reactions in scenarios A-C (see Schemes 1-3; Figure 12, Figure 14, Figure 15). No symmetry breaking occurred in parameter sets A, B, E, F, H-J, M and N. In parameter set P (see Figure 16), the overtaking non-selective background reaction results in an already built-up *ee* with a predominantly formed (*R*)-enantiomer to decrease again to 0.
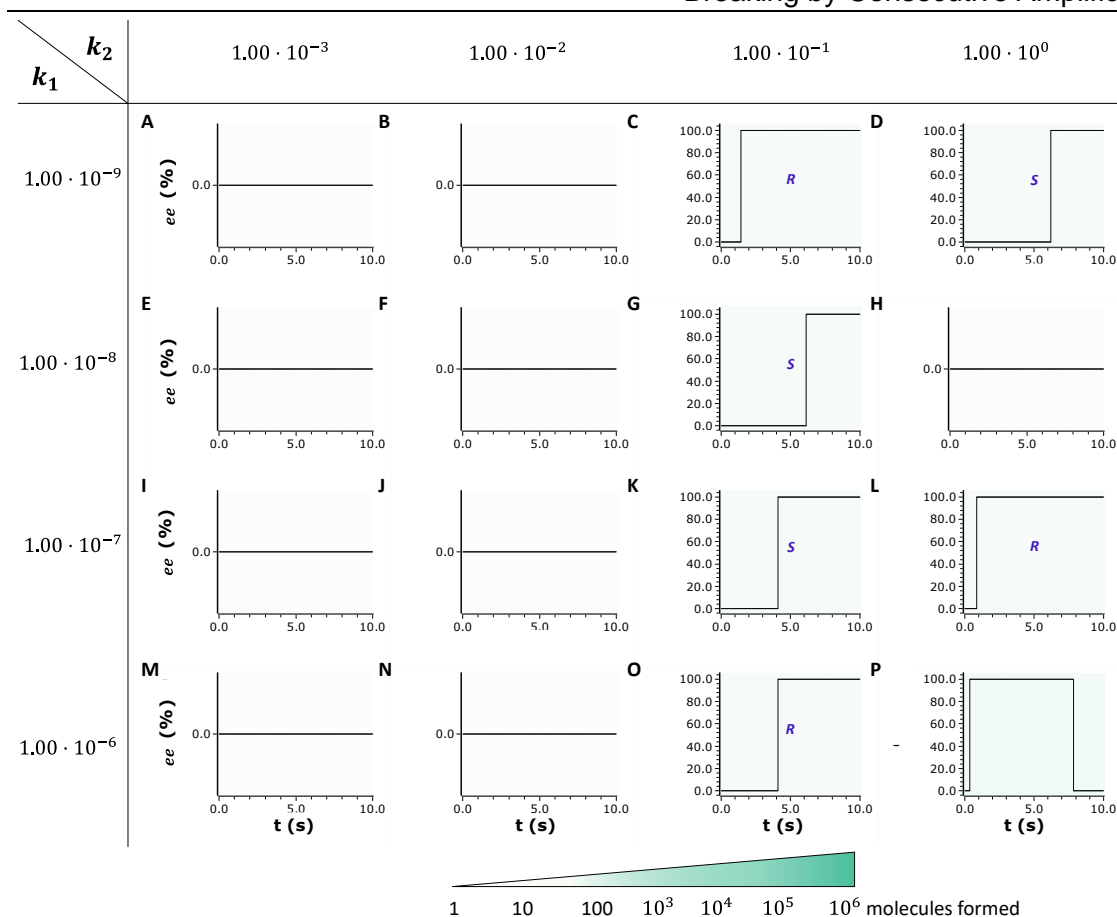
Figure 16: Scenario D: *ee* versus time courses for the simulations of scenario D with the *SMK.exe* tool. The respective stereo descriptor shows for each plot which stereoisomer was predominantly formed after 10 seconds, where applicable. The following reaction rate constants k_x were permuted: k_1: $1.00 \cdot 10^{-9}$ (**A** − **D**), $1.00 \cdot 10^{-8}$ (**E** − **H**), $1.00 \cdot 10^{-7}$ (**I** − **L**), $1.00 \cdot 10^{-6}$ (**M** − **P**), and k_2: $1.00 \cdot 10^{-3}$ (**A, E, I, M**), $1.00 \cdot 10^{-2}$ (**B, F, J, N**), $1.00 \cdot 10^{-1}$ (**C, G, K, O**), $1.00 \cdot 10^{0}$ (**D, H, L, P**)]. Figure according to L. Huber and O. Trapp, Symmetry breaking by consecutive amplification: Efficient paths to homochirality. *Origins of Life and Evolution of Biospheres*, 2022, *52*(1-3), 75-91.[251] Copyright by Creative Commons Attribution 4.0 International License CC BY.

Parameter set D in scenario D, which can be described as the "most inefficient" process with very few product molecules formed, however, exhibits a remarkably high *ee* value. In view of the results of scenarios A, B and C, this is a highly interesting result, because it could be a starting point for achieving very high enantioselectivities in a cascade of successive reactions. It is possible to imagine that such a process with building enantioselectivities would be very robust.

Now, the question arises why a very inefficient process leads to very high enantioselectivities and finally to a largely homochiral system?

This phenomenon could be explained by the fact that such a process is able to thin out the initially random formation of product enantiomers. While this process continues to proceed in the background, it leads in a long-term with a high probability to the formation of a racemic

seed. The production of molecules with the same sense of chirality is guaranteed by the initiation of amplification with a single molecule seed due to the decreasing probability of a random process. A similar, very well-known and in nature well proven reaction on the single molecule level should be mentioned in this context, namely the fertilisation of an egg cell and the subsequent cell division.

3.2.2.3 Statistical Analysis

In order to obtain statistical data for a given set of parameters, the simulations were repeated several times to investigate the effects of randomness on symmetry breaking. For the initial symmetry-breaking processes, this is important, molecules with (*R*)- or (*S*)-configuration are randomly generated as a seed for the subsequent reactions.

A set of a particular scenario, here the parameter set D of scenario A (Scheme 8), was selected exemplarily, repeated and a statistical analysis was carried out to examine the randomness of the seeding process and the variation from set to set. The set consisting of 50 repetitions with the reaction rate constants $k_1 = 1.00 \cdot 10^{-9}$, $k_2 = 1.00 \cdot 10^0$ was calculated and analysed.
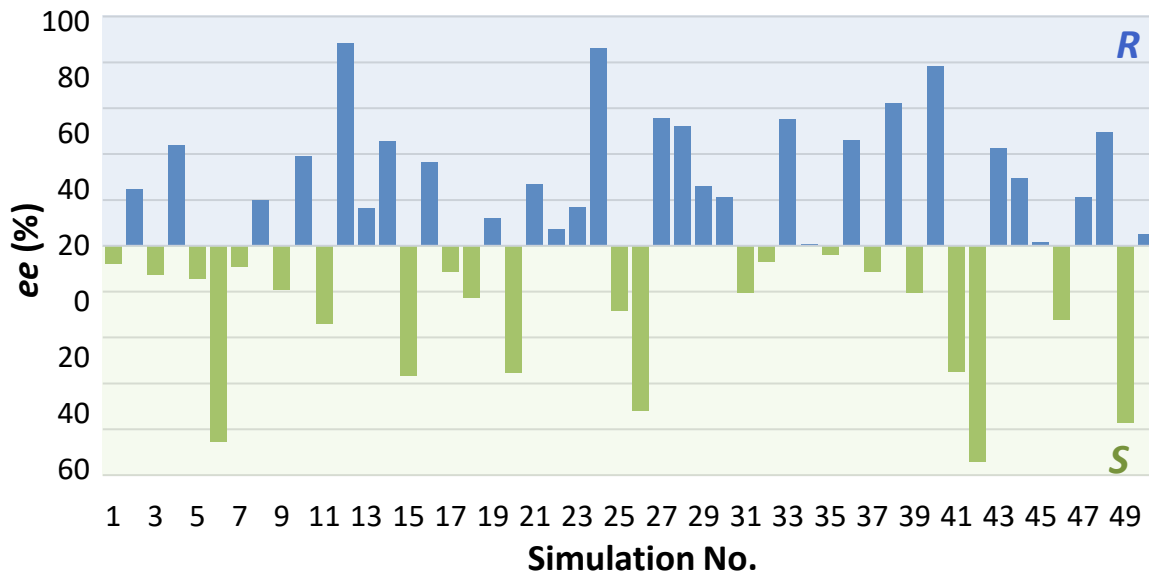
Figure 17: Statistical analysis for scenario A: 50 repetitions of the simulation with the parameter set D, $k_1 = 1.00 \cdot 10^{-9}$, $k_2 = 1.00 \cdot 10^0$. Figure according to L. Huber and O. Trapp, Symmetry breaking by consecutive amplification: Efficient paths to homochirality. *Origins of Life and Evolution of Biospheres*, 2022, *52*(1-3), 75-91.[251] Copyright by Creative Commons Attribution 4.0 International License CC BY.

In the group of repeated simulations, the average *ee* for 50 replicates was 35% *ee* with a standard deviation σ of 26% *ee*. Simulation no. 42 shows an *ee* of 94.1% *ee* for the (*S*)-enantiomer, which shows that even very high *ee* values also can occur. It is remarkable

that such high *ee* values occur randomly under these conditions, despite the deviations and considerable scatter.

A long simulation run of 500 s was performed to investigate the ratio of the total number of (R)- and (S)-enantiomers. The result of (R)-enantiomers (243919) to (S)-enantiomers (230542) indicates that the total ratio of (R)- to (S)-enantiomers is approximately 1:1. The statistical analysis of the obtained *ee* values for scenario A (see Figure 17) confirms that the formation of a preferred enantiomer is random. We can thus conclude that there is no bias in the simulation process.

Given that especially in the simulations of the latter scenarios (scenarios C and D) only a few molecules are formed, we extended the simulation times to 80 s for each of the examples presented here (see Figure 18).
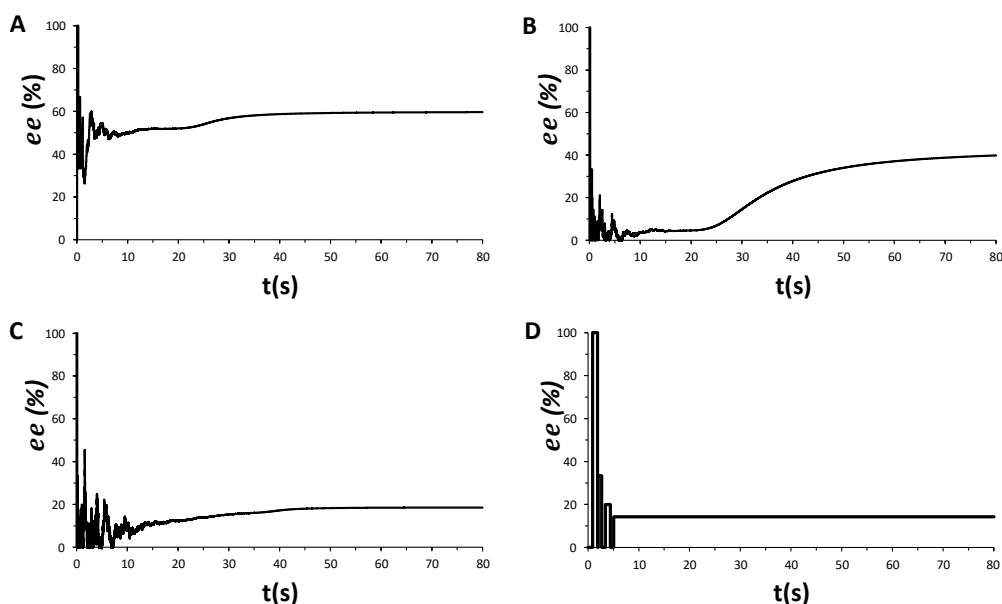
Figure 18: Extended simulated reaction profiles of 80 s for **A** scenario A with reaction rate constants k_1: $1.00 \cdot 10^{-9}$, and k_2: 1.00, and starting concentrations of $1000\ mM$ **A**, $1000\ mM$ **B. B**: scenario B with reaction rate constants k_1: $1.00 \cdot 10^{-9}$, k_2: 1.00, and k_3: 0.1 and starting concentrations of $1000\ mM$ **A**, $1000\ mM$ **B. C**: scenario C with reaction rate constants k_1: $1.00 \cdot 10^{-8}$, k_2: 1.00, and k_3: 0.1, and starting concentrations of $1000\ mM$ **A**, $1000\ mM$ **B. D**: scenario D reaction rate constants k_1: $1.00 \cdot 10^{-7}$, k_2: 1.00, and starting concentrations of $1\ mM$ **A**, $1\ mM$ **B**, $1000\ mM$ **D**, $1000\ mM$ **E**. Figure according to L. Huber and O. Trapp, Symmetry breaking by consecutive amplification: Efficient paths to homochirality. *Origins of Life and Evolution of Biospheres*, 2022, *52*(1-3), 75-91.[251] Copyright by Creative Commons Attribution 4.0 International License CC BY.

The trend already observed in the first 10 s could be confirmed by the reaction profiles thus obtained and it can be shown that a bias of the enantiomeric ratio manifests itself over a longer period of time. Another remarkable feature is that the scenarios presented here lead to a symmetry break after only a few seconds, which in some cases leads to amplification and in other cases to convergence.

3.3 Summary and Conclusion

In view of the emergence of homochirality and prebiotic complexity, this part of the thesis investigated a possibility to observe symmetry breaking on a molecular level. Therefore, an efficient simulation tool to predict reactions occurring on a molecular level based on a stochastic algorithm was developed. The focus of the tool was to enable efficient simulations on a workstation computer within a reasonable timeframe, while being able to apply the tool to a desired response scenario.
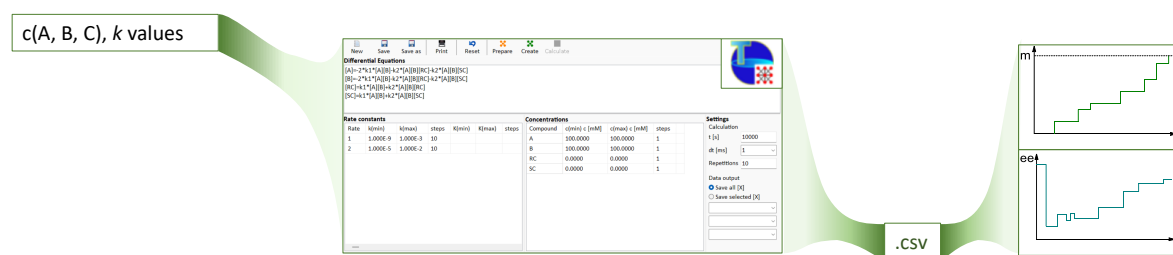
Figure 19: Schematic overview of the workflow of the versatile *SMK.exe* tool.

Four different reaction scenarios were investigated with this tool, comprising three autocatalytic reactions and one reaction cascade. The common denominator of these scenarios was the initiation by a stochastically occurring reaction, yielding product enantiomers. In the first scenario investigated, these enantiomers serve as catalyst in an autocatalytic process. In the second case, a dimerization of the enantiomers to a homochiral dimer is implemented while the third scenario considers the formation of a transient catalyst. This simulates a reaction cascade that is broadly occurring in nature.

The simulated reactions start with a substrate pool and only a single catalyst molecule. The results of the simulations demonstrated that interlocking processes, e.g., forming catalysts, transient catalysts, autocatalytic systems, or reaction cascades, which consecutively built on one another and lead to a kinetic acceleration, can amplify a statistically occurring symmetry breaking very well.

In general, a process where the downstream reactions are faster was observed to achieve and enhance symmetry breaking more efficiently. Interestingly, the actually "most inefficient" initial processes lead to high *ee* values and represent the most efficient scenarios with regard to achieving symmetry breaking. This is the case when single enantiomers are formed slowly, and the subsequent amplification process is fast and selective. Therefore, it is conceivable that a process that already forces an imbalance in favour of one of the enantiomers in the first step, e.g., by polarised light or enantiotopic faces of a crystal, can be efficiently amplified through a fast subsequent reaction or reaction cascade.

However, when the rates of the competing processes converge, a racemic mixture of products is obtained and no symmetry breaking occurs.

For the scenarios in which a transient catalyst and the reaction cascade of coupled processes are formed, the highest *ee* values and the most efficient symmetry breaking processes were found.

In addition, the occurrence of symmetry breaking was investigated for its degree of dependence on randomness. The results of the statistical analysis and a simulation carried out over a long period of time confirm that there is no bias within the system and that the formation of a preferred enantiomer is random.

These results point in a promising direction and thus provide an important contribution for the experimental implementation and identification of symmetry-breaking processes that may have led to a shift out of thermodynamic equilibrium during the Origin of Life and were thus essential for the Origin of Life.

Chapter 4

The Tipping Point

in the Atmosphere of a Planet

4.1 Fundamentals and Previous Research

Modelling planetary atmospheres can be a protracted task. To develop an appropriate model for atmospheric simulations, atmospheric processes - chemical and physical - must be considered. These may include i.a., temperature gradients, radiation flux, scattering, emission, winds, precipitation, absorption, elementary reactions (reactions in homogeneous and heterogeneous phases), diffusion, convection, intrinsic luminosity and the outgassing of the chosen planet. Since this multitude of factors can hardly be represented by a single experiment, interesting sub-areas are often investigated separately. However, as already mentioned, a model therefore only offers the possibility of exploring one aspect of a complex and multivariate system in nature. In the case of the atmosphere of the early Earth, this is complicated by the fact that there are no original samples with which to compare these models.

This part of the thesis therefore focuses on parameters for an atmospheric model of an arbitrary planet, using principles accepted in the literature and an experimental data set.

The composition of the early Earth's atmosphere is a heavily discussed topic in the OoL community (see Chapter 2.1.3).[50] The atmospheric composition of the early Earth is commonly considered to consist predominantly of molecular carbon dioxide CO_2, from outgassing volcanoes, N_2, and H_2O.[17] With the high abundance of CO_2 on the early Earth, mechanisms of CO_2 activation and fixation are to be considered. Remarkable results were found i.a., by MORAN et al. (see Scheme 12) supporting the metabolism first theory (see Chapter 2).[256,257]
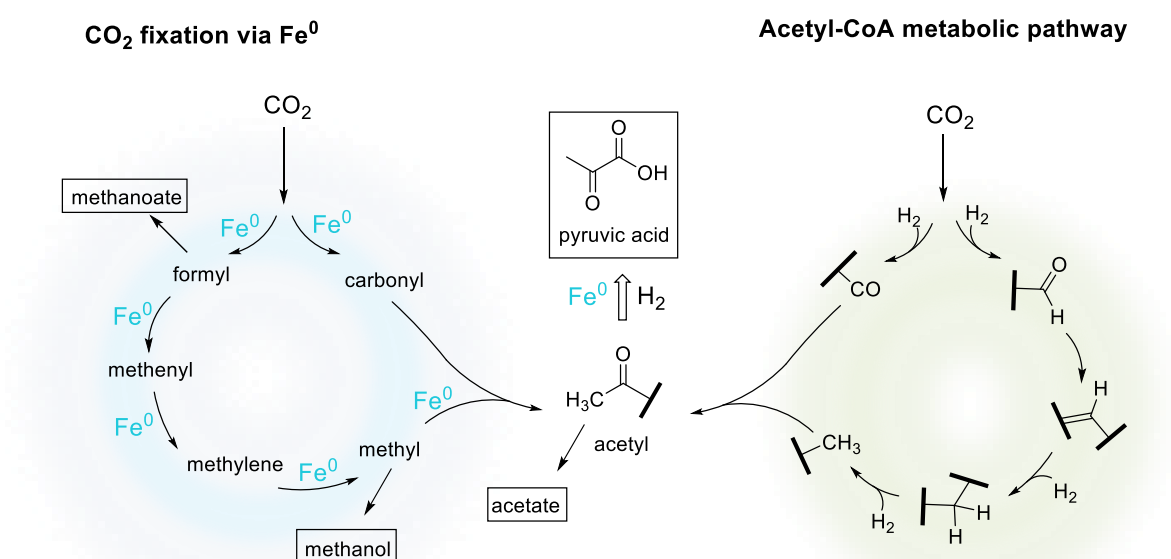
Scheme 12: Different types of CO_2 fixation: MORAN's synthetic pathway via elemental iron on the left and canonical enzyme-mediated (not explicitly shown) acetyl-CoA metabolic pathway using H_2 on the right. Molecules in boxes are identified products. Pyruvate is the common C-C bond linkage product of both pathways. Illustration based on literature reference [256].

The influx of meteorites can also be regarded as an undisputed and, thanks to some existing samples, also analytically proven source of material. Meteorites consist of 93-95% iron, 2% nickel, 2% cobalt and traces of iridium and are suitable as metal catalysts, e.g., for FISCHER-TROPSCH-type reactions.[266] When entering the denser atmosphere, these meteorites partially evaporate and form highly reactive iron and metal nanoparticles (see Figure 23).

The modelling of complex processes is a valuable method to gain additional insights that would otherwise be difficult to access experimentally. The terrestrial atmosphere is a suitable candidate that has been explored theoretically investigating comprising i.a., thermodynamic and kinetic models. Unlike exoplanetary systems, atmospheric conditions on the early Earth cannot be studied spectroscopically and must therefore be simulated *in silico* or in the laboratory.

HASHIMOTO et al. examined the composition of a mixed atmosphere of the early Earth towards the end of the accretion of planetesimals and calculated the thermodynamic equilibrium of a six-element system.[65] Atmospheric calculations based on a physical and nonequilibrium chemical model of atmosphere of the early Earth was considered by PEARCE et al.[258] KURAMOTO et al.[259] have performed numerical simulations of the hydrodynamic escape of hydrogen by solving the one-dimensional reaction equation. Their results in their model indicate a homopause mixing ratio of H_2 of below 1%. A different approach was followed by KULIKOV et al., using a diffusive-gravitational equilibrium and heat balance model, considering the influence of the changing active young sun.[260] A kinetics code for modelling exoplanetary atmospheres that focused on hot gas giants was developed by HOBBS et al.[261]

The variety of methods and models employed and tested shows how many different approaches are possible in order to elucidate this unsolved research conundrum.

The basic assumption in this work is that the early Earth's atmosphere consisted mainly of nitrogen and carbon dioxide, with local presence of water vapour, which later led to the formation of hydrogen when water reacted with iron. This is supported by the fact that the compositions of the oldest sedimentary rocks indicate high amounts of CO_2 and N_2.[262] The CO_2 considered in our model is the exclusive carbon bearing starting material, which is not uncommon in literature.[263]

4.2 Objective

Researchers in various areas of science are investigating in depth the elementary question of how life came into being, both in the laboratory and through simulations. The formulation of hypotheses and the planning of model systems is an essential step in this process. However, since this endeavour must be able to cover an enormously large and diverse chemical space, all these models so far are just that: models. An approach to being able to cover a partial problem in the large OoL area.

The aim of this project was to contribute to this area by using computer simulations to enable a system that cannot be observed in the laboratory over the desired time span and due to of analytical complexity.

The specific question to be studied in this part of the thesis was the change in the composition of the prebiotic Earth. Catalytic processes, CO_2 fixation and the build-up of small organic molecules, which are essential for the formation of the building blocks of life, were considered.

For this purpose, a suitable chemical model had to be created that includes kinetic framework conditions obtained from experimental data by the TRAPP group.

To be able to carry out the given framework conditions of a simulation in this volume and time scale, a version of the existing *RNA.exe* program had to be extended accordingly. The simulation results obtained were then to be evaluated and their significance discussed in the OoL context. One of the essential questions when examining the simulated reaction profiles was: If carbon dioxide is present in the atmosphere, how quickly is it consumed, and what is the significance of this for today's search for life on another planet?

4.3 Results and Discussion

A large chemical model, based on what we know of the early Earth, is required to perform a long-term simulation of the atmosphere of a chosen planet. The tool to calculate the concentrations of building blocks known to be critical to the Origin of Life, such as alcohols, alkanes and aldehydes, will be introduced. The examination of a prebiotically relevant chemical network to understand linkages is presented. In addition, an example calculation of whether a process progresses productively or breaks down and observation of how fast this happens is discussed.

4.3.1 The *RNA.exe* program

The existing reaction network analysis tool *RNA.exe* based on an adaptive fourth order Runge–Kutta algorithm, programmed in Pascal (Embarcadero Delphi XE 7), to tackle sets of differential equations for large-scale chemical reaction networks, was further refined and developed within the scope of this work.[220,251,264] The program can be used on a regular desktop computer without impairment of simultaneously operating programs.

A flowchart for how the *RNA.exe* program can be used is shown in Figure 20. The influences of the experimental results are shown by light blue arrows and lead to the selection of the input parameters. The input data is processed and .csv files of the created set are saved for comprehensibility and reproducibility. The tool solves the ODEs, that are presented as input in the interface, and allows for multiparameter variation. The user interface of the *RNA.exe* program is shown in Figure 21. Input fields for ODEs, settings, and parameter inputs, i.e., rate constants k and concentrations, as well as an interface area that simplifies file management and access to previous projects were implemented.
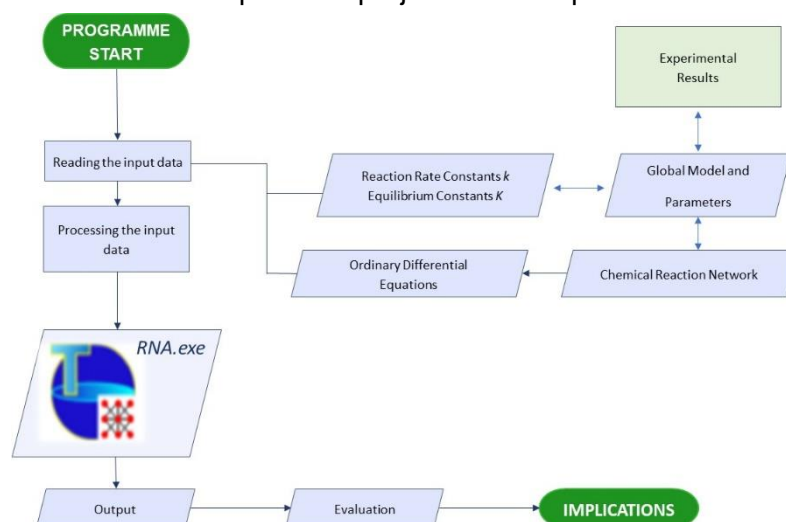
Figure 20: Schematic flowchart for the application of the *RNA.exe* program. The influence of the information obtained from experimental data is shown as a double arrow.
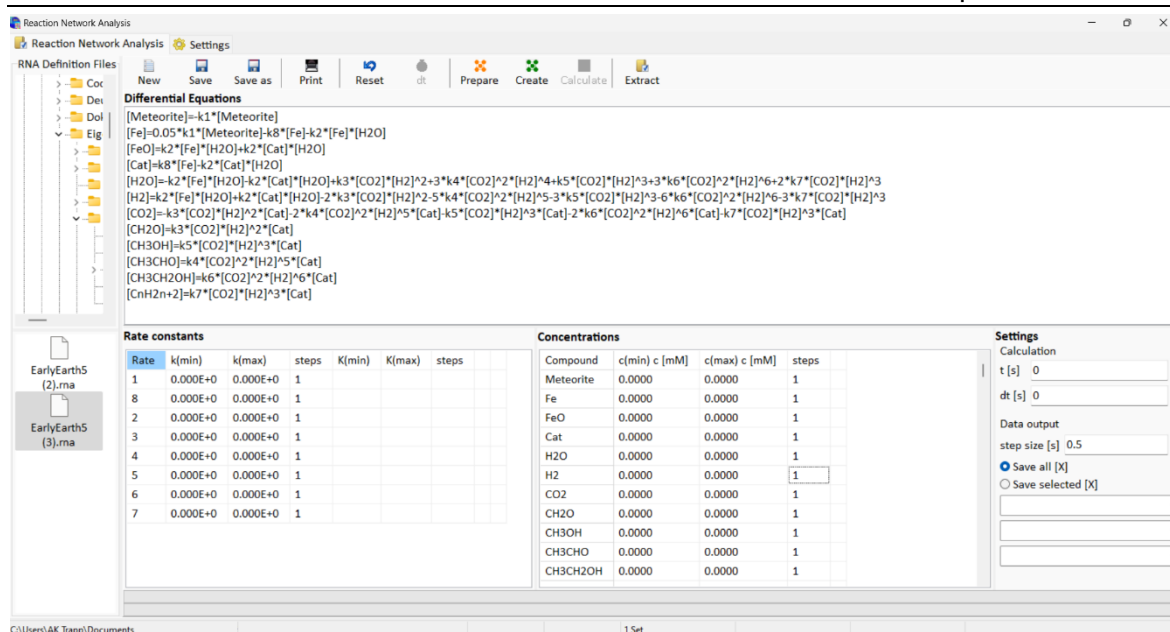
Figure 21: *RNA.exe* user interface with input fields for differential equations, settings, and parameter inputs such as rate constants *k* and concentrations as well as an interface area that simplifies file management and access to previous projects (upper and lower left). Only part of input fields for concentrations are shown.

The total of kinetic profiles that were calculated with *RNA.exe* ranged from 9000 to 360000 with computational speeds per profile ranging from $0.9 - 14.3 \frac{s}{profile}$.

The reaction volume model for the atmosphere of the given planet was obtained from the layer-by-layer calculation of the pressure and temperature dependence using the temperature-corrected barometric equation. This resulted in the reaction volume model with an atmosphere up to 60 km. The global traces of the cubic and thus standardized micro reactors within the simulated atmosphere (see Figure 22) resulted in integral sums of the substances formed and are saved in output .csv files.
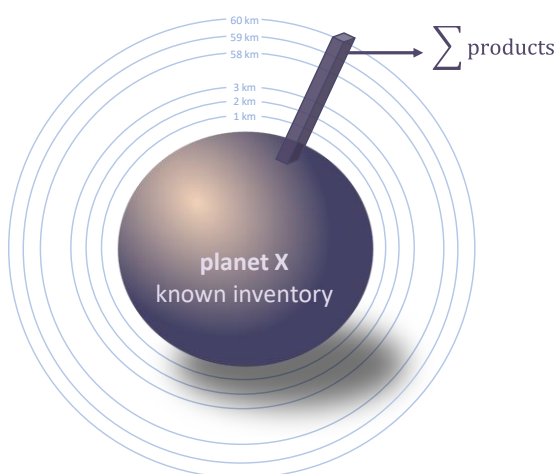
Figure 22: Schematic representation of an arbitrarily enlarged microreactor within the first 60 km of the atmosphere of a planet to simulate integral sums of products within the standardized volume**.**

4.3.2 The Model Structure

The global model of the planet's atmosphere is schematically shown in Figure 23. For this particular simulation, the initial conditions were chosen as an example based on the early Earth. Any other exoplanet atmosphere about which compositional information is available can be simulated accordingly.
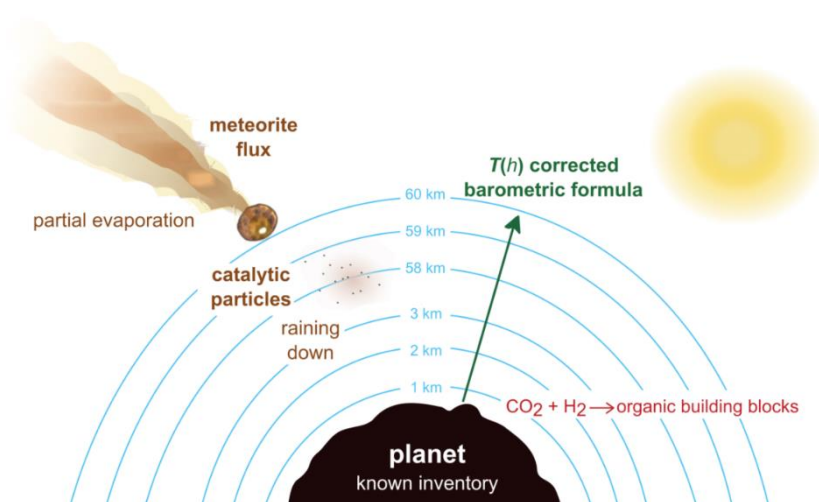
Figure 23: Setting for the global model of the planetary example used in the model. Meteorite flux with subsequent partial evaporation, the atmosphere up to 60 km and the schematic formation of building blocks are depicted.

The starting amount of CO_2 was set to at $1.7 \cdot 10^{14}$ Gt, assuming that all available carbon must have been present exclusively as CO_2. The total amount of the two other major components were set at $5.8 \cdot 10^{13}$ Gt N_2 whose total amount has not changed since the formation of the Earth, and $1.39 \cdot 10^9$ Gt H_2O.

As shown in Figure 23 and previously discussed (see Chapter 2.1), the particles formed during the bombardment of meteorites and their partial vaporisation leads to the formation of highly reactive metal, especially iron, nanoparticles, that can then act as catalysts.[265] The assumption is made here that only 5% are iron meteorites and that of these iron meteorites only 5% are subsequently available for catalysis; this was taken into account in the initial conditions. The final composition of the atmosphere depends on the available catalytically active material and thus on the meteorite flux. During the simulations, the amount of catalytically accessible material per year and thus the amount of catalytically available material is varied (Fe, see legend of Figure 24 ($10^{-2} – 10^{-5}$)). A system using iron nanoparticles as catalysts was investigated in detail by Trapp et al., demonstrating prebiotically plausible carbon dioxide activation.[266]

A global model (see Scheme 13) of the chemical reactions in the atmosphere and on the surface of a prototype planet was developed using the reaction rate constants k_n and equilibrium constants K_n derived from the above-mentioned experimental data (see Appendix Table 70). The model has an atmosphere up to 60 km and the temperature was set at 500 °C considering experimental setups and prebiotically relevant reaction condition scenarios.[266]

4.3.3 The Chemical Reaction Network

The starting materials of the investigated reaction network were carbon dioxide, as exclusive carbon source, water, and meteorites, as educt for the catalysts. Starting from meteoritic material, elemental iron (Fe^0) and water are formed in the preliminary reaction with the reaction constant k_1. This reaction is necessary to provide the starting materials CO_2 and H_2 for the subsequent formation of the prebiotically important small organic molecules.

The model network applied for the simulation is shown in Scheme 13.
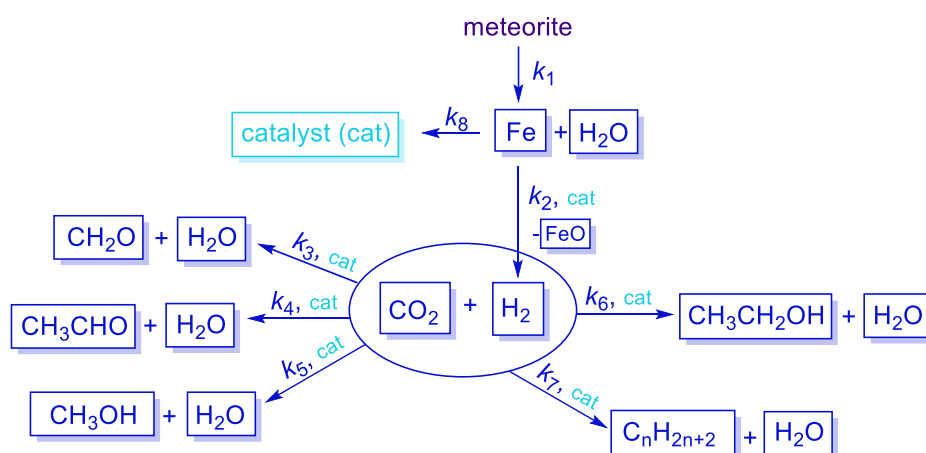
Scheme 13: The chemical network underlying the simulation of the atmosphere. The framed molecules represent observed products in the simulation.

Scheme 14 shows an extended reaction network that, in addition to the model reactions, shows exemplary pathways to more complex prebiotic building blocks such as sugars, amino acids and nucleosides to illustrate the importance of the simulated reaction network for the subsequent building block formations.
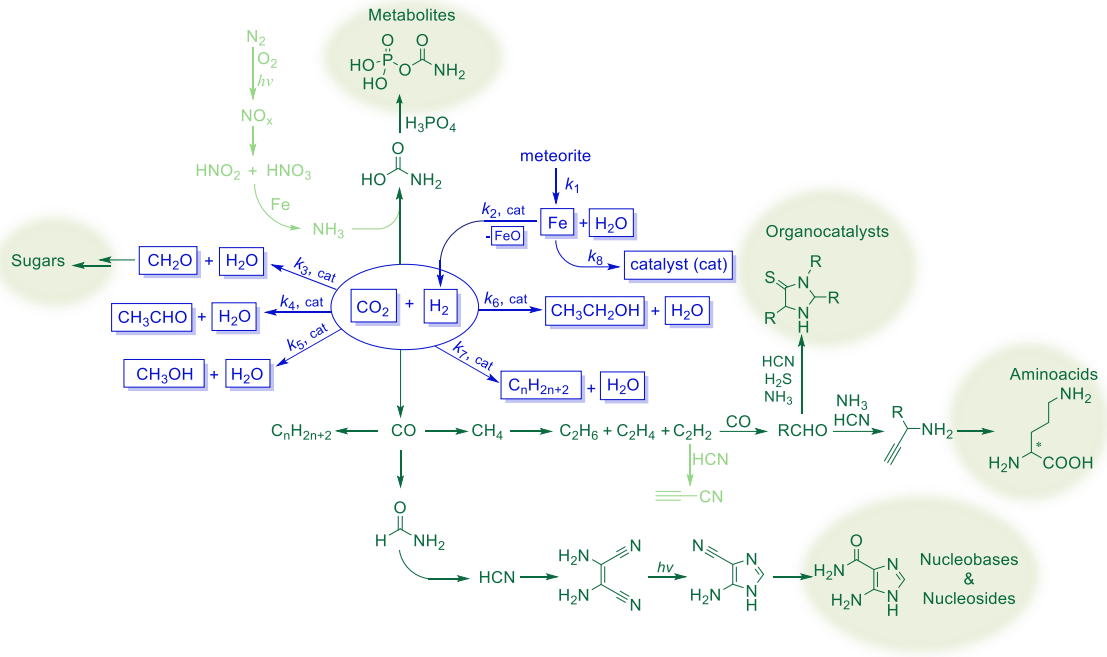
Scheme 14: Extended chemical network towards building blocks of life. Molecules in the boxes were observed in the simulation. Prebiotic routes explored by the TRAPP group[119,267] are shown (dark green) as well as examples of routes discussed in the literature [268,269] (light green). The substance classes relevant for the Origin of Life are shaded.

The underlying ODEs, that were used for the simulation are shown in Eqs. 31-42:

$$\frac{d[\text{Meteorite}]}{dt} = -k_1[\text{Meteorite}] \tag{31}$$

$$\frac{d[\text{Fe}]}{dt} = 0.05k_1[\text{Meteorite}] - k_8[\text{Fe}] - k_2[\text{Fe}][\text{H}_2\text{O}] \tag{32}$$

$$\frac{d[\text{FeO}]}{dt} = k_2[\text{Fe}][\text{H}_2\text{O}] + k_2[\text{Cat}][\text{H}_2\text{O}] \tag{33}$$

$$\frac{d[\text{Cat}]}{dt} = k_8[\text{Fe}] - k_2[\text{Cat}][\text{H}_2\text{O}] \tag{34}$$

$$\frac{d[\text{H}_2\text{O}]}{dt} = -k_2[\text{Fe}][\text{H}_2\text{O}] - k_2[\text{Cat}][\text{H}_2\text{O}] + k_3[\text{CO}_2][\text{H}_2]^2 + 3\,k_4[\text{CO}_2]^2[\text{H}_2]^4 + k_5[\text{CO}_2][\text{H}_2]^3 + 3k_6[\text{CO}_2]^2[\text{H}_2]^6 + 2k_7[\text{CO}_2][\text{H}_2]^3 \tag{35}$$

$$\frac{d[\text{H}_2]}{dt} = k_2[\text{Fe}][\text{H}_2\text{O}] + k_2[\text{Cat}][\text{H}_2\text{O}] - 2k_3[\text{CO}_2][\text{H}_2]^2 - 5k_4[\text{CO}_2]^2[\text{H}_2]^5 - 3k_5[\text{CO}_2][\text{H}_2]^3 - 6k_6[\text{CO}_2]^2[\text{H}_2]^6 - 3k_7[\text{CO}_2][\text{H}_2]^3 \tag{36}$$

$$\frac{d[\text{CO}_2]}{dt} = -k_3[\text{CO}_2][\text{H}_2]^2[\text{Cat}] - 2k_4[\text{CO}_2]^2[\text{H}_2]^5[\text{Cat}] - k_5[\text{CO}_2][\text{H}_2]^3[\text{Cat}] - 2k_6[\text{CO}_2]^2[\text{H}_2]^6[\text{Cat}] - k_7[\text{CO}_2][\text{H}_2]^3[\text{Cat}] \tag{37}$$

$$\frac{d[\text{CH}_2\text{O}]}{dt} = k_3[\text{CO}_2][\text{H}_2]^2[\text{Cat}] \tag{38}$$

$$\frac{d[CH_3CHO]}{dt} = k_4[CO_2]^2[H_2]^5[Cat] \tag{39}$$

$$\frac{d[CH_3OH]}{dt} = k_5[CO_2][H_2]^3[Cat] \tag{40}$$

$$\frac{d[CH_3CH_2OH]}{dt} = k_6[CO_2]^2[H_2]^6[Cat] \tag{41}$$

$$\frac{d[C_nH_{2n+2}]}{dt} = k_7[CO_2][H_2]^3[Cat] \tag{42}$$

The meteorite material reacts to form elemental iron (Fe^0) in a preceding reaction with the reaction rate constant k_1. The elemental iron can then either react with water to form hydrogen, with the reaction rate constant k_2, or in a further reaction form the active nanoparticle catalyst used in the network (k_8). The oxygen-rich environment results from the formation of water in the system as a by-product of the reduction step to Fe^0. The formation of hydrogen from elemental iron and water is prebiotically plausible and discussed in the literature.[270]

The CO_2 fixation by catalysis towards formaldehyde (k_3), acetaldehyde (k_4), methanol (k_5), ethanol (k_6) and various alkanes (k_7) was simulated and the global traces of the integral sums of products were obtained.

The complex chemical network model (Scheme 13) was simplified by disregarding the mechanisms of depletion of the formed organic molecules, while still taking into account the mechanism of depletion for the catalyst. For computability reasons, this reaction network was deliberately designed to focus on the formation of the organic molecules without including depletion processes, resulting in a *pseudo* accumulation of organic material that would naturally have undergone subsequent reactions or decomposition reactions. These alcohols and alkanes, as well as the more oxygen rich compounds such as aldehydes (e.g., formaldehyde and acetaldehyde), are important intermediates for further reactions yielding higher molecular building blocks for the Origin of Life.

4.3.4 Simulation Results

With the reaction network and the ODEs in hand, the change in atmospheric composition based on this chemical network with different amounts of catalytically available material was investigated. The global traces of the cubic and thus standardised microreactors (see Figure 22) within the simulated atmosphere yielded integral sums of the substances formed (see Figure 24). The time span simulated was 100 Myr but since the carbonaceous species in the simulation show plateau formation after 5-10 Myr, depending on the catalyst loading, only the first 20 Myr are shown.
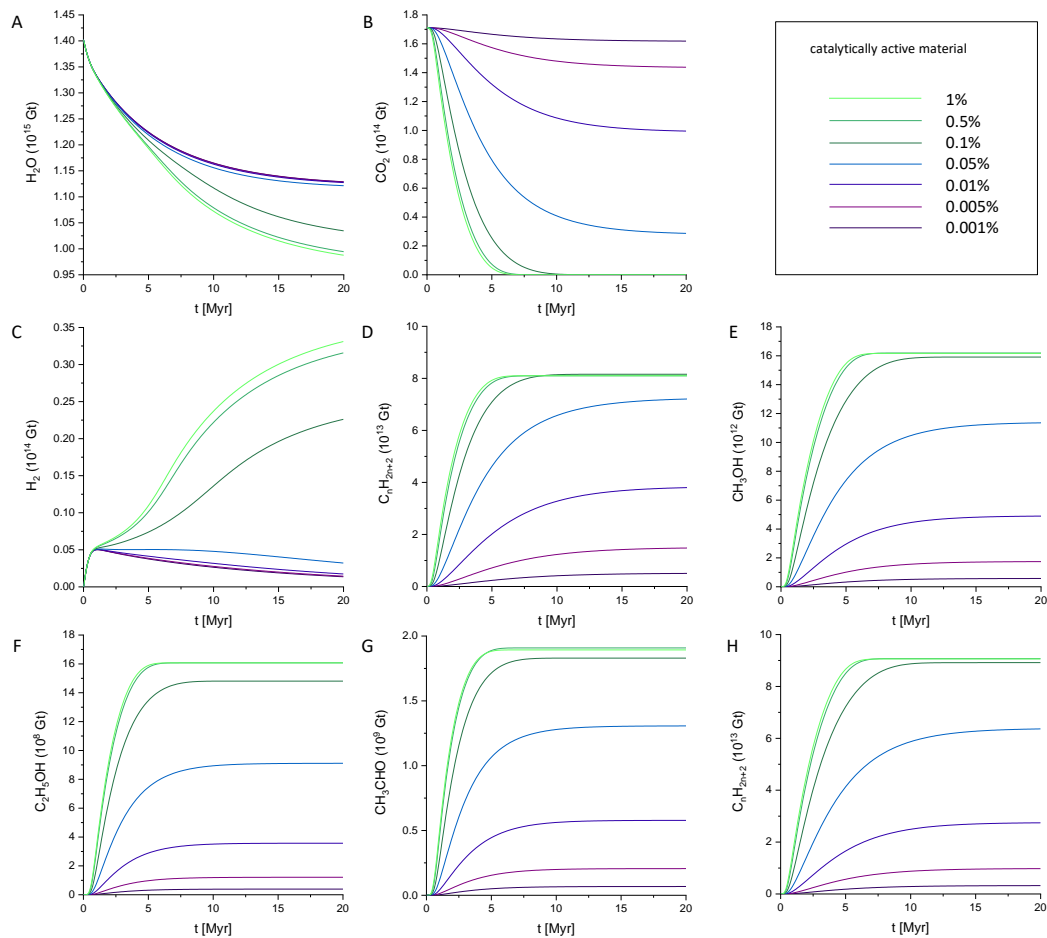
Figure 24: Simulations of the concentration courses, i.e., the integral sum of the products, over a period of 100 Myr, 20 Myr of which are shown. Amounts of catalytically active material: 1% (bright green), 0.5% (green), 0.1% (dark green), 0.05% (light blue), 0.01% (dark blue), 0.005% (purple), 0.001% (dark indigo).

The formation of H_2 (Figure 24, C) evidently is essential for the entire system to continue and thus represents the tipping point of the system. At catalyst loadings of 0.001-0.05%, the simulated total H_2 accumulation reaches a local maximum after which the concentration decreases asymptotically. Here it must be emphasised again that this system only takes into account a pseudo built-up of the simulated products. At higher concentrations of the active catalyst sufficient H_2 is formed to allow the CO_2 fixation to continue. The iron particles are oxidized by water and H_2 is released. Should this redox process come to a standstill at a certain point because not enough material is supplied in from external sources, then this H_2 formation will stop – representing the tipping point of the system.

In general, remarkable dependencies of the catalyst loading for the formation of H_2 can be observed over time. At the smallest tested amount of catalytically active material of 0.001%, it can be stated that the planet, with the particular example of the early Earth, would never

have reached the state where CO_2 would have been completely transformed into organic material. If this does not happen, a planet is dead and life as we know it will never evolve.

Heating up the atmosphere leads to the formation of water during the reduction step, and when the planet cools down, this process will stop. On the other hand, if a lot of hydrogen is formed, the atmosphere is heated up and the carbon inventory will subsequently be transformed into alkanes, alcohols, formaldehyde, and acetaldehyde.

These results indicate that the CO_2 atmosphere was probably consumed in less than 20 Myr, depending on the amount of catalytically active material (see Figure 24, B). This is a fairly rapid process, given the typical prebiotic timescales. This CO_2 consumption in itself, however, is important for the chemical processes on the early Earth to get started, as the composition of the atmosphere affects the material flux and the transmission of light of different wavelengths.[59] Thus, without the decrease in CO_2 in the atmosphere, UV light would have been absorbed and would not be available as an energy source for chemical reactions.

To demonstrate the direct dependence on catalyst loading, a different visualization method was chosen for the same data set. Two representatively selected amounts of catalytically active material, the highest and lowest investigated, were chosen and the amounts of molecules formed and consumed for are shown in Figure 25. These integral sums of products were calculated for the total amount of 100 Myr but are shown only for the first 10 Myr until plateau formation.
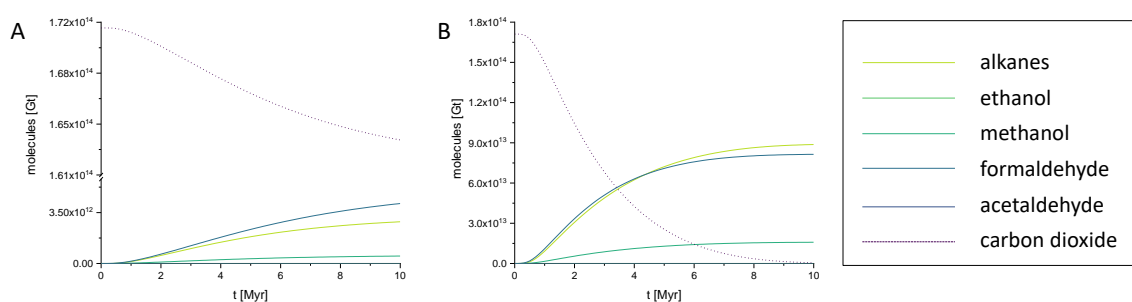
Figure 25: Simulations of amounts of formed molecules in gigatonnes (Gt) for alkanes, ethanol, methanol, formaldehyde, acetaldehyde, and CO_2 depicted over a period of 10 Myr. Amounts of catalytically active material: A: 0.001%; B: 1%.

The general trend is that with higher catalyst loading, CO_2 fixation proceeds faster and the overall yield increases. The two extreme values for catalyst loading scenarios are depicted in Figure 25, with the lowest being 0.001% (A) and the highest at 1% (B). At the minimum catalyst loading, the product composition consists mainly of formaldehyde, alkanes, and methanol. The amount of catalytically available material at 1% shows a different product

composition. Here, mainly alkanes, formaldehyde, and methanol are formed, and a higher overall yield is achieved. The formation of alkanes exceeds that of the other substance classes.

The fact that oxygenated products are formed even if the ratio of the effectively simulated partial pressures of CO_2 and H_2 is varied demonstrates the robustness of the reaction pathways within the investigated reaction system. This is particularly important considering that these oxygenated products play a crucial role in the formation of carbohydrates, amino acids and ultimately the emergence of life.

The products predominantly formed in the comparative experimental study in the TRAPP group with catalytically active particles obtained from the iron and nickel rich *Campo del Cielo* meteorite supported on Montmorillonite at 300 °C at 45 bar were the oxygenated products methanol, ethanol and acetaldehyde.[266] Both, the *in vitro* and *in silico* experiments thus show a very robust pathway towards the building blocks for life via CO_2 fixation.

4.4 Summary and Conclusion

A robust and deliberately broad-based kinetic model of the evolution of the early Earth's atmosphere was developed, whose orders of magnitudes of the parameter set are based on experimental data.

With kinetic modelling of a CO_2 fixation by catalysis markers were identified that can lead to the Origin of Life and its preservation. The conundrum here is how quickly CO_2 can be converted into organic matter and what conditions must be met to ensure that such a process is not interrupted, thus preventing subsequent processes such as the activation of nitrogen. This large-scale *in silico* catalysis of prebiotically plausible building blocks from atmospheric gases for an arbitrary planet provided insights into the dependencies on H_2 formation and consumption, identifying the tipping point of the model atmosphere.

Furthermore, the decrease in the concentration of CO_2 is essential for the possibility of photosynthesis and photochemistry to subsequently take place. The fixation of CO_2 within the determined time spam of about 20 – 100 Myr is a rather fast process.

The dependencies on catalyst loadings and therefore on external material influx were shown and the according product distribution was discussed.

These implications for a possible emergence that once existed on a given planet and a possible emergence in the future are an important starting point for further astrochemical research, as the concentration of certain gases indicates whether a planet can provide the basis for the emergence of life on the early Earth as well as other metallosilicate exoplanets with comparable geological and atmospheric compositions.

Chapter 5

System Validation of the *RNA.exe* Tool
for a SOAI Autocatalysis

5.1 Objective

The aim of this part of the thesis was to validate the further developed and refined reaction network analysis tool *RNA.exe*. This tool is based on an adaptive fourth order Runge–Kutta algorithm and programmed in Pascal (Embarcadero Delphi XE 7) and was employed in Chapter 4 to simulate a large-scale data set of an atmosphere.[264]

In order to consider the simulated output of *RNA.exe* as valuable data, the program must be validated, and the accuracy of the predicted values determined by comparing with an experimentally obtained data set. After the experimental kinetic investigation of the Soai reaction was successfully conducted in the Trapp working group using FIA-HPLC-MS measurements, an experimental data set could be used for the validation of the *RNA.exe* tool. The established hemiacetal model was used as the underlying reaction network.[220]

How well is the RNA.exe tool able to simulate representative kinetic data for a given reaction network system? For this validation, the simulated sets from the *RNA.exe* tool were compared with an experimentally obtained set and the variance of the 100 best fit sets was to be determined. Furthermore, the aim was to provide insight into how the method deals with experimental "out-layer" sets that cannot be covered by the dataset.

5.2 Results

In order to be able to determine exact k values with the developed tool the following questions have to be answered: Will the simulated sets be able to "hit" the values of the original experimental data set? Out of the vast number of simulated sets how many of the calculated data sets come close to the original data set at all?

5.2.1 Methodology and Setup

Figure 26 schematically explains the goal and setup of the validation experiment depicting the combined representation of the original data set values and the simulated ones.
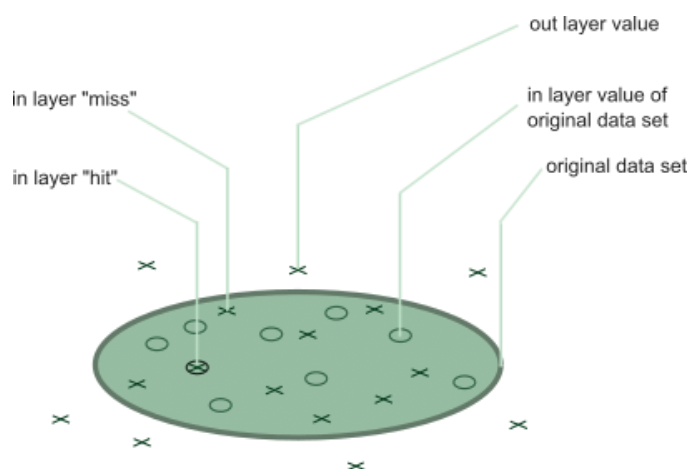
Figure 26: Schematic cluster of the original data set, the "in layer" hits and "out layer" values that were attempted within this validation setup. Original data set values (circle),

Underlying Reaction Mechanism and ODEs

The mechanism is composed of three different, simultaneously occurring processes: the formation of the zinc alcoholates, the established dimer formation and the two postulated catalytic cycles with hemiacetal structures.

The starting point is the reaction of the two alcohol enantiomers **(R)-1** and **(S)-1** with diisopropylzinc to form the corresponding zinc alcoholates **(R)-2** and **(S)-2** (see Scheme 15). These zinc alcoholates can self-assemble into various dimeric structures, see Chapter 2.2.3.1. The two homochiral dimers **(R,R)-3** and **(S,S)-3** are in equilibrium with the monomers and remain in solution. The heterochiral dimeric structure **(R,S)-3** has a lower solubility and is less catalytically active, this is taken into account by the equilibrium constant K_d for the equilibrium with the undissolved form **(R,S)-3$_{solid}$** in the ODE.

The monomeric zinc alcoholates **2** can undergo an equilibrium reaction with the aldehyde **4** to form the enantiomeric zinc-complexed hemiacetal structures **5**. The equilibrium here lies on the alcoholate side, as previous NMR studies have shown.[220] The subsequent coordination of another aldehyde molecule and then the transfer of the alkyl group leads to **6**. Alkylation of the aldehyde to **(*R,R,R*)-** or **(*S,S,S*)-7** follows, during which the formation of further chiral centres promotes enantioselectivity yet again. The dimer hemiacetals **(*R,R,R,R*)-** or **(*S,S,S,S*)-8** are formed after another coordination of an aldehyde after which the catalytic cycle is closed yielding the enantiomeric zinc-complexed hemiacetal structures **(*R,R*)-5** and **(*S,S*)-5**.
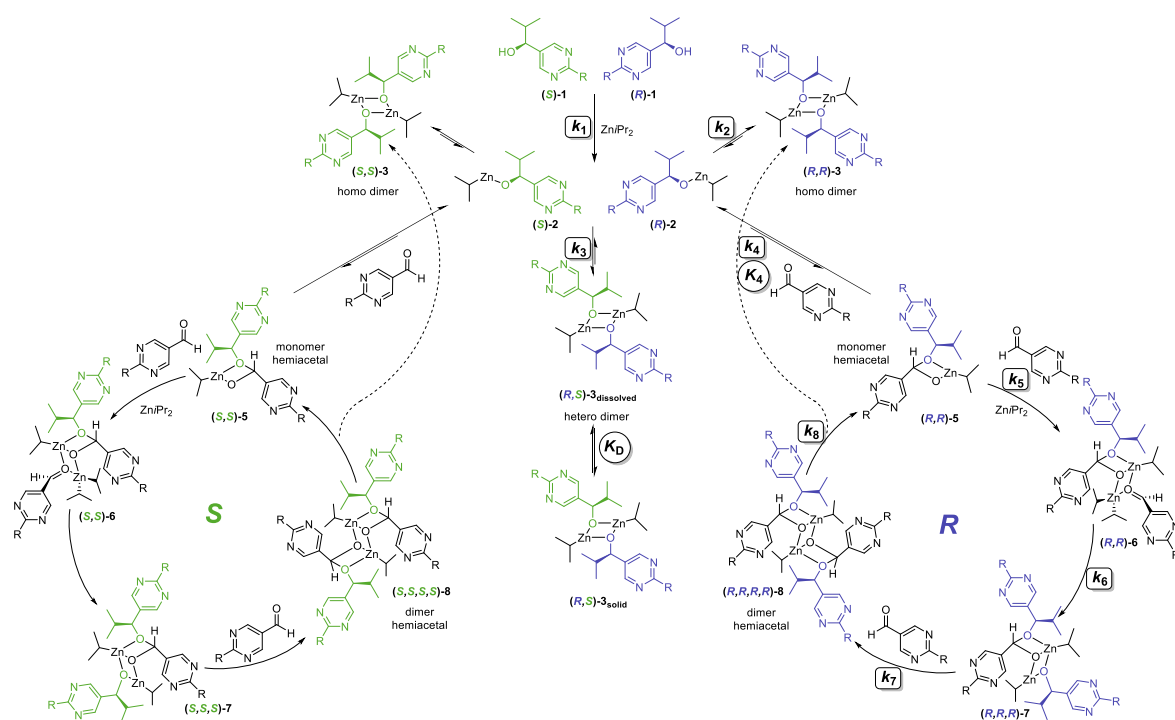
Scheme 15: SOAI reaction network with reaction rate constants used for the simulation and validation of the *RNA.exe* tool.

Heterochiral dimer assembly can account for the enantioselectivity and stereo amplification of the reaction. If an alcohol enantiomer is predominantly formed, statistically more homochiral dimers are formed. If its mirror image is included, it will be incorporated into heterochiral dimers, which are more difficult to dissolve, and thus be withdrawn from the system. As a result, the ratio of alcohol available for catalysis is shifted even further to the side of the alcohol monomer, which has already been incorporated in excess.[138]

User Interface for Validation

The user interface of the *RNA.exe* program is shown in Figure 27. The ODEs of the previously discussed reaction network are written into the field intended for this purpose. The reaction rates and concentrations can be entered in the corresponding input fields. The step size (Δt) of the output data and the duration of the simulated reaction time can also be set.
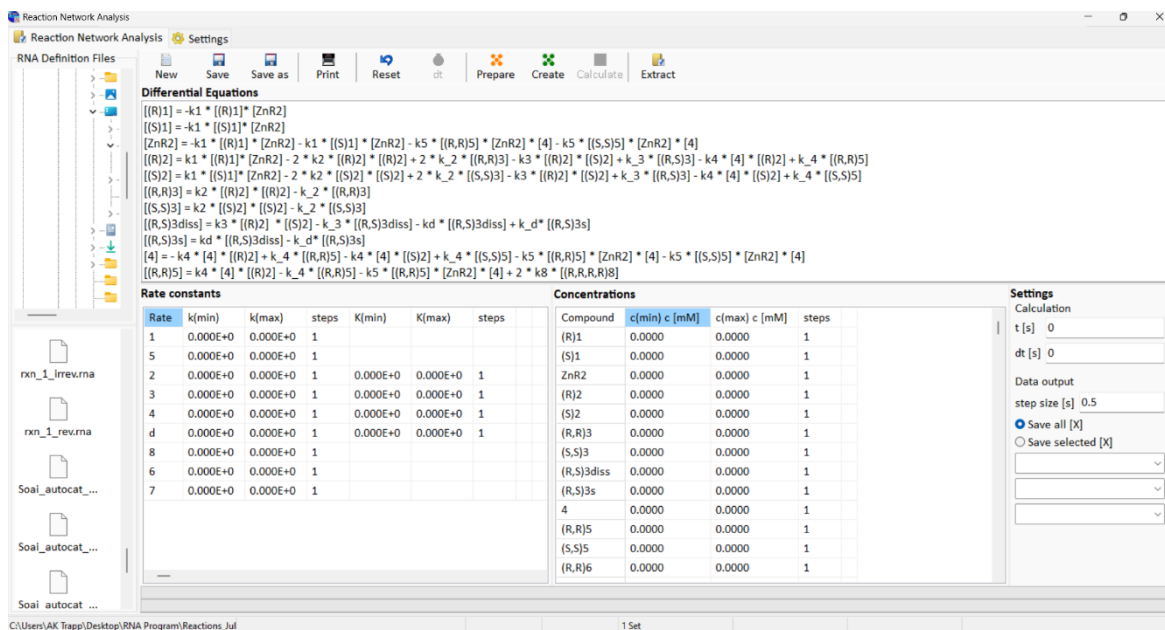
Figure 27: User interface of the *RNA.exe* program with input fields for differential equations, settings, and parameter inputs such as rate constants, concentrations, and an interface area that simplifies file management and access to previous projects. For visibility reasons only part of the ODEs and input fields for concentrations are shown.

5.2.1.1 Original Data Set Values

Experimental data for the SOAI reaction of the 2-((trimethylsilyl)ethynyl)pyrimidine-5-carbaldehyde system was obtained by PATRICK MÖHLER.[271] Kinetic FIA measurements with the TMS-substituted pyrimidine aldehyde were carried out and analysed and the experimental insights and parameters were used for the original data set.

2-(TMS-ethynyl)-pyrimidine-5-carbaldehyde
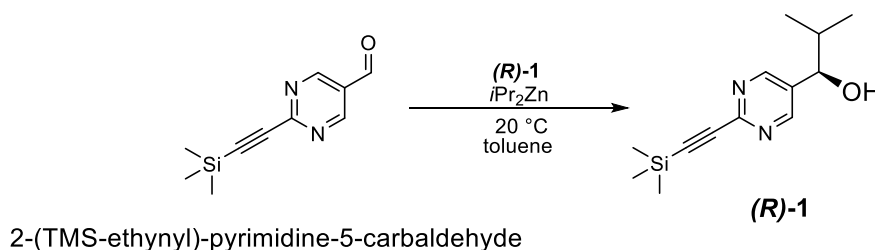
Scheme 16: Reaction scheme for the SOAI reaction system used for the validation of the *RNA.exe* tool.

The reaction rate constants for the original data set are listed in Table 3.

Table 3: Reaction rate constants for reaction steps of the SOAI reaction of the 2-((trimethylsilyl)ethynyl)pyrimi-dine-5-carbaldehyde system.

Reaction step	k or K^1
k_1	150
k_2	500
k_3	500
k_d	200
k_4	0.01
k_5	50
k_6	0.5
k_7	15
k_8	0.5
K_2	200
K_D	10000
K_4	5
S_f	0.0001

1) The respective units can be derived from the differential equations (see Chapter 7.3 Appendix).

Two sets of experiments were conducted, with either constant aldehyde or alcohol concentrations while varying the respective other concentration. When varying the aldehyde concentrations (35 mM, 25 mM, 20 mM, 10 mM) the alcohol concentration was set at 1.5 mM. The alcohol concentrations chosen were 5 mM, 1.5 mM or 0.5 mM at constant aldehyde concentration of 25 mM.
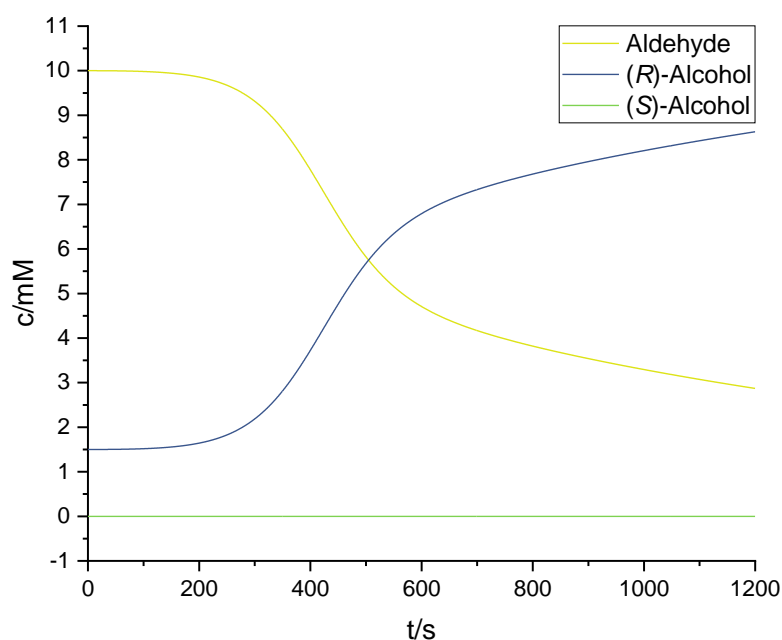
Figure 28: Concentration course of the SOAI Reaction: original data set concentration course for the set of 25 mM aldehyde, 1.5 mM (*R*)-alcohol, 50 mM diisopropylzinc.

Figure 28 shows an exemplary plot of one set of the original data set derived from the experimental data with 25 mM aldehyde, 1.5 mM (*R*)-alcohol, 50 mM diisopropylzinc and exhibits an *ee* of 99.9999933% *ee*.

5.2.2 Simulation Results

5.2.2.1 Accuracy of the Program Simulation

First, the accuracy of the RNA.exe program was to be determined. A total of 32805 sets were simulated, all of whom were compared graphically with the values of the original data set. The variance σ^2 of the best 100 simulated data sets ranged from $\sigma^2_{\#1} = 0.02444735$ to $\sigma^2_{\#100} = 0.05464338$, which signifies a very good agreement with the experimentally obtained values.
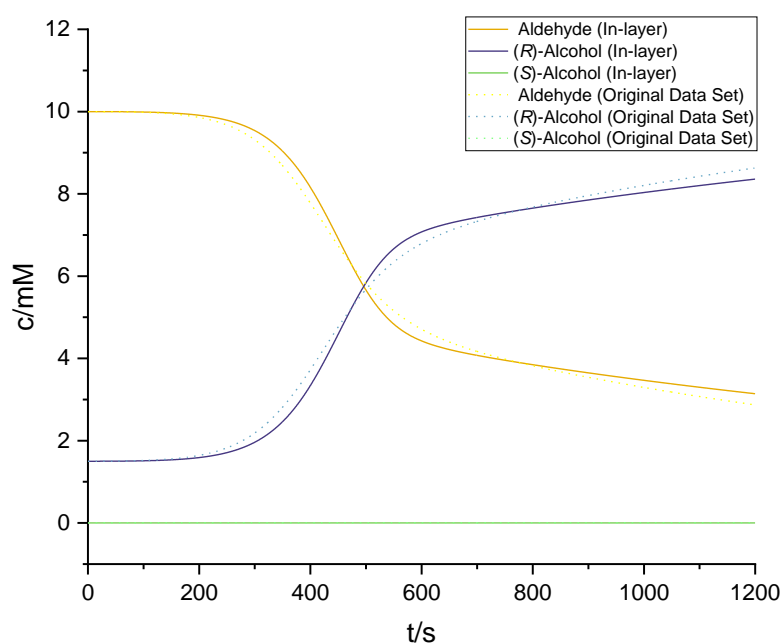
Figure 29: Concentration courses of the Soai Reaction: original data set (bold line) versus the set of the "in layer" hit sets with the highest hit accuracy i.e., the smallest σ² (dotted line).

A schematic overview for the visualisation of the refinement method is shown in Figure 30.
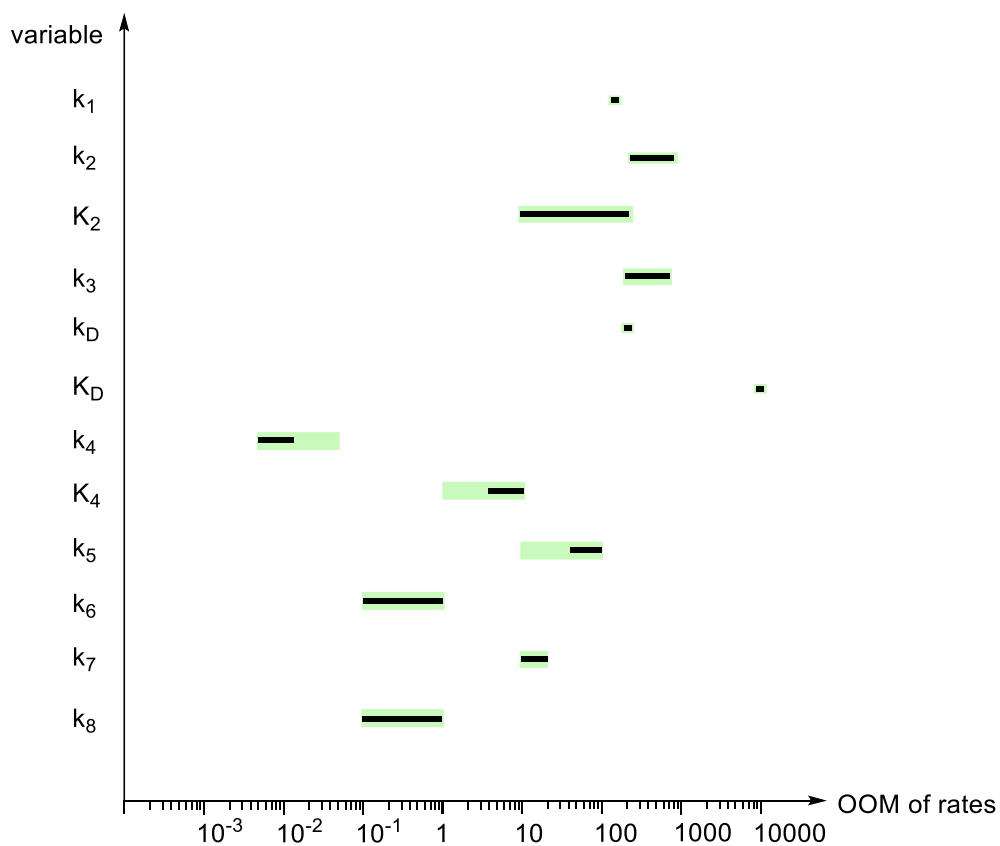
Figure 30: Variables ranges (reaction rate constant and equilibrium constants) for applied data sets plotted against the order of magnitude (OOM) of the rates: range of the unrefined parameters (bright green), ranges of refined parameters (black).

5.2.2.2 Experimental Out-Layers

An additional question was: how does the method cope with experimental "out-layer" sets that cannot be covered by the dataset? Figure 31 shows how much influence individual deviations have on the overall system.
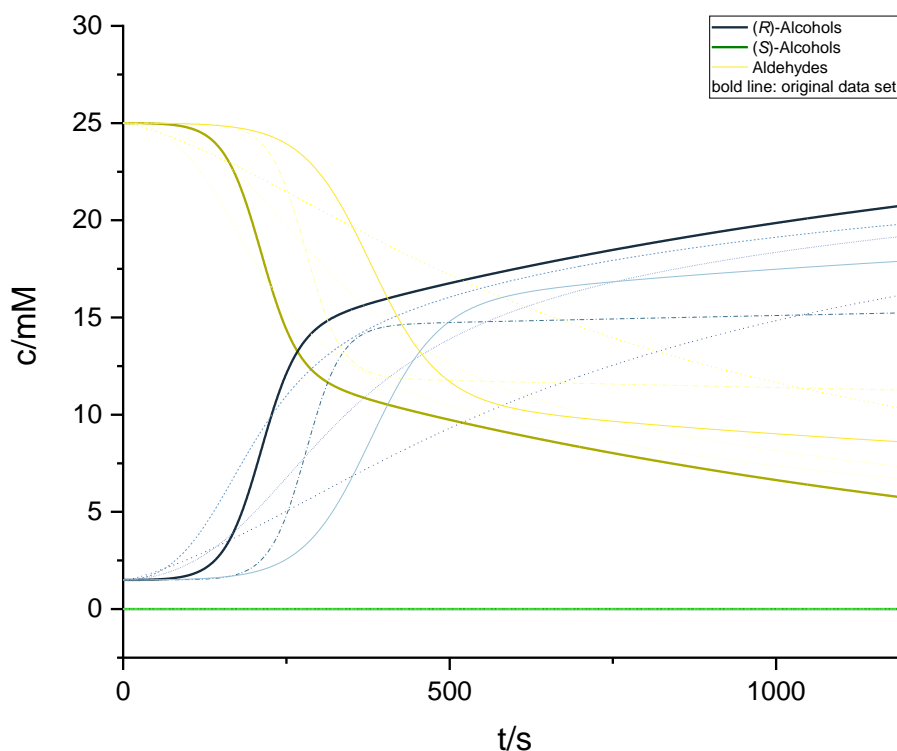
Figure 31: Concentration course comparison of "out layer miss" data set versus the original reference set.

The results show how drastically the discrepancy of the concentration courses vary if even only one of the reaction rate constants does not match the original data set. Table 4 shows that although most of the k values match very well, the values for the monomer hemiacetal formation (k_4) and for the rate determining step (k_7) do not coincide with the referenced set. This results in vast deviations and no matching pairs are obtained with the given parameters.

Table 4: Kinetic values of the simulated out layer sets in comparison to the original data set values (highlighted in blue). Kinetic values of the simulated sets that match the original data set are highlighted in green, the discrepancies are highlighted in yellow.

	#1	#2	#3	#4	#5	Original data set values
k_1	150	150	150	150	150	150
k_2	500	500	500	500	500	500
k_3	500	500	500	500	500	500
k_d	200	200	200	200	200	200
k_4	0.20	0.20	0.0007	0.005	0.20	0.10
k_5	50	50	50	50	50	50
k_6	0.50	0.50	0.50	0.50	0.50	0.50
k_7	100	3	15	2	15	15
k_8	0.50	0.50	0.50	0.50	0.50	0.50
S_f	0.0001	0.0001	0.0001	0.0001	0.0001	0.0001
σ^2	1.5089	2.7969	5.8529	7.3916	17.9354	0.0000

1) The respective units can be derived from the differential equations (see Chapter 7.3 Appendix).

5.2.2.3 Determination of the reaction orders

For the determination of the rate law of a chemical reaction, there are different methods. The method of initial velocities is often used in combination with the isolation method. A starting substance A is used in varying initial concentrations, all other reactants in excess, so that the following equations for the reaction velocity v result:

$$v = \frac{d[A]}{dt} = k \cdot [A]^a \tag{43}$$

$$\log\left(\frac{d[A]}{dt}\right) = \log(k) + a \cdot \log([A]) \tag{44}$$

Subsequently, the reaction order a of the starting material A can be determined from the slope by the linear fitting of equation (44). The initial rate can be determined by the initial change in concentration. The sigmoidal reaction course characteristic of autocatalysis makes this a calculation more complicated. Although this mathematical approach does not quite meet the complex reaction network of the autocatalysed Soai reaction, the *AMPCAT.exe* program and the varying initial concentrations of the three reaction components aldehyde, alcohol, and zinc organyl can provide an impression of the respective influences on the course of the reaction.

Graphical determination of the reaction orders by linear regression analysis by double logarithmic plotting of the initial rates versus the concentration of the respective substance were conducted (see Figure 32).

The resulting reaction orders for the aldehyde with a reaction order of 2.0, the alcohol of 0.8, and the zinc organyl one of 0.0133 agrees well with the expected values of 2.0 in relation to the aldehyde, 1.0 in relation to the alcohol and 0 for the diisopropyl zinc.

$$\lg(v_0) = 0.0133 \cdot \lg([Zn]_0) - 5.7590$$

$$\lg(v_0) = 2.00179 \cdot \lg([aldehyde]_0) - 2.5704$$

$$\lg(v_0) = 0.8566 \cdot \lg([alcohol]_0) - 4.23064$$
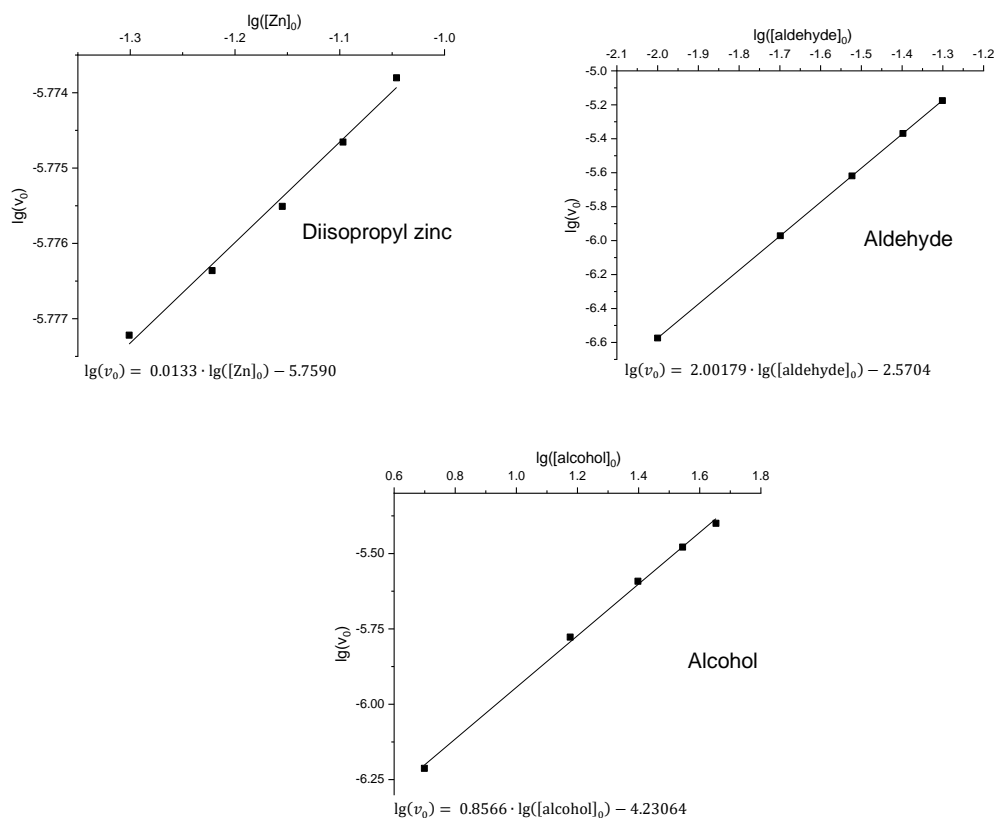
Figure 32: Graphical determination of the reaction orders by linear regression analysis of $log(v0)$ *versus* $log(c(substance)$ of: diisopropylzinc, the aldehyde, the (*R*)-alcohol and of the original data set according to equation (47). The slope of the linear regression gives the reaction order.

5.3 Summary

The simulation program *RNA.exe*, which was specially designed and further developed for the different chemical scenarios on the basis of a Runge–Kutta algorithm, was successfully validated with an experimentally obtained data set. The results simulated by the program were compared with the experimentally obtained concentration courses and kinetic data. The sensitivity of the reaction network was shown with even minor discrepancies between sets having a major influence on the system's kinetics.

Chapter 6

Summary and Conclusion

In this dissertation, reaction network systems were investigated with the help of purpose build simulation tools. The aim was to develop, implement and validate two robust and versatile network analysis programs with distinct applications and subsequently to apply them in relevant models for the elucidation of the Origin of Life (see Figure 33). One tool was to be employed for simulations at the molecular level to gain insights regarding the emergence of homochirality while the other was designed for large-scale *in silico* catalysis and applied to simulate a planet's atmosphere and an autocatalytic reaction network.

In the first part of the thesis, a way to observe symmetry breaking at the molecular level was investigated. Therefore, an efficient simulation software tool, *SMK.exe,* was developed for predicting reactions at the molecular level based on a stochastic algorithm. This program is designed to provide efficient simulations on a workstation computer within a short period of time, i.e., the computation time for a calculated set is in the order of seconds. It is possible to feed a desired reaction network in form of ODEs into the network analysis program, making it a very versatile tool that can be adapted for a variety of different chemical reaction networks. The program structure and workflow of the algorithm were described, and input and output requirements were considered. Furthermore, the *SMK.exe* tool was validated in terms of its reproducibility. A statistical analysis and a long-term simulation confirmed that there was no bias within the system and that the formation of a preferred enantiomer was random.

With regard to the emergence of homochirality and prebiotic complexity, four different reaction scenarios were investigated, including three autocatalytic reactions and one reaction cascade. These scenarios start with a substrate pool and only a single catalyst molecule and involve the initiation of a stochastic reaction that yields product enantiomers. In the first scenario, these enantiomers serve as a catalyst in an autocatalytic process, while in the second scenario a dimerisation of the enantiomers to a homochiral dimer is considered. This was followed by a simulation of the formation of a transient catalyst in an autocatalytic process. The last scenario investigated was a reaction cascade, as often found in nature processes.

Overall, processes where the downstream reactions are faster were able to achieve and enhance symmetry breaking more efficiently. An interesting insight from these molecular-level simulations was that those initial processes which are the most "inefficient" lead to high *ee* values and are thus actually the most efficient scenarios in terms of achieving symmetry breaking. To achieve this, individual enantiomers must be formed slowly, but the subsequent amplification process must be fast and selective. A commonality of all the systems where no symmetry breaking occurred is that the rates of the competing processes

converged, giving only a racemic product mixture. The highest *ee* values and the most efficient symmetry breaking processes were found for the scenarios in which a transient catalyst was formed and for the scenario of the reaction cascade of coupled processes.

In summary, the conducted simulations demonstrated that interlocking processes, such as the formation of transient catalysts, autocatalytic systems or reaction cascades, which consecutively build on each other and lead to a kinetic acceleration, can very well amplify a statistically occurring symmetry breaking.

In the second part of the thesis (Chapter 4), the development of the atmosphere of a planet during a catalytic CO_2 fixation was simulated and evaluated. The chemoinformatics program *RNA.exe* was developed further and deployed for this purpose. *RNA.exe* was validated in the third subject area (Chapter 5) using experimental kinetic data on the SOAI reaction. As the basis for the calculations in Chapter 4, a robust and deliberately broad kinetic model of the early Earth's atmosphere was established. The kinetic data required for this to form the basis of the parameter set are derived from experimental data from the TRAPP working group.[266] With this model, a large-scale *in silico* catalysis was carried out for the time period of 100 Myr in which organic molecules were formed from atmospheric gases. The dependencies on the amount of catalytically active material and thus on substance influx on an early Earth-like planet were shown and the corresponding product distribution discussed. Thereby the velocity and the given conditions of the conversion of CO_2 into organic matter were investigated to prevent such a process from interrupting and thus inhibiting subsequent processes leading to the emergence of life. The effects of the decrease in CO_2 concentration are an essential prerequisite for photosynthesis and photochemical processes to take place. The determined timespan necessary for complete CO_2 fixation in the model system lies between 20 and 100 Myr, depending on the amount of catalytically active material, which is a very rapid process in the large Origin of Life context. Crucial here is the formation and consumption of H_2, which represents the tipping point in the model atmosphere studied.

Since the concentration of certain gases indicates whether a planet has the basis for the Origin of Life, these findings are an important indication for research into the Origin of Life on the early Earth as well as other metallosilicate exoplanets with comparable geological and atmospheric compositions.

Figure 33: Graphic summary of "*In silico* Investigations towards Homochirality with Regard to the Origin of Life: Symmetry Breaking by Consecutive Amplification, Atmospheric Modelling of a Reaction Network in a Prebiotic Context and System Validation for a SOAI Autocatalysis". *SMK.exe* was coded and employed to investigate symmetry breaking on a molecular level whereas the *RNA.exe* tool was further developed, validated with a SOAI reaction system, and used to simulate the atmosphere of the early Earth.

Chapter 7

Appendix

7.1 Appendix: Symmetry Breaking Simulations with *SMK.exe*

The original output intervals are set to 0.001 s steps, here only time values with significant change are shown for readability reasons, otherwise 10000 entries would have been necessary. These output files exist, please contact the author for further inquiry if data is needed. Subset D of Scenario A is shown in greater detail exemplarily (see Table 8).

7.1.1 Scenario A

Table 5: Symmetry breaking simulation scenario A, subset A.

t /s	[A]	[B]	[RC]	[SC]
0	602214076	602214076	0	0
0.162	602214075	602214075	1	0
1	602214071	602214071	4	1
2	602214070	602214070	5	1
2.98	602214067	602214067	6	3
3	602214067	602214067	6	3
4	602214067	602214067	6	3
5	602214067	602214067	6	3
6	602214067	602214067	6	3
7	602214067	602214067	6	3
8	602214067	602214067	6	3
9	602214067	602214067	6	3
10	602214067	602214067	6	3

Table 6: Symmetry breaking simulation scenario A, subset B.

t /s	[A]	[B]	[RC]	[SC]
0	602214076	602214076	0	0
0.008	602214075	602214075	0	1
0.18	602214074	602214074	0	2
0.425	602214073	602214073	1	2
1	602214073	602214073	1	2
2	602214070	602214070	4	2
3	602214067	602214067	4	5
4	602214067	602214067	4	5
5	602214067	602214067	4	5
6	602214066	602214066	4	6
7	602214066	602214066	4	6
8	602214066	602214066	4	6
9	602214066	602214066	4	6
10	602214066	602214066	4	6

Table 7: Symmetry breaking simulation scenario A, subset C.

t /s	[A]	[B]	[RC]	[SC]

0	602214076	602214076	0	0
0.052	602214075	602214075	1	0
0.46	602214071	602214071	4	1
1	602214066	602214066	7	3
2	602214033	602214033	32	11
3	602213968	602213968	84	24
4	602213834	602213834	199	43
5	602213564	602213564	415	97
6	602212987	602212987	893	196
7	602211688	602211688	1972	416
8	602209123	602209123	4684	872
9	602201953	602201953	11240	3456
10	602184237	602184237	24303	9489

Table 8: Symmetry breaking simulation scenario A, subset D.

t /s	[A]	[B]	[RC]	[SC]
0	602214076	602214076	0	0
0.017	602214075	602214075	1	0
0.019	602214074	602214074	1	1
0.122	602214073	602214073	2	1
0.212	602214072	602214072	3	1
0.229	602214071	602214071	4	1
0.318	602214070	602214070	5	1
0.433	602214069	602214069	5	2
0.545	602214068	602214068	5	3
0.618	602214067	602214067	6	3
0.625	602214066	602214066	7	3
0.649	602214065	602214065	7	4
0.751	602214064	602214064	8	4
0.76	602214063	602214063	8	5
0.94	602214062	602214062	9	5
1.011	602214061	602214061	10	5
1.109	602214060	602214060	11	5
1.143	602214059	602214059	12	5
1.187	602214058	602214058	13	5
1.199	602214057	602214057	14	5
1.23	602214056	602214056	15	5
1.256	602214055	602214055	16	5
1.27	602214054	602214054	16	6
1.273	602214053	602214053	17	6
1.283	602214052	602214052	17	7
1.322	602214051	602214051	18	7
1.365	602214050	602214050	19	7
1.421	602214049	602214049	20	7
1.427	602214048	602214048	20	8
1.497	602214047	602214047	21	8
1.499	602214046	602214046	21	9
1.52	602214045	602214045	21	10
1.521	602214044	602214044	22	10
1.534	602214043	602214043	22	11
1.536	602214042	602214042	23	11

1.543	602214041	602214041	24	11
1.544	602214040	602214040	25	11
1.582	602214039	602214039	26	11
1.649	602214038	602214038	26	12
1.655	602214037	602214037	27	12
2	602214026	602214026	34	16
3	602213953	602213953	85	38
4	602213808	602213808	202	66
5	602213502	602213502	446	128
6	602212847	602212847	934	295
7	602211441	602211441	2024	611
8	602208553	602208553	4255	1268
9	602202588	602202588	8819	2669
10	602190357	602190357	18202	5517

Table 9: Symmetry breaking simulation scenario A, subset E.

t /s	[A]	[B]	[RC]	[SC]
0	602214076	602214076	0	0
0.046	602214075	602214075	0	1
0.091	602214074	602214074	0	2
0.201	602214073	602214073	1	2
1	602214062	602214062	6	8
2	602214049	602214049	12	15
3	602214043	602214043	15	18
4	602214035	602214035	21	20
5	602214032	602214032	22	22
6	602214031	602214031	22	23
7	602214030	602214030	22	24
8	602214027	602214027	23	26
9	602214024	602214024	25	27
10	602214021	602214021	28	27

Table 10: Symmetry breaking simulation scenario A, subset F.

t /s	[A]	[B]	[RC]	[SC]
0	602214076	602214076	0	0
0.027	602214075	602214075	0	1
0.129	602214074	602214074	0	2
0.339	602214070	602214070	1	5
0.738	602214066	602214066	4	6
1	602214059	602214059	8	9
2	602214040	602214040	17	19
3	602214030	602214030	21	25
4	602214026	602214026	23	27
5	602214019	602214019	24	33
6	602214014	602214014	26	36
7	602214011	602214011	28	37
8	602214009	602214009	30	37
9	602214006	602214006	33	37
10	602214003	602214003	34	39

Table 11: Symmetry breaking simulation scenario A, subset G.

t /s	[A]	[B]	[RC]	[SC]
0	602214076	602214076	0	0
0.047	602214075	602214075	1	0
0.053	602214074	602214074	2	0
1	602214043	602214043	22	11
2	602213961	602213961	67	48
3	602213793	602213793	160	123
4	602213437	602213437	352	287
5	602212649	602212649	780	647
6	602211023	602211023	1677	1376
7	602207653	602207653	3564	2859
8	602200849	602200849	7397	5830
9	602186669	602186669	15271	12136
10	602157125	602157125	31705	25246

Table 12: Symmetry breaking simulation scenario A, subset H.

t /s	[A]	[B]	[RC]	[SC]
0	602214076	602214076	0	0
0.052	602214075	602214075	0	1
0.086	602214074	602214074	1	1
1	602214060	602214060	8	8
2	602214041	602214041	19	16
3	602214030	602214030	22	24
4	602214020	602214020	28	28
5	602214017	602214017	30	29
6	602214009	602214009	35	32
7	602214008	602214008	36	32
8	602214007	602214007	37	32
9	602214004	602214004	39	33
10	602214001	602214001	41	34

Table 13: Symmetry breaking simulation scenario A, subset I.

t /s	[A]	[B]	[RC]	[SC]
0	602214076	602214076	0	0
0.001	602214075	602214075	1	0
0.003	602214074	602214074	2	0
0.044	602214066	602214066	10	0
0.089	602214055	602214055	15	6
0.17	602214041	602214041	22	13
0.3	602214011	602214011	43	22
0.369	602213992	602213992	50	34
0.444	602213972	602213972	65	39
0.483	602213964	602213964	71	41

0.61	602213937	602213937	88	51
1	602213862	602213862	125	89
2	602213713	602213713	192	171
3	602213619	602213619	247	210
4	602213550	602213550	281	245
5	602213505	602213505	303	268
6	602213474	602213474	319	283
7	602213452	602213452	329	295
8	602213431	602213431	338	307
9	602213415	602213415	347	314
10	602213405	602213405	353	318

Table 14: Symmetry breaking simulation scenario A, subset J.

t /s	[A]	[B]	[RC]	[SC]
0	602214076	602214076	0	0
0.011	602214074	602214074	2	0
0.014	602214073	602214073	2	1
0.032	602214068	602214068	5	3
0.56	602213951	602213951	67	58
1	602213869	602213869	107	100
2	602213728	602213728	174	174
3	602213647	602213647	211	218
4	602213593	602213593	240	243
5	602213557	602213557	255	264
6	602213513	602213513	276	287
7	602213480	602213480	290	306
8	602213446	602213446	304	326
9	602213407	602213407	320	349
10	602213375	602213375	334	367

Table 15: Symmetry breaking simulation scenario A, subset K.

t /s	[A]	[B]	[RC]	[SC]
0	602214076	602214076	0	0
0.006	602214075	602214075	1	0
0.013	602214074	602214074	1	1
0.02	602214073	602214073	1	2
0.03	602214069	602214069	2	5
0.079	602214062	602214062	4	10
0.16	602214039	602214039	16	21
0.2	602214024	602214024	25	27
0.28	602213997	602213997	37	42
1	602213706	602213706	178	192
2	602212859	602212859	573	644
3	602211032	602211032	1381	1663
4	602207264	602207264	3005	3807

5	602199321	602199321	6561	8194
6	602182870	602182870	14005	17201
7	602148923	602148923	29411	35742
8	602077896	602077896	61520	74660
9	601928684	601928684	128912	156480
10	601619871	601619871	268331	325874

Table 16: Symmetry breaking simulation scenario A, subset L.

t /s	[A]	[B]	[RC]	[SC]
0	602214076	602214076	0	0
0.002	602214075	602214075	1	0
0.005	602214074	602214074	1	1
0.023	602214071	602214071	1	4
0.1	602214051	602214051	11	14
0.34	602214009	602214009	36	31
0.376	602213998	602213998	39	39
0.43	602213985	602213985	45	46
0.5	602213965	602213965	54	57
0.58	602213942	602213942	64	70
0.81	602213902	602213902	80	94
1	602213867	602213867	98	111
2	602213732	602213732	159	185
3	602213648	602213648	196	232
4	602213593	602213593	228	255
5	602213544	602213544	251	281
6	602213493	602213493	280	303
7	602213455	602213455	299	322
8	602213418	602213418	314	344
9	602213393	602213393	327	356
10	602213372	602213372	339	365

Table 17: Symmetry breaking simulation scenario A, subset M.

t /s	[A]	[B]	[RC]	[SC]
0	602214076	602214076	0	0
0.001	602214074	602214074	2	0
0.003	602214072	602214072	3	1
0.008	602214060	602214060	8	8
0.014	602214046	602214046	14	16
0.03	602214000	602214000	43	33
0.08	602213881	602213881	103	92
0.18	602213641	602213641	214	221
0.44	602213062	602213062	504	510
0.58	602212779	602212779	640	657
0.77	602212429	602212429	815	832
1	602211995	602211995	1022	1059
2	602210737	602210737	1662	1677
3	602209950	602209950	2069	2057

4	602209363	602209363	2365	2348
5	602208892	602208892	2583	2601
6	602208517	602208517	2778	2781
7	602208205	602208205	2917	2954
8	602207949	602207949	3061	3066
9	602207753	602207753	3167	3156
10	602207579	602207579	3258	3239

Table 18: Symmetry breaking simulation scenario A, subset N.

t /s	[A]	[B]	[RC]	[SC]
0	602214076	602214076	0	0
0.001	602214074	602214074	1	1
0.002	602214071	602214071	3	2
0.003	602214066	602214066	6	4
0.02	602214021	602214021	30	25
0.14	602213730	602213730	170	176
0.65	602212548	602212548	782	746
1	602211886	602211886	1111	1079
2	602210604	602210604	1735	1737
3	602209696	602209696	2212	2168
4	602209046	602209046	2528	2502
5	602208551	602208551	2754	2771
6	602208109	602208109	2987	2980
7	602207743	602207743	3174	3159
8	602207437	602207437	3338	3301
9	602207150	602207150	3479	3447
10	602206908	602206908	3600	3568

Table 19: Symmetry breaking simulation scenario A, subset O.

t /s	[A]	[B]	[RC]	[SC]
0	602214076	602214076	0	0
0.001	602214072	602214072	1	3
0.03	602214005	602214005	31	40
0.39	602213006	602213006	581	489
1	602210381	602210381	1886	1809
2	602202275	602202275	5985	5816
3	602184541	602184541	14954	14581
4	602146575	602146575	34096	33405
5	602066774	602066774	74670	72632
6	601901028	601901028	158761	154287
7	601556260	601556260	333222	324594
8	600838945	600838945	697225	677906
9	599358951	599358951	1447068	1408057
10	596324404	596324404	2985646	2904026

Table 20: Symmetry breaking simulation scenario A, subset P.

t /s	[A]	[B]	[RC]	[SC]
0	602214076	602214076	0	0
0.001	602214073	602214073	3	0
0.002	602214071	602214071	3	2
0.02	602214017	602214017	20	39
0.086	602213851	602213851	100	125
0.413	602213025	602213025	500	551
1	602211921	602211921	1064	1091
2	602210700	602210700	1694	1682
3	602209818	602209818	2140	2118
4	602209198	602209198	2442	2436
5	602208737	602208737	2669	2670
6	602208393	602208393	2836	2847
7	602208109	602208109	2979	2988
8	602207868	602207868	3107	3101
9	602207658	602207658	3229	3189
10	602207493	602207493	3306	3277

7.1.2 Scenario B

Table 21: Symmetry breaking simulation scenario B, subset A.

t /s	[A]	[B]	[RC]	[SC]	[RDcat]	[SDcat]
0	602214076	602214076	0	0	0	0
1	602214075	602214075	1	0	0	0
2	602214073	602214073	3	0	0	0
3	602214073	602214073	3	0	0	0
4	602214071	602214071	4	1	0	0
5	602214070	602214070	4	2	0	0
6	602214070	602214070	4	2	0	0
7	602214070	602214070	4	2	0	0
8	602214070	602214070	4	2	0	0
9	602214070	602214070	4	2	0	0
10	602214069	602214069	4	3	0	0

Table 22: Symmetry breaking simulation scenario B, subset B.

t /s	[A]	[B]	[RC]	[SC]	[RDcat]	[SDcat]
0	602214076	602214076	0	0	0	0
0.598	602214075	602214075	1	0	0	0
0.621	602214074	602214074	1	1	0	0

1	602214073	602214073	2	1	0	0
2	602214070	602214070	3	3	0	0
3	602214070	602214070	3	3	0	0
4	602214069	602214069	3	4	0	0
5	602214068	602214068	4	4	0	0
6	602214068	602214068	4	4	0	0
7	602214067	602214067	5	4	0	0
8	602214067	602214067	5	4	0	0
9	602214067	602214067	5	4	0	0
10	602214067	602214067	5	4	0	0

Table 23: Symmetry breaking simulation scenario B, subset C.

t /s	[A]	[B]	[RC]	[SC]	[RDcat]	[SDcat]
0	602214076	602214076	0	0	0	0
0.115	602214075	602214075	1	0	0	0
0.389	602214074	602214074	2	0	0	0
1	602214073	602214073	3	0	0	0
1.618	602214070	602214070	5	1	0	0
2	602214070	602214070	5	1	0	0
3	602214069	602214069	6	1	0	0
4	602214068	602214068	6	2	0	0
5	602214068	602214068	6	2	0	0
6	602214067	602214067	6	3	0	0
7	602214065	602214065	8	3	0	0
8	602214065	602214065	8	3	0	0
9	602214065	602214065	8	3	0	0
10	602214063	602214064	8	3	1	0

Table 24: Symmetry breaking simulation scenario B, subset D.

t /s	[A]	[B]	[RC]	[SC]	[RDcat]	[SDcat]
0	602214076	602214076	0	0	0	0
0.13	602214075	602214075	0	1	0	0
0.391	602214074	602214074	1	1	0	0
1	602214072	602214072	2	2	1	0
2	602214070	602214070	2	4	1	0
3	602214070	602214070	2	4	1	0
4	602214070	602214070	2	4	1	0
5	602214069	602214069	2	5	1	0
6	602214065	602214066	3	6	1	1
7	602214065	602214066	3	6	1	1
8	602214064	602214065	3	7	1	1
9	602214064	602214065	3	7	1	1
10	602214064	602214065	3	7	1	1

Table 25: Symmetry breaking simulation scenario B, subset E.

t /s	[A]	[B]	[RC]	[SC]	[RDcat]	[SDcat]
0	602214076	602214076	0	0	0	0
0.015	602214075	602214075	1	0	0	0

0.33	602214071	602214071	5	0	0	0
0.408	602214069	602214069	6	1	0	0
1	602214060	602214061	10	4	1	0
2	602214039	602214041	19	14	1	1
3	602214026	602214029	27	17	2	1
4	602214021	602214024	29	20	2	1
5	602214016	602214019	33	21	2	1
6	602214008	602214011	35	27	2	1
7	602214004	602214007	38	28	2	1
8	602214000	602214004	38	30	3	1
9	602213992	602213998	36	36	5	1
10	602213989	602213995	38	37	5	1

Table 26: Symmetry breaking simulation scenario B, subset F.

t /s	[A]	[B]	[RC]	[SC]	[RDcat]	[SDcat]
0	602214076	602214076	0	0	0	0
0.008	602214075	602214075	1	0	0	0
0.214	602214071	602214071	4	1	0	0
1	602214060	602214060	9	7	0	0
2	602214048	602214048	16	12	0	0
3	602214037	602214038	19	18	1	0
4	602214029	602214030	24	21	1	0
5	602214021	602214023	26	25	1	1
6	602214014	602214017	29	27	1	2
7	602214010	602214013	29	31	1	2
8	602214008	602214012	29	31	1	3
9	602214002	602214006	34	32	1	3
10	602213996	602214002	35	33	3	3

Table 27: Symmetry breaking simulation scenario B, subset G.

t /s	[A]	[B]	[RC]	[SC]	[RDcat]	[SDcat]
0	602214076	602214076	0	0	0	0
0.037	602214075	602214075	0	1	0	0
0.29	602214072	602214072	1	3	0	0
1	602214061	602214061	6	9	0	0
2	602214047	602214048	11	16	0	1
3	602214035	602214037	16	21	0	2
4	602214030	602214032	18	24	0	2
5	602214025	602214027	21	26	0	2
6	602214017	602214020	25	28	1	2
7	602214007	602214010	32	31	1	2
8	602214000	602214004	34	34	2	2
9	602213995	602214001	34	35	3	2
10	602213987	602213994	38	37	3	3

Table 28: Symmetry breaking simulation scenario B, subset H.

t /s	[A]	[B]	[RC]	[SC]	[RDcat]	[SDcat]

0	602214076	602214076	0	0	0	0
0.001	602214075	602214075	0	1	0	0
0.055	602214074	602214074	1	1	0	0
0.57	602214055	602214056	13	6	0	1
1	602214044	602214046	16	12	1	1
2	602214029	602214032	22	19	1	1
3	602214022	602214026	24	22	1	1
4	602214014	602214019	27	25	1	1
5	602214008	602214014	29	27	1	1
6	602214003	602214009	32	29	1	1
7	602214001	602214007	33	30	1	1
8	602213996	602214004	32	32	1	1
9	602213992	602214000	36	32	1	1
10	602213985	602213994	38	35	1	1

Table 29: Symmetry breaking simulation scenario B, subset I.

t /s	[A]	[B]	[RC]	[SC]	[RDcat]	[SDcat]
0	602214076	602214076	0	0	0	0
0.006	602214075	602214075	0	1	0	0
0.01	602214074	602214074	1	1	0	0
0.062	602214062	602214063	6	6	1	0
0.34	602214007	602214008	35	32	1	0
0.64	602213949	602213950	54	71	1	0
1	602213893	602213894	83	98	1	0
2	602213745	602213750	164	157	3	2
3	602213628	602213638	210	218	5	5
4	602213528	602213544	250	266	8	8
5	602213459	602213476	275	308	8	9
6	602213418	602213436	292	330	8	10
7	602213389	602213409	301	346	9	11
8	602213372	602213394	306	354	11	11
9	602213358	602213380	311	363	11	11
10	602213351	602213375	311	366	11	13

Table 30: Symmetry breaking simulation scenario B, subset J.

t /s	[A]	[B]	[RC]	[SC]	[RDcat]	[SDcat]
0	602214076	602214076	0	0	0	0
0.008	602214074	602214074	1	1	0	0
0.106	602214052	602214052	14	10	0	0
0.19	602214036	602214036	20	20	0	0
0.725	602213905	602213906	75	94	1	0
1	602213856	602213857	99	119	1	0
2	602213711	602213718	164	187	2	5
3	602213612	602213629	206	224	8	9
4	602213534	602213559	243	249	12	13
5	602213471	602213498	285	266	12	15
6	602213413	602213447	312	283	15	19

7	602213365	602213405	334	297	16	24
8	602213319	602213368	357	302	20	29
9	602213288	602213341	369	313	23	30
10	602213263	602213323	372	321	27	33

Table 31: Symmetry breaking simulation scenario B, subset K.

t /s	[A]	[B]	[RC]	[SC]	[RDcat]	[SDcat]
0	602214076	602214076	0	0	0	0
0.004	602214075	602214075	1	0	0	0
0.014	602214074	602214074	1	1	0	0
0.106	602214059	602214059	10	7	0	0
0.48	602213968	602213968	60	48	0	0
1	602213864	602213868	114	90	3	0
2	602213708	602213718	187	161	5	2
3	602213601	602213613	225	226	5	2
4	602213511	602213529	260	269	5	2
5	602213444	602213469	284	298	5	2
6	602213396	602213425	299	323	5	2
7	602213361	602213399	312	327	5	2
8	602213326	602213370	324	338	5	2
9	602213292	602213343	340	342	5	2
10	602213261	602213316	351	354	1	6

Table 32: Symmetry breaking simulation scenario B, subset L.

t /s	[A]	[B]	[RC]	[SC]	[RDcat]	[SDcat]
0	602214076	602214076	0	0	0	0
0.001	602214075	602214075	0	1	0	0
0.005	602214074	602214074	1	1	0	0
0.08	602214059	602214059	10	7	0	0
0.4	602213983	602213983	51	42	0	0
0.654	602213925	602213926	71	78	1	0
1	602213857	602213860	107	106	2	1
2	602213733	602213741	168	159	3	2
3	602213638	602213656	210	192	6	3
4	602213543	602213566	254	233	4	1
5	602213457	602213487	286	273	5	1
6	602213415	602213450	308	283	5	1
7	602213369	602213408	323	306	4	1
8	602213328	602213371	339	323	3	1
9	602213294	602213345	342	338	8	1
10	602213257	602213313	355	352	4	0

Table 33: Symmetry breaking simulation scenario B, subset M.

t /s	[A]	[B]	[RC]	[SC]	[RDcat]	[SDcat]
0	602214076	602214076	0	0	0	0
0.001	602214075	602214075	0	1	0	0
0.002	602214073	602214073	2	1	0	0
0.01	602214058	602214058	10	8	0	0

0.15	602213717	602213717	171	188	0	0
0.425	602213031	602213032	507	536	0	1
0.445	602212989	602212992	527	554	1	2
1	602212021	602212032	1021	1012	2	9
2	602210634	602210674	1723	1639	18	22
3	602209569	602209668	2241	2068	48	51
4	602208832	602208994	2575	2345	80	82
5	602208260	602208481	2790	2584	113	108
6	602207802	602208071	2986	2750	140	129
7	602207408	602207718	3165	2883	158	152
8	602207097	602207452	3291	2978	181	174
9	602206853	602207239	3400	3051	195	191
10	602206624	602207043	3462	3152	213	206

Table 34: Symmetry breaking simulation scenario B, subset N.

t /s	[A]	[B]	[RC]	[SC]	[RDcat]	[SDcat]
0	602214076	602214076	0	0	0	0
0.001	602214074	602214074	0	2	0	0
0.002	602214069	602214069	2	5	0	0
0.05	602213952	602213952	55	69	0	0
0.21	602213573	602213574	238	263	1	0
0.395	602213120	602213123	463	487	2	1
1	602211908	602211933	1048	1070	10	15
2	602210509	602210577	1718	1713	25	43
3	602209397	602209520	2232	2201	52	71
4	602208683	602208869	2568	2453	80	106
5	602208125	602208369	2806	2657	105	136
6	602207639	602207940	3005	2830	133	163
7	602207266	602207610	3146	2976	151	184
8	602206951	602207347	3273	3060	171	213
9	602206682	602207124	3377	3133	195	233
10	602206422	602206904	3483	3207	215	253

Table 35: Symmetry breaking simulation scenario B, subset O.

t /s	[A]	[B]	[RC]	[SC]	[RDcat]	[SDcat]
0	602214076	602214076	0	0	0	0
0.001	602214072	602214072	0	4	0	0
0.002	602214069	602214069	1	6	0	0
0.08	602213871	602213871	112	93	0	0
0.209	602213571	602213572	252	251	0	1
0.303	602213342	602213345	371	357	1	2
0.438	602213075	602213083	512	473	4	4
1	602211967	602211984	1083	992	6	5
2	602210470	602210539	1788	1680	20	19
3	602209458	602209590	2244	2110	32	26
4	602208620	602208807	2619	2463	34	27
5	602207978	602208223	2904	2704	40	25

6	602207480	602207773	3105	2905	46	25
7	602207041	602207393	3278	3053	37	33
8	602206667	602207084	3403	3172	50	37
9	602206312	602206770	3546	3302	39	21
10	602205993	602206505	3655	3404	39	27

Table 36: Symmetry breaking simulation scenario B, subset P.

t /s	[A]	[B]	[RC]	[SC]	[RDcat]	[SDcat]
0	602214076	602214076	0	0	0	0
0.001	602214068	602214068	2	6	0	0
0.03	602214003	602214003	33	40	0	0
0.22	602213522	602213523	259	293	0	0
0.489	602212964	602212966	541	567	0	1
0.575	602212805	602212809	627	636	1	2
1	602212027	602212042	1018	1001	3	6
2	602210511	602210576	1753	1682	15	20
3	602209384	602209513	2269	2165	26	33
4	602208568	602208755	2653	2481	33	37
5	602207874	602208126	2956	2742	40	35
6	602207322	602207632	3182	2952	38	34
7	602206873	602207242	3340	3125	34	37
8	602206476	602206903	3470	3276	36	30
9	602206122	602206607	3596	3388	39	39
10	602205840	602206376	3695	3469	41	29

7.1.3 Scenario C

Table 37: Symmetry breaking simulation scenario C, subset A.

t /s	[A]	[B]	[RC]	[SC]	[Dimer]
0	602214076	602214076	0	0	0
0.329	602214075	602214075	1	0	0
0.766	602214074	602214074	1	1	0
1	602214074	602214074	1	1	0
2	602214073	602214073	1	2	0
3	602214073	602214073	1	2	0
4	602214071	602214071	1	4	0
5	602214071	602214071	1	4	0
6	602214071	602214071	0	3	1
7	602214071	602214071	0	3	1
8	602214070	602214070	1	3	1
9	602214070	602214070	1	3	1
10	602214070	602214070	1	3	1

Table 38: Symmetry breaking simulation scenario C, subset B.

t /s	[A]	[B]	[RC]	[SC]	[Dimer]

0	602214076	602214076	0	0	0
1	602214076	602214076	0	0	0
1.115	602214075	602214075	0	1	0
1.191	602214074	602214074	1	1	0
2	602214073	602214073	2	1	0
3	602214071	602214071	2	3	0
4	602214071	602214071	2	3	0
5	602214071	602214071	2	3	0
6	602214071	602214071	2	3	0
7	602214071	602214071	2	3	0
8	602214071	602214071	2	3	0
9	602214070	602214070	3	3	0
10	602214069	602214069	3	4	0

Table 39: Symmetry breaking simulation scenario C, subset C.

t /s	[A]	[B]	[RC]	[SC]	[Dimer]
0	602214076	602214076	0	0	0
0.121	602214075	602214075	1	0	0
1	602214073	602214073	2	0	1
2	602214070	602214070	4	0	1
3	602214052	602214052	19	3	1
4	602214015	602214015	48	11	1
5	602213960	602213960	91	23	1
6	602213823	602213823	188	63	1
7	602213534	602213534	400	140	1
8	602212929	602212929	831	314	1
9	602211726	602211726	1742	606	1
10	602209191	602209191	3611	1272	1

Table 40: Symmetry breaking simulation scenario C, subset D.

t /s	[A]	[B]	[RC]	[SC]	[Dimer]
0	602214076	602214076	0	0	0
0.04	602214075	602214075	1	0	0
0.773	602214071	602214071	4	0	1
1	602214067	602214067	7	0	1
2	602214046	602214046	25	3	1
3	602214007	602214007	56	11	1
4	602213932	602213932	117	25	1
5	602213782	602213782	237	55	1
6	602213481	602213481	474	119	1
7	602212855	602212855	974	245	1
8	602211552	602211552	2003	519	1
9	602208779	602208779	4225	1070	1
10	602203047	602203047	8881	2146	1

Table 41: Symmetry breaking simulation scenario C, subset E.

t /s	[A]	[B]	[RC]	[SC]	[Dimer]
0	602214076	602214076	0	0	0
0.067	602214075	602214075	0	1	0
0.117	602214073	602214073	1	2	0
0.38	602214066	602214066	3	7	0
1	602214053	602214053	11	12	0
2	602214042	602214042	17	17	0
3	602214034	602214034	19	21	1
4	602214025	602214025	24	25	1
5	602214019	602214019	27	28	1
6	602214012	602214012	30	32	1
7	602214007	602214007	33	34	1
8	602214003	602214003	36	35	1
9	602214001	602214001	37	36	1
10	602214000	602214000	38	36	1

Table 42: Symmetry breaking simulation scenario C, subset F.

t /s	[A]	[B]	[RC]	[SC]	[Dimer]
0	602214076	602214076	0	0	0
0.038	602214075	602214075	1	0	0
0.076	602214074	602214074	1	1	0
0.17	602214070	602214070	3	3	0
0.24	602214066	602214066	6	4	0
0.598	602214055	602214055	16	5	0
1	602214051	602214051	17	8	0
2	602214046	602214046	20	10	0
3	602214042	602214042	23	11	0
4	602214026	602214026	33	17	0
5	602214023	602214023	36	17	0
6	602214018	602214018	39	19	0
7	602214015	602214015	40	21	0
8	602214012	602214012	42	22	0
9	602214009	602214009	43	24	0
10	602214003	602214003	47	26	0

Table 43: Symmetry breaking simulation scenario C, subset G.

t /s	[A]	[B]	[RC]	[SC]	[Dimer]
0	602214076	602214076	0	0	0
0.021	602214075	602214075	1	0	0
0.395	602214067	602214067	8	1	0
0.6	602214059	602214059	13	4	0
1	602214044	602214044	21	11	0
2	602213963	602213963	61	52	0
3	602213762	602213762	191	123	0
4	602213377	602213377	413	286	0

5	602212602	602212602	864	610	0
6	602210888	602210888	1835	1351	1
7	602207404	602207404	3872	2798	1
8	602200008	602200008	8139	5927	1
9	602184667	602184667	17017	12390	1
10	602152748	602152748	35587	25739	1

Table 44: Symmetry breaking simulation scenario C, subset H.

t /s	[A]	[B]	[RC]	[SC]	[Di-mer]
0	602214076	602214076	0	0	0
0.006	602214075	602214075	0	1	0
0.074	602214074	602214074	1	1	0
0.265	602214065	602214065	5	6	0
0.718	602214043	602214043	16	17	0
0.844	602214034	602214034	21	21	0
1	602214021	602214021	30	25	0
2	602213926	602213926	78	70	1
3	602213720	602213720	164	190	1
4	602213335	602213335	349	390	1
5	602212522	602212522	716	836	1
6	602210764	602210764	1531	1779	1
7	602207168	602207168	3186	3720	1
8	602199687	602199687	6610	7777	1
9	602184490	602184490	13574	16010	1
10	602152133	602152133	28491	33450	1

Table 45: Symmetry breaking simulation scenario C, subset I.

t /s	[A]	[B]	[RC]	[SC]	[Di-mer]
0	602214076	602214076	0	0	0
0.005	602214075	602214075	1	0	0
0.008	602214073	602214073	2	1	0
0.058	602214060	602214060	10	6	0
0.258	602214002	602214002	38	36	0
0.454	602213951	602213951	63	62	0
0.496	602213942	602213942	64	70	0
0.885	602213872	602213872	95	107	1
1	602213846	602213846	106	122	1
2	602213684	602213684	192	198	1
3	602213607	602213607	224	243	1
4	602213539	602213539	256	279	1
5	602213476	602213476	285	313	1

6	602213431	602213431	308	335	1
7	602213402	602213402	324	348	1
8	602213380	602213380	329	365	1
9	602213355	602213355	337	382	1
10	602213330	602213330	346	398	1

Table 46: Symmetry breaking simulation scenario C, subset J.

t /s	[A]	[B]	[RC]	[SC]	[Di-mer]
0	602214076	602214076	0	0	0
0.011	602214075	602214075	0	1	0
0.025	602214071	602214071	1	4	0
0.084	602214052	602214052	10	14	0
0.64	602213925	602213925	70	81	0
0.924	602213869	602213869	97	110	0
1	602213857	602213857	101	118	0
2	602213724	602213724	164	188	0
3	602213620	602213620	223	233	0
4	602213528	602213528	265	283	0
5	602213489	602213489	283	302	1
6	602213447	602213447	304	323	1
7	602213403	602213403	326	345	1
8	602213370	602213370	343	361	1
9	602213346	602213346	355	373	1
10	602213326	602213326	364	384	1

Table 47: Symmetry breaking simulation scenario C, subset K.

t /s	[A]	[B]	[RC]	[SC]	[Di-mer]
0	602214076	602214076	0	0	0
0.002	602214075	602214075	1	0	0
0.02	602214071	602214071	4	1	0
0.233	602214003	602214003	40	33	0
0.588	602213880	602213880	100	96	0
1	602213667	602213667	214	195	0
2	602212853	602212853	617	606	0
3	602211019	602211019	1531	1526	0
4	602207081	602207081	3496	3497	1
5	602198985	602198985	7527	7560	2
6	602181791	602181791	16011	16270	2
7	602146188	602146188	33651	34233	2
8	602072413	602072413	69803	71852	4
9	601919563	601919563	144800	149673	20
10	601603017	601603017	299868	311011	90

Table 48: Symmetry breaking simulation scenario C, subset L.

t /s	[A]	[B]	[RC]	[SC]	[Di-mer]

0	602214076	602214076	0	0	0
0.003	602214075	602214075	0	1	0
0.007	602214072	602214072	3	1	0
0.054	602214060	602214060	6	10	0
0.37	602213964	602213964	50	62	0
0.84	602213767	602213767	144	165	0
1	602213672	602213672	188	216	0
2	602212739	602212739	665	672	0
3	602210709	602210709	1708	1659	0
4	602206456	602206456	3903	3717	0
5	602197796	602197796	8442	7838	0
6	602179768	602179768	17784	16524	0
7	602141869	602141869	37279	34928	0
8	602063935	602063935	77164	72975	1
9	601901397	601901397	160326	152321	16
10	601565108	601565108	332081	316715	86

Table 49: Symmetry breaking simulation scenario C, subset M.

t /s	[A]	[B]	[RC]	[SC]	[Di-mer]
0	602214076	602214076	0	0	0
0.001	602214074	602214074	1	1	0
0.04	602214005	602214005	43	28	0
0.14	602213749	602213749	175	152	0
0.45	602213024	602213024	535	517	0
1	602211951	602211951	1037	1086	1
2	602210437	602210437	1766	1871	1
3	602209439	602209439	2261	2374	1
4	602208740	602208740	2594	2740	1
5	602208237	602208237	2854	2983	1
6	602207810	602207810	3051	3213	1
7	602207484	602207484	3213	3377	1
8	602207250	602207250	3325	3499	1
9	602207063	602207063	3413	3598	1
10	602206901	602206901	3486	3687	1

Table 50: Symmetry breaking simulation scenario C, subset N.

t /s	[A]	[B]	[RC]	[SC]	[Di-mer]
0	602214076	602214076	0	0	0
0.001	602214075	602214075	0	1	0
0.002	602214072	602214072	1	3	0
0.1	602213865	602213865	106	105	0
0.35	602213267	602213267	407	402	0
1	602212004	602212004	1009	1063	0
2	602210521	602210521	1753	1802	0
3	602209477	602209477	2263	2334	1
4	602208743	602208743	2650	2681	1
5	602208159	602208159	2953	2962	1
6	602207687	602207687	3158	3229	1

7	602207308	602207308	3329	3437	1
8	602206933	602206933	3505	3636	1
9	602206653	602206653	3633	3788	1
10	602206371	602206371	3756	3947	1

Table 51: Symmetry breaking simulation scenario C, subset O.

t /s	[A]	[B]	[RC]	[SC]	[Dimer]
0	602214076	602214076	0	0	0
0.002	602214075	602214075	0	1	0
0.003	602214071	602214071	3	2	0
0.02	602214020	602214020	32	24	0
0.1	602213822	602213822	141	113	0
0.37	602213063	602213063	517	496	0
1	602210349	602210349	1905	1822	0
2	602202098	602202098	6105	5873	0
3	602184259	602184259	15220	14597	0
4	602146196	602146196	34682	33198	0
5	602066730	602066730	75061	72281	2
6	601900484	601900484	159788	153764	20
7	601556027	601556027	334769	323084	98
8	600840748	600840748	698081	674417	415
9	599368864	599368864	1444656	1396956	1800
10	596355900	596355900	2970735	2871667	7887

Table 52: Symmetry breaking simulation scenario C, subset P.

t /s	[A]	[B]	[RC]	[SC]	[Dimer]
0	602214076	602214076	0	0	0
0.001	602214071	602214071	3	2	0
0.02	602214018	602214018	26	32	0
0.12	602213757	602213757	150	169	0
0.37	602213007	602213007	533	536	0
0.61	602212178	602212178	948	950	0
0.91	602210801	602210801	1651	1624	0
1	602210357	602210357	1878	1841	0
2	602202320	602202320	5917	5839	0
3	602184621	602184621	14814	14639	1
4	602147152	602147152	33472	33446	3
5	602068083	602068083	72988	72995	5
6	601903923	601903923	154471	155642	20
7	601563182	601563182	324107	326631	78
8	600854809	600854809	676293	682130	422
9	599396129	599396129	1399756	1414661	1765
10	596419538	596419538	2876617	2902429	7746

7.1.4 Scenario D

Table 53: Symmetry breaking simulation scenario D, subset A.

t /s	[A]	[B]	[RCat]	[SCat]	[D]	[E]	[RF]	[SF]
0	602214	602214	0	0	301107038	301107038	0	0
1	602214	602214	0	0	301107038	301107038	0	0
2	602214	602214	0	0	301107038	301107038	0	0
3	602214	602214	0	0	301107038	301107038	0	0
4	602214	602214	0	0	301107038	301107038	0	0
5	602214	602214	0	0	301107038	301107038	0	0
6	602214	602214	0	0	301107038	301107038	0	0
7	602214	602214	0	0	301107038	301107038	0	0
8	602214	602214	0	0	301107038	301107038	0	0
9	602214	602214	0	0	301107038	301107038	0	0
10	602214	602214	0	0	301107038	301107038	0	0

Table 54: Symmetry breaking simulation scenario D, subset B.

t /s	[A]	[B]	[RCat]	[SCat]	[D]	[E]	[RF]	[SF]
0	602214	602214	0	0	301107038	301107038	0	0
1	602214	602214	0	0	301107038	301107038	0	0
2	602214	602214	0	0	301107038	301107038	0	0
3	602214	602214	0	0	301107038	301107038	0	0
4	602214	602214	0	0	301107038	301107038	0	0
5	602214	602214	0	0	301107038	301107038	0	0
6	602214	602214	0	0	301107038	301107038	0	0
7	602214	602214	0	0	301107038	301107038	0	0
8	602214	602214	0	0	301107038	301107038	0	0
9	602214	602214	0	0	301107038	301107038	0	0
10	602214	602214	0	0	301107038	301107038	0	0

Table 55: Symmetry breaking simulation scenario D, subset C.

t /s	[A]	[B]	[RCat]	[SCat]	[D]	[E]	[RF]	[SF]
0	602214	602214	0	0	301107038	301107038	0	0
1	602214	602214	0	0	301107038	301107038	0	0
1.425	602214	602214	0	0	301107037	301107037	1	0
2	602214	602214	0	0	301107037	301107037	1	0
3	602214	602214	0	0	301107037	301107037	1	0
4	602214	602214	0	0	301107037	301107037	1	0
5	602214	602214	0	0	301107037	301107037	1	0
6	602214	602214	0	0	301107037	301107037	1	0
7	602214	602214	0	0	301107037	301107037	1	0
8	602214	602214	0	0	301107037	301107037	1	0
9	602214	602214	0	0	301107037	301107037	1	0
10	602214	602214	0	0	301107037	301107037	1	0

Table 56: Symmetry breaking simulation scenario D, subset D.

t /s	[A]	[B]	[RCat]	[SCat]	[D]	[E]	[RF]	[SF]

0	602214	602214	0	0	301107038	301107038	0	0
1	602214	602214	0	0	301107038	301107038	0	0
2	602214	602214	0	0	301107038	301107038	0	0
3	602214	602214	0	0	301107038	301107038	0	0
4	602214	602214	0	0	301107038	301107038	0	0
5	602214	602214	0	0	301107038	301107038	0	0
6	602214	602214	0	0	301107038	301107038	0	0
6.194	602214	602214	0	0	301107037	301107037	1	0
7	602214	602214	0	0	301107037	301107037	1	0
8	602214	602214	0	0	301107037	301107037	1	0
9	602214	602214	0	0	301107037	301107037	1	0
10	602214	602214	0	0	301107037	301107037	1	0

Table 57: Symmetry breaking simulation scenario D, subset E.

t /s	[A]	[B]	[RCat]	[SCat]	[D]	[E]	[RF]	[SF]
0	602214	602214	0	0	301107038	301107038	0	0
1	602214	602214	0	0	301107038	301107038	0	0
2	602214	602214	0	0	301107038	301107038	0	0
3	602214	602214	0	0	301107038	301107038	0	0
4	602214	602214	0	0	301107038	301107038	0	0
5	602214	602214	0	0	301107038	301107038	0	0
6	602214	602214	0	0	301107038	301107038	0	0
7	602214	602214	0	0	301107038	301107038	0	0
8	602214	602214	0	0	301107038	301107038	0	0
9	602214	602214	0	0	301107038	301107038	0	0
10	602214	602214	0	0	301107038	301107038	0	0

Table 58: Symmetry breaking simulation scenario D, subset F.

t /s	[A]	[B]	[RCat]	[SCat]	[D]	[E]	[RF]	[SF]
0	602214	602214	0	0	301107038	301107038	0	0
1	602214	602214	0	0	301107038	301107038	0	0
2	602214	602214	0	0	301107038	301107038	0	0
3	602214	602214	0	0	301107038	301107038	0	0
4	602214	602214	0	0	301107038	301107038	0	0
5	602214	602214	0	0	301107038	301107038	0	0
6	602214	602214	0	0	301107038	301107038	0	0
7	602214	602214	0	0	301107038	301107038	0	0
8	602214	602214	0	0	301107038	301107038	0	0
9	602214	602214	0	0	301107038	301107038	0	0
10	602214	602214	0	0	301107038	301107038	0	0

Table 59: Symmetry breaking simulation scenario D, subset G.

t /s	[A]	[B]	[RCat]	[SCat]	[D]	[E]	[RF]	[SF]
0	602214	602214	0	0	301107038	301107038	0	0
1	602214	602214	0	0	301107038	301107038	0	0
2	602214	602214	0	0	301107038	301107038	0	0
3	602214	602214	0	0	301107038	301107038	0	0
4	602214	602214	0	0	301107038	301107038	0	0
5	602214	602214	0	0	301107038	301107038	0	0
6	602214	602214	0	0	301107038	301107038	0	0

6.126	602214	602214	0	1	301107037	301107037	0	1
7	602214	602214	0	1	301107037	301107037	0	1
8	602214	602214	0	1	301107037	301107037	0	1
9	602214	602214	0	1	301107037	301107037	0	1
10	602214	602214	0	1	301107037	301107037	0	1

Table 60: Symmetry breaking simulation scenario D, subset H.

t /s	[A]	[B]	[RCat]	[SCat]	[D]	[E]	[RF]	[SF]
0	602214	602214	0	0	301107038	301107038	0	0
1	602214	602214	0	0	301107038	301107038	0	0
2	602214	602214	0	0	301107038	301107038	0	0
3	602214	602214	0	0	301107038	301107038	0	0
4	602214	602214	0	0	301107038	301107038	0	0
5	602214	602214	0	0	301107038	301107038	0	0
6	602214	602214	0	0	301107038	301107038	0	0
7	602214	602214	0	0	301107038	301107038	0	0
8	602214	602214	0	0	301107038	301107038	0	0
9	602214	602214	0	0	301107038	301107038	0	0
10	602214	602214	0	0	301107038	301107038	0	0

Table 61: Symmetry breaking simulation scenario D, subset I.

t /s	[A]	[B]	[RCat]	[SCat]	[D]	[E]	[RF]	[SF]
0	602214	602214	0	0	301107038	301107038	0	0
1	602214	602214	0	0	301107038	301107038	0	0
2	602214	602214	0	0	301107038	301107038	0	0
3	602214	602214	0	0	301107038	301107038	0	0
4	602214	602214	0	0	301107038	301107038	0	0
5	602214	602214	0	0	301107038	301107038	0	0
6	602214	602214	0	0	301107038	301107038	0	0
7	602214	602214	0	0	301107038	301107038	0	0
8	602214	602214	0	0	301107038	301107038	0	0
9	602214	602214	0	0	301107038	301107038	0	0
10	602214	602214	0	0	301107038	301107038	0	0

Table 62: Symmetry breaking simulation scenario D, subset J.

t /s	[A]	[B]	[RCat]	[SCat]	[D]	[E]	[RF]	[SF]
0	602214	602214	0	0	301107038	301107038	0	0
1	602214	602214	0	0	301107038	301107038	0	0
2	602214	602214	0	0	301107038	301107038	0	0
3	602214	602214	0	0	301107038	301107038	0	0
4	602214	602214	0	0	301107038	301107038	0	0
5	602214	602214	0	0	301107038	301107038	0	0
6	602214	602214	0	0	301107038	301107038	0	0
7	602214	602214	0	0	301107038	301107038	0	0
8	602214	602214	0	0	301107038	301107038	0	0
9	602214	602214	0	0	301107038	301107038	0	0

10	602214	602214	0	0	301107038	301107038	0	0

Table 63: Symmetry breaking simulation scenario D, subset K.

t /s	[A]	[B]	[RCat]	[SCat]	[D]	[E]	[RF]	[SF]
0	602214	602214	0	0	301107038	301107038	0	0
1	602214	602214	0	0	301107038	301107038	0	0
2	602214	602214	0	0	301107038	301107038	0	0
3	602214	602214	0	0	301107038	301107038	0	0
4	602214	602214	0	0	301107038	301107038	0	0
4.099	602214	602214	0	1	301107037	301107037	0	1
5	602214	602214	0	1	301107037	301107037	0	1
6	602214	602214	0	1	301107037	301107037	0	1
7	602214	602214	0	1	301107037	301107037	0	1
8	602214	602214	0	1	301107037	301107037	0	1
9	602214	602214	0	1	301107037	301107037	0	1
10	602214	602214	0	1	301107037	301107037	0	1

Table 64: Symmetry breaking simulation scenario D, subset L.

t /s	[A]	[B]	[RCat]	[SCat]	[D]	[E]	[RF]	[SF]
0	602214	602214	0	0	301107038	301107038	0	0
0.852	602214	602214	1	0	301107037	301107037	1	0
1	602214	602214	1	0	301107037	301107037	1	0
2	602214	602214	1	0	301107037	301107037	1	0
3	602214	602214	1	0	301107037	301107037	1	0
4	602214	602214	1	0	301107037	301107037	1	0
5	602214	602214	1	0	301107037	301107037	1	0
6	602214	602214	1	0	301107037	301107037	1	0
7	602214	602214	1	0	301107037	301107037	1	0
8	602214	602214	1	0	301107037	301107037	1	0
9	602214	602214	1	0	301107037	301107037	1	0
10	602214	602214	1	0	301107037	301107037	1	0

Table 65: Symmetry breaking simulation scenario D, subset M.

t /s	[A]	[B]	[RCat]	[SCat]	[D]	[E]	[RF]	[SF]
0	602214	602214	0	0	301107038	301107038	0	0
1	602214	602214	0	0	301107038	301107038	0	0
2	602214	602214	0	0	301107038	301107038	0	0
3	602214	602214	0	0	301107038	301107038	0	0
4	602214	602214	0	0	301107038	301107038	0	0
5	602214	602214	0	0	301107038	301107038	0	0
6	602214	602214	0	0	301107038	301107038	0	0
7	602214	602214	0	0	301107038	301107038	0	0
8	602214	602214	0	0	301107038	301107038	0	0
9	602214	602214	0	0	301107038	301107038	0	0
10	602214	602214	0	0	301107038	301107038	0	0

Table 66: Symmetry breaking simulation scenario D, subset N.

t /s	[A]	[B]	[RCat]	[SCat]	[D]	[E]	[RF]	[SF]
0	602214	602214	0	0	301107038	301107038	0	0
1	602214	602214	0	0	301107038	301107038	0	0
2	602214	602214	0	0	301107038	301107038	0	0
3	602214	602214	0	0	301107038	301107038	0	0
4	602214	602214	0	0	301107038	301107038	0	0
5	602214	602214	0	0	301107038	301107038	0	0
6	602214	602214	0	0	301107038	301107038	0	0
7	602214	602214	0	0	301107038	301107038	0	0
8	602214	602214	0	0	301107038	301107038	0	0
9	602214	602214	0	0	301107038	301107038	0	0
10	602214	602214	0	0	301107038	301107038	0	0

Table 67: Symmetry breaking simulation scenario D, subset O.

t /s	[A]	[B]	[RCat]	[SCat]	[D]	[E]	[RF]	[SF]
0	602214	602214	0	0	301107038	301107038	0	0
0.021	602214	602214	0	1	301107037	301107037	0	1
1	602214	602214	0	1	301107037	301107037	0	1
2	602214	602214	0	1	301107037	301107037	0	1
3	602214	602214	0	1	301107037	301107037	0	1
4	602214	602214	0	1	301107037	301107037	0	1
5	602214	602214	0	1	301107037	301107037	0	1
6	602214	602214	0	1	301107037	301107037	0	1
7	602214	602214	0	1	301107037	301107037	0	1
8	602214	602214	0	1	301107037	301107037	0	1
9		602214	0	1	301107037	301107037	0	1
10	602214	602214	0	1	301107037	301107037	0	1

Table 68: Symmetry breaking simulation scenario D, subset P.

t /s	[A]	[B]	[RCat]	[SCat]	[D]	[E]	[RF]	[SF]
0	602214	602214	0	0	301107038	301107038	0	0
0.37	602214	602214	1	0	301107037	301107037	1	0
1	602214	602214	1	0	301107037	301107037	1	0
2	602214	602214	1	0	301107037	301107037	1	0
3	602214	602214	1	0	301107037	301107037	1	0
4	602214	602214	1	0	301107037	301107037	1	0
5	602214	602214	1	0	301107037	301107037	1	0
6	602214	602214	1	0	301107037	301107037	1	0
7	602214	602214	1	0	301107037	301107037	1	0
7.814	602214	602214	1	1	301107036	301107036	1	1
8	602214	602214	1	1	301107036	301107036	1	1
9	602214	602214	1	1	301107036	301107036	1	1
10	602214	602214	1	1	301107036	301107036	1	1

7.2 Appendix: The Tipping Point of the Atmosphere of a Planet

7.2.1 Temperature Correction

Assumption, that the atmosphere is homogeneously mixed and treated as if it was a perfect gas.

The calculation of the total pressure P as a function of the temperature T and total density ρ at any point in the atmosphere is carried out according to the following equations (45) and (46)[272]:

$$P = P_b \left[\frac{T_{Mg,b}}{T_{Mg,b} + L_{M,b} \cdot (H - H_b)} \right]^{\left[\frac{g_0' \cdot M_0}{R^* \cdot L_{Mg,b}} \right]} \tag{45}$$

$$P = P_b \cdot \exp \left[\frac{g_0' \cdot M_0 (H - H_b)}{R^* \cdot T_{Mg,b}} \right] \tag{46}$$

As mixing is dominant in the space between the surface and 80 km altitude, M_0 remains constant at its sea-level value M_0.

$$M_g = M_0 \tag{47}$$

7.2.2 Values for Geopotential Height Values

Table 69: Values for Geopotential Height Values H_b and L.

Calculated Atmosphere	Geopotential Height H_b (km´)	Molecular-scale Temperature Gradient $L_{M,b}$ (K/ km´)	Form of function relating T to H
0 km	0	-6.5	Linear
	11	0.0	Linear
	20	1.0	Linear
	32	2.8	Linear
	47	0.0	Linear
60 km	51	-2.8	Linear
	71	-2.0	Linear

7.2.3 Reaction Rate Constants for the Simulation

The reaction rate constants, that were used for the simulation are shown in Table 70.

Table 70: Reaction rate constants k_{1-8} for the simulation in chapter 4.

#	k_1	k_2	k_3	k_4	k_5	k_6	k_7	k_8
1	3.51E-08	7.54E-05	6.08E-02	2.07E-02	1.14E-01	1.73E-01	1.54E-01	1.00E-05
2	3.51E-08	7.54E-05	6.08E-02	2.07E-02	1.14E-01	1.73E-01	1.54E-01	3.16E-05
3	3.51E-08	7.54E-05	6.08E-02	2.07E-02	1.14E-01	1.73E-01	1.54E-01	1.00E-04
4	3.51E-08	7.54E-05	6.08E-02	2.07E-02	1.14E-01	1.73E-01	1.54E-01	3.16E-04
5	3.51E-08	7.54E-05	6.08E-02	2.07E-02	1.14E-01	1.73E-01	1.54E-01	1.00E-03
6	3.51E-08	7.54E-05	6.08E-02	2.07E-02	1.14E-01	1.73E-01	1.54E-01	3.16E-03
7	3.51E-08	7.54E-05	6.08E-02	2.07E-02	1.14E-01	1.73E-01	1.54E-01	1.00E-02

7.3 Appendix: System Validation of the *RNA.exe* tool for a S<small>OAI</small> Autocatalysis

7.3.1 ODEs of the kinetic model

Based on the reaction mechanism postulated in the T<small>RAPP</small> working group (Scheme 15), the following system of differential equations was derived to describe the reaction kinetics of the S<small>OAI</small> reaction.

A selectivity factor S_f was defined to account for the ratio of the formation of the stereoisomers **(R,R)-5** and **(S,S)-5** and the corresponding autocatalytic cycle.

Time-dependent concentration changes

The time-dependent concentration changes are shown below with molecular structures shown exemplarily for (*R*)-enantiomers:
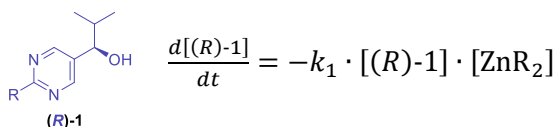
$$\frac{d[(R)\text{-}1]}{dt} = -k_1 \cdot [(R)\text{-}1] \cdot [\text{ZnR}_2]$$

$$\frac{d[(S)\text{-}1]}{dt} = -k_1 \cdot [(S)\text{-}1] \cdot [\text{ZnR}_2]$$

$$\frac{d[\text{ZnR}_2]}{dt} = -k_1 \cdot [(R)\text{-}1] \cdot [\text{ZnR}_2] - k_1 \cdot [(S)\text{-}1] \cdot [\text{ZnR}_2] - k_5 \cdot [(R,R)\text{-}5] \cdot [\text{ZnR}_2][4]$$
$$-k_5 \cdot [(S,S)\text{-}5] \cdot [\text{ZnR}_2] \cdot [4]$$

$$\frac{d[(R)\text{-}2]}{dt} = k_1 \cdot [(R)\text{-}1] \cdot [\text{ZnR}_2] - 2 \cdot k_2 \cdot [(R)\text{-}2]^2$$
$$+2 \cdot k_{-2} \cdot [(R,R)\text{-}3] - k_3 \cdot [(R)\text{-}2][(S)\text{-}2]$$
$$-k_{-3} \cdot [(R,S)\text{-}3_{diss}] - k_4 \cdot [(R)\text{-}2] \cdot [4] + k_{-4} \cdot [(R,R)\text{-}5]$$
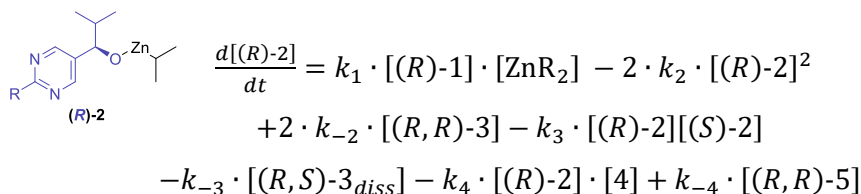
$$\frac{d[(S)\text{-}2]}{dt} = k_1 \cdot [(S)\text{-}1] \cdot [\text{ZnR}_2] - 2 \cdot k_2 \cdot [(S)\text{-}2]^2 + 2 \cdot k_{-2} \cdot [(S,S)\text{-}3] - k_3 \cdot [(R)\text{-}2][(S)\text{-}2] -$$
$$k_{-3} \cdot [(R,S)\text{-}3_{diss}] - k_4 \cdot [(S)\text{-}2] \cdot [4] + k_{-4} \cdot [(S,S)\text{-}5]$$
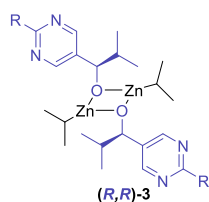
$$\frac{d[(R,R)\text{-}3]}{dt} = k_2 \cdot [(R)\text{-}2]^2 - k_{-2} \cdot [(R,R)\text{-}3]$$

$$\frac{d[(S,S)\text{-}3]}{dt} = k_2 \cdot [(S)\text{-}2]^2 - (S,S)\text{-}3]$$

(R,R)-3
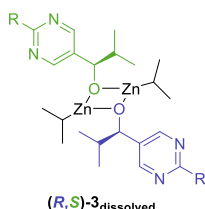
$$\frac{d[(R,S)\text{-}3_{diss}]}{dt} = k_3 \cdot [(R)\text{-}2][(S)\text{-}2] - k_{-3} \cdot [(R,S)\text{-}3_{diss}]$$
$$- k_{\mathrm{d}} \cdot [(R,S)\text{-}3_{diss}] + k_{-\mathrm{d}} \cdot [(R,S)\text{-}3_{solid}]$$

(R,S)-3$_{dissolved}$
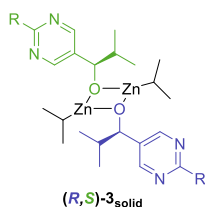
$$\frac{d[(R,S)\text{-}3_{solid}]}{dt} = k_{\mathrm{d}}[(R,S)\text{-}3_{diss}] - k_{-\mathrm{d}} \cdot [(R,S)\text{-}3_{solid}]$$

(R,S)-3$_{solid}$
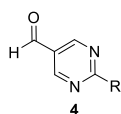
$$\frac{d[4]}{dt} = -k_4 \cdot [(R)\text{-}2] \cdot [4] - k_4 \cdot [(S)\text{-}2] \cdot [4]$$
$$+ k_{-4} \cdot [(R,R)\text{-}5] + k_{-4} \cdot [(S,S)\text{-}5]$$
$$- k_5 \cdot [(R,R)\text{-}5] \cdot [\mathrm{ZnR_2}] \cdot [4] - k_{-5} \cdot [(S,S)\text{-}5] \cdot [\mathrm{ZnR_2}] \cdot [4]$$
$$- k_7 \cdot [(R,R,R)\text{-}7] \cdot [4] - k_7 \cdot [(S,S,S)\text{-}7] \cdot [4]$$

4
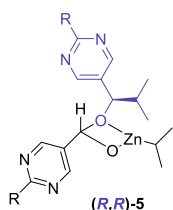
$$\frac{d[(R,R)\text{-}5]}{dt} = k_4 \cdot [(R)\text{-}2] \cdot [4] - k_{-4} \cdot [(R,R)\text{-}5]$$
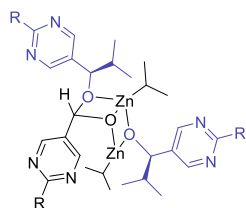$$- k_5 \cdot [(R,R)5] \cdot [\mathrm{ZnR_2}] \cdot [4] + 2 \cdot k_8 \cdot [(R,R,R,R)\text{-}8]$$

(R,R)-5

$$\frac{d[(S,S)\text{-}5]}{dt} = k_4 \cdot [(S)\text{-}2] \cdot [4] - k_{-4} \cdot [(S,S)\text{-}5]$$
$$- k_5 \cdot [(S,S)5] \cdot [\mathrm{ZnR_2}] \cdot [4] + 2 \cdot k_8 \cdot [(S,S,S,S)\text{-}8]$$
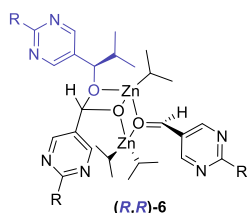
$$\frac{d[(R,R)\text{-}6]}{dt} = k_5 \cdot [(R,R)\text{-}5] \cdot [\mathrm{ZnR_2}] \cdot [4] - k_6 \cdot [(R,R)\text{-}6]$$

(R,R)-6

$$\frac{d[(S,S)\text{-}6]}{dt} = k_5 \cdot [(S,S)\text{-}5] \cdot [\mathrm{ZnR_2}] \cdot [4] - k_6 \cdot [(S,S)\text{-}6]$$

(*R*,*R*,*R*)-**7**

$$\frac{d[(R,R,R)\text{-}7]}{dt} = k_6 \cdot [(R,R)\text{-}6] - k_7 \cdot [(R,R,R)\text{-}7] \cdot [4]$$

$$\frac{d[(S,S,S)\text{-}7]}{dt} = k_6 \cdot [(S,S)\text{-}6] - k_7 \cdot [(S,S,S)\text{-}7] \cdot [4]$$
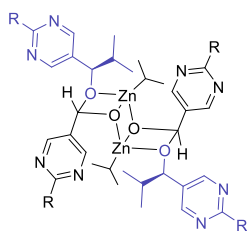
(*R*,*R*,*R*,*R*)-**8**

$$\frac{d[(R,R,R,R)\text{-}8]}{dt} = k_7 \cdot [(R,R,R)\text{-}7] \cdot [4] - k_8 \cdot [(R,R,R,R)\text{-}8]$$

$$\frac{d[(S,S,S,S)\text{-}8]}{dt} = k_7 \cdot [(S,S,S)\text{-}7] \cdot [4] - k_8 \cdot [(S,S,S,S)\text{-}8]$$

Chapter 8

Bibliography

[1] Banzhaf, W., McMullin, B. (2012). In *Handbook of Natural Computing* (Eds.: G. Rozenberg, T. Bäck, J. N. Kok), Springer Berlin Heidelberg, Berlin, Heidelberg, 1805-1834.

[2] Ehlmann, B. L., Anderson, F. S., Andrews-Hanna, J., Catling, D. C., Christensen, P. R., Cohen, B. A., Dressing, C. D., Edwards, C. S., Elkins-Tanton, L. T., Farley, K. A., Fassett, C. I., Fischer, W. W., Fraeman, A. A., Golombek, M. P., Hamilton, V. E., Hayes, A. G., Herd, C. D. K., Horgan, B., Hu, R., Jakosky, B. M., Johnson, J. R., Kasting, J. F., Kerber, L., Kinch, K. M., Kite, E. S., Knutson, H. A., Lunine, J. I., Mahaffy, P. R., Mangold, N., McCubbin, F. M., Mustard, J. F., Niles, P. B., Quantin-Nataf, C., Rice, M. S., Stack, K. M., Stevenson, D. J., Stewart, S. T., Toplis, M. J., Usui, T., Weiss, B. P., Werner, S. C., Wordsworth, R. D., Wray, J. J., Yingst, R. A., Yung, Y. L., Zahnle, K. J. (2016). The sustainability of habitability on terrestrial planets: Insights, questions, and needed measurements from Mars for understanding the evolution of Earth-like worlds. *Journal of Geophysical Research: Planets*, *121*(10), 1927-1961.

[3] Hyodo, R., Usui, T. (2021). Searching for life on Mars and its moons. *Science*, *373*(6556), 742-742.

[4] Wong, M. L., Bartlett, S., Chen, S., Tierney, L. (2022). Searching for Life, Mindful of Lyfe's Possibilities. *Life*, *12*(6), 783.

[5] McKay, C. P. (2022). Habitability in the Solar System beyond the Earth and the search for life. In *New Frontiers in Astrobiology* (pp. 167-177). Elsevier.

[6] Avalos, M., Babiano, R., Cintas, P., Jiménez, J. L., Palacios, J. C. (2000). From parity to chirality: chemical implications revisited. *Tetrahedron: Asymmetry*, *11*(14), 2845-2874.

[7] Avalos, M., Babiano, R., Cintas, P., Jiménez, J. L., Palacios, J. C. (2000). Chiral autocatalysis: where stereochemistry meets the origin of life. *Chemical Communications*, (11), 887-892.

[8] Brack, A. (2013). Clay minerals and the origin of life. In *Developments in Clay Science* (Vol. 5, pp. 507-521). Elsevier.

[9] Ruiz-Mirazo, K., Briones, C., de la Escosura, A. (2014). Prebiotic systems chemistry: new perspectives for the origins of life. *Chemical reviews*, *114*(1), 285-366.

[10] Yadav, M., Kumar, R., Krishnamurthy, R. (2020). Chemistry of abiotic nucleotide synthesis. *Chemical reviews*, *120*(11), 4766-4805.

[11] Höglund, P., Eriksson, T., Björkman, S. (1998). A double-blind study of the sedative effects of the thalidomide enantiomers in humans. *Journal of pharmacokinetics and biopharmaceutics*, *26*, 363-383.

[12] Evans, A. M., Nation, R. L., Sansom, L. N., Bochner, F., Somogyi, A. A. (1991). Effect of racemic ibuprofen dose on the magnitude and duration of platelet cyclo-oxygenase inhibition: relationship between inhibition of thromboxane production and the plasma unbound concentration of S (+)-ibuprofen. *British journal of clinical pharmacology*, *31*(2), 131-138.

[13] Knowles, W. S. (2002). Asymmetric hydrogenations (Nobel lecture). *Angewandte Chemie International Edition*, *41*(12), 1998-2007.

[14] Noyori, R. (2002). Asymmetric catalysis: science and opportunities (Nobel lecture). *Angewandte Chemie International Edition*, *41*(12), 2008-2022.

[15] Sharpless, K. B. (2002). Searching for new reactivity (Nobel lecture). *Angewandte Chemie International Edition*, *41*(12), 2024-2032.

[16] Joyce, G. F., Deamer, D. W., Fleischaker, G. (1994). Origins of life: the central concepts. *Deamer, DW*.

[17] Trail, D., Watson, E. B., Tailby, N. D. (2011). The oxidation state of Hadean magmas and implications for early Earth's atmosphere. *Nature*, *480*(7375), 79-82.

[18] Bruylants, G., Bartik, K., Reisse, J. (2011). Prebiotic chemistry: a fuzzy field. *Comptes Rendus Chimie*, *14*(4), 388-391.

[19] Nisbet, E. G., Sleep, N. H. (2001). The habitat and nature of early life. *Nature*, *409*(6823), 1083-1091.

[20] Oparin, A. I. (1961). Life: Its Nature. *Origin and Development. Edinburgh: Oliver & Boyd*.

[21] Waddington, C. H. (1968). Towards a theoretical biology. *Nature*, *218*(5141), 525-527.

[22] Küppers, B. O. (1990). Information and the Origin of Life. Cambridge (Mass.).

[23] Yockey, H. P. (2002). Information theory, evolution and the origin of life. *Information Sciences*, *141*(3-4), 219-225.

[24] Walker, S. I., Davies, P. C. (2013). The algorithmic origins of life. *Journal of the Royal Society Interface*, *10*(79), 20120869.

[25] Astrobiology at NASA. Life In The Universe. About Life Detection https://astrobiology.nasa.gov/research/life-detection/about/#:~:text=The%20NASA%20definition%20of%20life,life%20we%20know%20%E2%80%94Terran%20life. (Accessed on 21.02.23)

[26] Prigogine, I., Nicolis, G., Babloyantz, A. (1972). Thermodynamics of evolution I. *Physics today*, *25*(11), 23-28.

[27] Dalrymple, G. B. (2001). The age of the Earth in the twentieth century: a problem (mostly) solved. *Geological Society, London, Special Publications*, *190*(1), 205-221.

[28] Oparin, A. I. (1953). *The Origin of Life: Transl. with Annot. by Sergius Morgulis*. Dover Publ.

[29] Miller, S. L. (1974). The origins of life on the earth. *Concept of Modern biology series*.

[30] A. Pross, What is Life?: How Chemistry Becomes Biology, Oxford Landmark Science (OUP Oxford, 2012).

[31] Wu, L.-F., Sutherland, J. D. (2019). Provisioning the origin and early evolution of life. *Emerging Topics in Life Sciences, 3*(5), 459-468.

[32] Bouvier, A., Wadhwa, M. (2010). The age of the Solar System redefined by the oldest Pb–Pb age of a meteoritic inclusion. *Nature geoscience*, *3*(9), 637-641.

[33] Bottke, W. F., Vokrouhlický, D., Marchi, S., Swindle, T., Scott, E. R. D., Weirich, J. R., Levison, H. (2015). Dating the Moon-forming impact event with asteroidal meteorites. *Science*, *348*(6232), 321-323.

[34] Herwartz, D., Pack, A., Friedrichs, B., Bischoff, A. (2014). Identification of the giant impactor Theia in lunar rocks. *Science*, *344*(6188), 1146-1150.

[35] Halliday, A. N. (2008). A young Moon-forming giant impact at 70–110 million years accompanied by late-stage mixing, core formation and degassing of the Earth. *Philosophical Transactions of the Royal Society A: Mathematical, Physical and Engineering Sciences*, *366*(1883), 4163-4181.

[36] Wilde, S. A., Valley, J. W., Peck, W. H., Graham, C. M. (2001). Evidence from detrital zircons for the existence of continental crust and oceans on the Earth 4.4 Gyr ago. *Nature*, *409*(6817), 175-178.

[37] Peck, W. H., Valley, J. W., Wilde, S. A., Graham, C. M. (2001). Oxygen isotope ratios and rare earth elements in 3.3 to 4.4 Ga zircons: Ion microprobe evidence for high $\delta 18O$ continental crust and oceans in the Early Archean. *Geochimica et Cosmochimica Acta*, *65*(22), 4215-4229.

[38] Mojzsis, S. J., Harrison, T. M., Pidgeon, R. T. (2001). Oxygen-isotope evidence from ancient zircons for liquid water at the Earth's surface 4,300 Myr ago. *Nature*, *409*(6817), 178-181.

[39] Schidlowski, M. (1988). A 3,800-million-year isotopic record of life from carbon in sedimentary rocks. *Nature*, *333*(6171), 313-318.

[40] Rosing, M. T. (1999). 13C-depleted carbon microparticles in > 3700-Ma sea-floor sedimentary rocks from West Greenland. *Science*, *283*(5402), 674-676.

[41] Ohtomo, Y., Kakegawa, T., Ishida, A., Nagase, T., Rosing, M. T. (2014). Evidence for biogenic graphite in early Archaean Isua metasedimentary rocks. *Nature Geoscience*, *7*(1), 25-28.

[42] Bell, E. A., Boehnke, P., Harrison, T. M., Mao, W. L. (2015). Potentially biogenic carbon preserved in a 4.1 billion-year-old zircon. *Proc. Natl. Acad. Sci. USA*, 14518-21.

[43] Javaux, E. J. (2019). Challenges in evidencing the earliest traces of life. *Nature*, *572*(7770), 451-460.

[44] Walter, M. R., Buick, R., Dunlop, J. S. R. (1980). Stromatolites 3,400–3,500 Myr old from the North pole area, Western Australia. *Nature*, *284*, 443-445.

[45] Byerly, G. R., Lower, D. R., Walsh, M. M. (1986). Stromatolites from the 3,300–3,500-Myr Swaziland Supergroup, Barberton Mountain Land, South Africa. *Nature*, *319*, 489-491.

[46] Allwood, A. C., Walter, M. R., Kamber, B. S., Marshall, C. P., Burch, I. W. (2006). Stromatolite reef from the Early Archaean era of Australia. *Nature*, *441*(7094), 714-718.

[47] Noffke, N., Christian, D., Wacey, D., Hazen, R. M. (2013). Microbially induced sedimentary structures recording an ancient ecosystem in the ca. 3.48 billion-year-old Dresser Formation, Pilbara, Western Australia. *Astrobiology*, *13*(12), 1103-1124.

[48] Schopf, J. W., Packer, B. M. (1987). Early Archean (3.3-billion to 3.5-billion-year-old) microfossils from Warrawoona Group, Australia. *Science*, *237*(4810), 70-73.

[49] Zahnle, K., Schaefer, L., Fegley, B. (2010). Earth's Earliest Atmospheres. Cold Spring Harbor, *Perps Biol. 2,* a004895.

[50] Kasting, J. F. (1993). Earth's early atmosphere. *Science*, *259*(5097), 920-926.

[51] Urey, H.C. (1959). The Atmospheres of the Planets. In: Flügge S. (eds) Astrophysics III: The Solar System / Astrophysik III: Das Sonnensystem. *Encyclopedia of Physics / Handbuch der Physik*, Vol. 11 / 52. Springer, Berlin, Heidelberg.

[52] Kasting, J. F., Howard, M. T. (2006). Atmospheric composition and climate on the early Earth. *Philosophical Transactions of the Royal Society B: Biological Sciences, 361*(1474), 1733–1742.

[53] Shaw, G. H. (2008). Earth's atmosphere – Hadean to early Proterozoic. *Chemie Der Erde - Geochemistry, 68*(3), 235–264.

[54] Morowitz, H. J. (1969). A mechanism for the amplification of fluctuations in racemic mixtures. *Journal of Theoretical Biology, 25*(3), 491–494.

[55] Lee, C. T. A., Yeung, L. Y., McKenzie, N. R., Yokoyama, Y., Ozaki, K., Lenardic, A. (2016). Two-step rise of atmospheric oxygen linked to the growth of continents. *Nature Geoscience*, *9*(6), 417-424.

[56] Lyons, T. W., Reinhard, C. T., Planavsky, N. J. (2014). The rise of oxygen in Earth's early ocean and atmosphere. *Nature*, *506*(7488), 307-315.

[57] Partin, C. A., Lalonde, S. V., Planavsky, N. J., Bekker, A., Rouxel, O. J., Lyons, T. W., Konhauser, K. O. (2013). Uranium in iron formations and the rise of atmospheric oxygen. *Chemical Geology*, *362*, 82-90.

[58] Huber, L., Trapp, O. (2022). First Steps of Prebiotic Chemistry Catalyzed by Minerals and Metals. In *Prebiotic Chemistry and Life's Origin* (pp. 77-123).

[59] Cnossen, I., Sanz-Forcada, J., Favata, F., Witasse, O., Zegers, T., Arnold, N.F. (2007). Habitat of early life: Solar X-ray and UV radiation at Earth's surface 4–3.5 billion years ago. *J. Geophys. Res. Planets*, *112*.

[60] Cohen, K. M., Finney, S. C., Gibbard, P. L., Fan, J. X. (2013). The ICS international chronostratigraphic chart. *Episodes Journal of International Geoscience*, *36*(3), 199-204.

[61] Bada, J. L., Bigham, C., Miller, S. L. (1994). Impact melting of frozen oceans on the early Earth: implications for the origin of life. *Proceedings of the National Academy of Sciences*, *91*(4), 1248-1250.

[62] Sagan, C., Chyba, C. (1997). The early faint sun paradox: Organic shielding of ultraviolet-labile greenhouse gases. *Science, 276*(5316), 1217-1221.

[63] Goldblatt, C., Claire, M. W., Lenton, T. M., Matthews, A. J., Watson, A. J., Zahnle, K. J. (2009). Nitrogen-enhanced greenhouse warming on early Earth. *Nature Geoscience*, *2*(12), 891-896.

[64] Goldblatt, C., Zahnle, K. J. (2011). Faint young Sun paradox remains. *Nature*, *474*(7349), E1-E1.

[65] Hashimoto, G. L., Abe, Y., Sugita, S. (2007). The chemical composition of the early terrestrial atmosphere: Formation of a reducing atmosphere from CI-like material. *Journal of Geophysical Research: Planets*, *112*(E5).

[66] Catling, D. C., Zahnle, K. J., McKay, C. P. (2001). Biogenic methane, hydrogen escape, and the irreversible oxidation of early Earth. *Science, 293*(5531), 839-843.

[67] Oparin, A. I. (1924). *Proiskhozhdenie zhizni* (The Origin of Life).Voennoe Izd. Ministerstva Obrony Sojuza SSR.

[68] Haldane, J. B. S. (1929). The origin of life. *Rationalist Annual*, *148*, 3-10.

[69] Miller, S. L. (1953). A production of amino acids under possible primitive earth conditions. *Science*, *117*(3046), 528-529.

[70] Calvin, M. (1956). Chemical Evolution and the Origin of Life. *American Scientist, 44*(3), 248-263.

[71] Hazen, R. M., Papineau, D., Bleeker, W., Downs, R. T., Ferry, J. M., McCoy, T. J., Sverjensky, D. A., Yang, H. (2008). Mineral evolution. *American Mineralogist*, *93*(11-12), 1693-1720.

[72] Barge, L. M. (2018). Considering planetary environments in origin of life studies. *Nature communications*, *9*(1), 5170.

[73] Frost, D. J., McCammon, C. A. (2008). The redox state of Earth's mantle. *Annu. Rev. Earth Planet. Sci.*, *36*, 389-420.

[74] Miller, S. L., Urey, H. C. (1953). Organic compound synthesis on the primitive Earth. Science 117:245-251.

[75] Thomson, S. J. (1961). Radiation Chemistry of Organic Compounds. *Nature, 191*(4786), 317–317.

[76] Lemmon, R. M. (1970). Chemical evolution. *Chemical Reviews, 70*(1), 95–109.

[77] Sagan, C., Khare, B. N. (1971). Long-Wavelength Ultraviolet Photoproduction of Amino Acids on the Primitive Earth. *Science, 173*(3995), 417–420.

[78] Miller, S. L., Urey, H. C., Oró, J. (1976). Origin of organic compounds on the primitive earth and in meteorites. *Journal of Molecular Evolution, 9*(1), 59–72.

[79] Rubenstein, E., Bonner, W. A., Noyes, H. P., Brown, G. S. (1983). Supernovae and life. *Nature*, *306*(5939), 118-118.

[80] Garzón, L., Garzón, M. L. (2001). Radioactivity as a significant energy source in prebiotic synthesis. *Origins of Life and Evolution of the Biosphere, 31*(1/2), 3–13.

[81] Bailey, J. (2001). Astronomical sources of circularly polarized light and the origin of homochirality. *Origins of Life and Evolution of the Biosphere*, *31*, 167-183.

[82] Darwin, C. (1871). Letter to J.D. Hooker; Hooker, J.D., Down, United Kingdom, published in: *Darwin Correspondence Project, "Letter no. 7471"*; Available online: http://www.darwinproject.ac.uk/DCP-LETT-7471 (accessed on January 17, 2023).

[83] Rode, B. M., Fitz, D., Jakschitz, T. (2007). The First Steps of Chemical Evolution towards the Origin of Life. *Chemistry & Biodiversity, 4*(12), 2674–2702.

[84] Bada, J.L. (2004) How life began on Earth: A status report. *Earth Planet. Sci. Lett.*, *226*, 1–15.

[85] Gull, M., Zhou, M., Fernández, F. M., Pasek, M. A. (2013). Prebiotic Phosphate Ester Syntheses in a Deep Eutectic Solvent. *Journal of Molecular Evolution, 78*(2), 109–117.

[86]   Menor-Salván, C., Marín-Yaseli, M. R. (2012). Prebiotic chemistry in eutectic solutions at the water–ice matrix. *Chemical Society Reviews,* 41(16), 5404.

[87]   Clark, B.C.; Kolb, V.M (2018). Comet Pond II: Synergistic Intersection of Concentrated Extra-terrestrial Materials and Planetary Environments to Form Procreative Darwinian Ponds. *Life*, *8*, 12.

[88]   Oberbeck, V. R., Aggarwal, H. (1991). Comet impacts and chemical evolution on the bombarded Earth. *Origins of Life and Evolution of the Biosphere,* 21(5-6), 317–338.

[89]   Clark, B. C. (1988). Primeval procreative comet pond. *Origins of Life and Evolution of the Biosphere,* 18(3), 209–238.

[90]   Chyba, C., Sagan, C. (1992). Endogenous production, exogenous delivery and impact-shock synthesis of organic molecules: an inventory for the origins of life. *Nature*, *355*(6356), 125-132.

[91]   Kitadai, N., Maruyama, S. (2018). Origins of building blocks of life: A review. *Geoscience Frontiers*, *9*(4), 1117-1153.

[92]   Callahan, M. P., Smith, K. E., Cleaves, H. J., Ruzicka, J., Stern, J. C., Glavin, D. P., House, C. H., Dworkin, J. P. (2011). Carbonaceous meteorites contain a wide range of extraterrestrial nucleobases. *Proceedings of the National Academy of Sciences*, *108*(34), 13995-13998.

[93]   Cronin, J. R., Pizzarello, S. (1997). Enantiomeric excesses in meteoritic amino acids. *Science*, *275*(5302), 951-955.

[94]   Pizzarello, S. (2004). Chemical evolution and meteorites: an update. *Origins of Life and Evolution of the Biosphere*, *34*, 25-34.

[95]   Pizzarello, S. (2006). The chemistry of life's origin: a carbonaceous meteorite perspective. *Accounts of Chemical Research*, *39*(4), 231-237.

[96]   Oró, J., Gibert, J., Lichtenstein, H., Wikstrom, S., Flory, D. A. (1971). Amino-acids, aliphatic and aromatic hydrocarbons in the Murchison meteorite. *Nature*, *230*, 105-106.

[97]   Miller, S. L. (1955). Production of some organic compounds under possible primitive earth conditions. *Journal of the American Chemical Society*, *77*(9), 2351-2361.

[98]   Epstein, S., Krishnamurthy, R. V., Cronin, J. R., Pizzarello, S., Yuen, G. U. (1987). Unusual stable isotope ratios in amino acid and carboxylic acid extracts from the Murchison meteorite. *Nature*, *326*(6112), 477-479.

[99]   Engel, M. H., Macko, S. A. (1997). Isotopic evidence for extraterrestrial non-racemic amino acids in the Murchison meteorite. *Nature*, *389*(6648), 265-268.

[100] Miyakawa, S., Yamanashi, H., Kobayashi, K., Cleaves, H. J., Miller, S. L. (2002). Prebiotic synthesis from CO atmospheres: implications for the origins of life. *Proceedings of the National Academy of Sciences*, *99*(23), 14628-14631.

[101] Hennet, R. C., Holm, N. G., Engel, M. H. (1992). Abiotic synthesis of amino acids under hydrothermal conditions and the origin of life: a perpetual phenomenon?. *Naturwissenschaften*, *79*, 361-365.

[102] Strecker, A. (1850). Ueber die künstliche Bildung der Milchsäure und einen neuen, dem Glycocoll homologen Körper. *Justus Liebigs Annalen der Chemie*, *75*(1), 27-45.

[103] Strecker, A. (1854). Ueber einen neuen aus Aldehyd-Ammoniak und Blausäure entstehenden Körper. *Justus Liebigs Annalen der Chemie*, *91*(3), 349-351.

[104] Hulshof, J., Ponnamperuma, C. (1976). Prebiotic condensation reactions in an aqueous medium: a review of condensing agents. *Origins of life*, *7*, 197-224.

[105] Sawai, H., Lohrmann, R., Orgel, L. E. (1975). Prebiotic peptide-formation in the solid state: II. Reaction of Glycine with Adenosine 5′-Triphosphate and P 1, P 2-Diadenosine-Pyrophosphate. *Journal of Molecular Evolution*, *6*, 165-184.

[106] Weber, A. L., Caroon, J. M., Warden, J. T., Lemmon, R. M., Calvin, M. (1977). Simultaneous peptide and oligonucleotide formation in mixtures of amino acid, nucleoside triphosphate, imidazole, and magnesium ion. *Biosystems*, *8*(4), 277-286.

[107] Schwendinger, M. G., Rode, B. M. (1989). Possible role of copper and sodium chloride in prebiotic evolution of peptides. *Analytical Sciences*, *5*(4), 411-414.

[108] Ferris, J. P., Hill Jr, A. R., Liu, R., Orgel, L. E. (1996). Synthesis of long prebiotic oligomers on mineral surfaces. *Nature*, *381*(6577), 59-61.

[109] Le Son, H., Suwannachot, Y., Bujdak, J., Rode, B. M. (1998). Salt-induced peptide formation from amino acids in the presence of clays and related catalysts. *Inorganica chimica acta*, *272*(1-2), 89-94.

[110] Kawamura, K., Takeya, H., Kushibe, T. (2009). Effect of condensation agents and minerals for oligopeptide formation under mild and hydrothermal conditions in related to chemical evolution of proteins. *Advances in space research*, *44*(2), 267-275.

[111] Canavelli, P., Islam, S., Powner, M. W. (2019). Peptide ligation by chemoselective aminonitrile coupling in water. *Nature*, *571*(7766), 546-549.

[112] Butlerow, A. (1861). Bildung einer zuckerartigen Substanz durch Synthese. *Justus Liebigs Annalen der Chemie*, *120*(3), 295-298.

[113] Ritson, D. J., Sutherland, J. D. (2013). Synthesis of aldehydic ribonucleotide and amino acid precursors by photoredox chemistry. *Angewandte Chemie International Edition*, *52*(22), 5845-5847.

[114] Ferus, M., Pietrucci, F., Saitta, A. M., Knížek, A., Kubelík, P., Ivanek, O., Shestivska, V., Civiš, S. (2017). Formation of nucleobases in a Miller–Urey reducing atmosphere. *Proceedings of the National Academy of Sciences*, *114*(17), 4306-4311.

[115] Powner, M. W., Gerland, B., Sutherland, J. D. (2009). Synthesis of activated pyrimidine ribonucleotides in prebiotically plausible conditions. *Nature*, *459*(7244), 239-242.

[116] Becker, S., Thoma, I., Deutsch, A., Gehrke, T., Mayer, P., Zipse, H., Carell, T. (2016). A high-yielding, strictly regioselective prebiotic purine nucleoside formation pathway. *Science*, *352*(6287), 833-836.

[117] Teichert, J. S., Kruse, F. M., Trapp, O. (2019). Direct prebiotic pathway to DNA nucleosides. *Angewandte Chemie*, *131*(29), 10049-10052.

[118] Gibard, C., Bhowmik, S., Karki, M., Kim, E. K., Krishnamurthy, R. (2018). Phosphorylation, oligomerization and self-assembly in water under potential prebiotic conditions. *Nature Chemistry*, *10*(2), 212-217.

[119] Bechtel, M., Hümmer, E., Trapp, O. (2022). Selective phosphorylation of RNA-and DNA-nucleosides under prebiotically plausible conditions. *ChemSystemsChem*.

[120] Ruiz-Mirazo, K., Briones, C., de la Escosura, A. (2014). Prebiotic systems chemistry: new perspectives for the origins of life. *Chemical reviews*, *114*(1), 285-366.

[121] Islam, S., Powner, M. W. (2017). Prebiotic systems chemistry: Complexity overcoming clutter. *Chem*, *2*(4), 470-501.

[122] Frenkel-Pinter, M., Samanta, M., Ashkenasy, G., Leman, L. J. (2020). Prebiotic peptides: Molecular hubs in the origin of life. *Chemical reviews*, *120*(11), 4707-4765.

[123] Hutchison III, C. A., Chuang, R. Y., Noskov, V. N., Assad-Garcia, N., Deerinck, T. J., Ellisman, M. H., Gill, J., Kannan, K., Karas, B. J., Ma, L., Pelletier, J. F., Qi, Z.-Q., Richter, R. A., Strychalski, E. A., Sun, L., Suzuki, Y., Tsvetanova, B., Wise, K. S., Smith, H. O., Glass, J. I., Merryman, C., Gibson, D. G., Venter, J. C. (2016). Design and synthesis of a minimal bacterial genome. *Science*, *351*(6280), aad6253.

[124] Koonin, E. V. (2003). Comparative genomics, minimal gene-sets and the last universal common ancestor. *Nature Reviews Microbiology*, *1*(2), 127-136.

[125] Johnson, A. P., Cleaves, H. J., Dworkin, J. P., Glavin, D. P., Lazcano, A., Bada, J. L. (2008). The Miller volcanic spark discharge experiment. *Science*, *322*(5900), 404-404.

[126] Groth, W., von Weyssenhoff, H. (1957). Photochemische bildung von aminosäuren aus mischungen einfacher Gase. *Naturwissenschaften*, *44*(19), 510-511.

[127] Harada, K., Fox, S. W. (1964). Thermal synthesis of natural amino-acids from a postulated primitive terrestrial atmosphere. *Nature*, *201*, 335-336.

[128] Huber, C., Kraus, F., Hanzlik, M., Eisenreich, W., Wächtershäuser, G. (2012). Elements of metabolic evolution. *Chemistry–A European Journal*, *18*(7), 2063-2080.

[129] Ludlow, R. F., Otto, S. (2008). Systems chemistry. *Chemical Society Reviews*, *37*(1), 101-108.

[130] Ashkenasy, G., Hermans, T. M., Otto, S., Taylor, A. F. (2017). Systems chemistry. *Chemical Society Reviews*, *46*(9), 2543-2554.

[131] Boekhoven, J. (2018). Complexity from small molecules. *Nature Nanotechnology*, *13*(11), 979-980.

[132] Gujarro, A., Yus, M. (2009). The origin of chirality in the molecules of life: a revision from awareness to the current theories and perspectives of this unsolved problem.

[133] Feringa, B. L., Van Delden, R. A. (1999). Absolute asymmetric synthesis: the origin, control, and amplification of chirality. *Angewandte Chemie International Edition*, *38*(23), 3418-3438.

[134] Pasteur, L. (1848). Sur les relations qui peuvent exister entre la forme crystalline, la composition chimique et le sens de la polarization rotatoire. *Annales Chimie Phys.*, *24*, 442-459.

[135] Pasteur, L. (1848). Memoires sur la relation qui peut exister entre la forme crystalline et al composition chimique, et sur la cause de la polarization rotatoire. *Compt. rend.*, *26*, 535-538.

[136] Gal, J. (2017). Pasteur and the art of chirality. *Nature chemistry*, *9*(7), 604-605.

[137] Thomson, W., Kelvin, B. (2010). *Baltimore lectures on molecular dynamics and the wave theory of light*. Cambridge University Press.

[138] Todd, M. H. (2002). Asymmetric autocatalysis: product recruitment for the increase in the chiral environment (PRICE). *Chemical Society Reviews*, *31*(4), 211-222.

[139] Satyanarayana, T., Abraham, S., Kagan, H. B. (2009). Nonlinear effects in asymmetric catalysis. *Angewandte Chemie International Edition*, *48*(3), 456-494.

[140] Blackmond, D. G. (2010). Kinetic aspects of non-linear effects in asymmetric synthesis, catalysis, and autocatalysis. *Tetrahedron: Asymmetry*, *21*(11-12), 1630-1634.

[141] Geiger, Y., Achard, T., Maisse-François, A., Bellemin-Laponnaz, S. (2020). Hyperpositive nonlinear effects in asymmetric catalysis. *Nature Catalysis*, *3*(5), 422-426.

[142] Frank, F. C. (1953). On spontaneous asymmetric synthesis. *Biochimica et biophysica acta*, *11*, 459-463.

[143] Horeau, A. (1969). Interactions d'énantiomères en solution; influence sur le pouvoir rotatoire: Pureté optique et pureté énantiomérique. *Tetrahedron Letters*, *10*(36), 3121-3124.

[144] Wynberg, H., Feringa, B. (1976). Enantiomeric recognition and interactions. *Tetrahedron*, *32*(22), 2831-2834.

[145] Puchot, C., Samuel, O., Dunach, E., Zhao, S., Agami, C., Kagan, H. B. (1986). Nonlinear effects in asymmetric synthesis. Examples in asymmetric oxidations and aldolization reactions. *Journal of the American Chemical Society*, *108*(9), 2353-2357.

[146] Finn, M. G., Sharpless, K. B. (1991). Mechanism of asymmetric epoxidation. 2. Catalyst structure. *Journal of the American Chemical Society*, *113*(1), 113-126.

[147] Girard, C., Kagan, H. B. (1998). Nonlinear effects in asymmetric synthesis and stereoselective reactions: ten years of investigation. *Angewandte Chemie International Edition*, *37*(21), 2922-2959.

[148] Oguni, N., Matsuda, Y., Kaneko, T. (1988). Asymmetric amplifying phenomena in enantiose-lective addition of diethylzinc to benzaldehyde. Journal of the American Chemical Society, 110(23), 7877-7878.

[149] Guillaneux, D., Zhao, S. H., Samuel, O., Rainford, D., Kagan, H. B. (1994). Nonlinear effects in asymmetric catalysis. *Journal of the American Chemical Society*, *116*(21), 9430-9439.

[150] Kitamura, M., Suga, S., Niwa, M., Noyori, R. (1995). Self and nonself recognition of asymmet-ric catalysts. Nonlinear effects in the amino alcohol-promoted enantioselective addition of di-alkylzincs to aldehydes. *Journal of the American Chemical Society*, *117*(17), 4832-4842.

[151] Blackmond, D. G. (1997). Mathematical models of nonlinear effects in asymmetric catalysis: new insights based on the role of reaction rate. *Journal of the American Chemical Soci-ety*, *119*(52), 12934-12939.

[152] Blackmond, D. G. (2000). Kinetic aspects of nonlinear effects in asymmetric catalysis. *Ac-counts of Chemical Research*, *33*(6), 402-411.

[153] Bonner, W. A. (1991). Terrestrial and extraterrestrial sources of molecular homochirality. *Ori-gins of Life and Evolution of the Biosphere*, *21*(5-6), 407-420.

[154] Haq, S., Liu, N., Humblot, V., Jansen, A. P. J., Raval, R. (2009). Drastic symmetry breaking in supramolecular organization of enantiomerically unbalanced monolayers at surfaces. *Nature Chemistry*, *1*(5), 409-414.

[155] Kurata, M., Yoshizawa, A. (2020). The formation of a chiral supramolecular structure acting as a template for chirality transfer. *Chemical Communications*, *56*(59), 8289-8292.

[156] Pincock, R. E., Perkins, R. R., Ma, A. S., Wilson, K. R. (1971). Probability distribution of enan-tiomorphous forms in spontaneous generation of optically active substances. *Sci-ence*, *174*(4013), 1018-1020.

[157] Fletcher, S. P., Bissette, A. J. (2013). Mechanism of Autocatalysis. *Angew. Chem., Int. Ed*, *52*, 12800-12826.

[158] Soai, K., Kawasaki, T., Matsumoto, A. (2014). Asymmetric autocatalysis of pyrimidyl alkanol and its application to the study on the origin of homochirality. *Accounts of Chemical Re-search*, *47*(12), 3643-3654.

[159] Norden, B. (1977). Was photoresolution of amino acids the origin of optical activity in life?. *Na-ture*, *266*(5602), 567-568.

[160] Bailey, J., Chrysostomou, A., Hough, J. H., Gledhill, T. M., McCall, A., Clark, S., Ménard, F., Tamura, M. (1998). Circular polarization in star-formation regions: Implications for biomolecu-lar homochirality. *Science*, *281*(5377), 672-674.

[161] Meinert, C., Hoffmann, S. V., Cassam-Chenaï, P., Evans, A. C., Giri, C., Nahon, L., Meierhen-rich, U. J. (2014). Photonenergy-controlled symmetry breaking with circularly polarized light. *Angewandte Chemie*, *126*(1), 214-218.

[162] Meierhenrich, U. J., Nahon, L., Alcaraz, C., Bredehöft, J. H., Hoffmann, S. V., Barbier, B., Brack, A. (2005). Asymmetrische Vakuum-UV-Photolyse der Aminosäure Leucin in fester Phase. *Angewandte Chemie*, *117*(35), 5774-5779.

[163] Kuhn, W., Knopf, E. (1930). Photochemische Erzeugung optisch aktiver Stoffe. *Naturwissen-schaften*, *18*(8), 183-183.

[164] Sögütoglu, L. C., Steendam, R. R., Meekes, H., Vlieg, E., Rutjes, F. P. (2015). Viedma ripen-ing: a reliable crystallisation method to reach single chirality. *Chemical Society Re-views*, *44*(19), 6723-6732.

[165] Quack, M. (2002). How important is parity violation for molecular and biomolecular chiral-ity?. *Angewandte Chemie International Edition*, *41*(24), 4618-4630.

[166] Lee, T. D., Yang, C. N. (1956). Question of parity conservation in weak interactions. *Physical Review*, *104*(1), 254.

[167] Yang, C. N. (1958). Law of parity conservation and other symmetry laws. *Science*, *127*(3298), 565-569.

[168] Lee, T. D. (1958). Weak interactions and nonconservation of parity. *Science*, *127*(3298), 569-573.

[169] Yamagata, Y. (1966). A hypothesis for the asymmetric appearance of biomolecules on earth. *Journal of Theoretical Biology*, *11*(3), 495-498.

[170] Tranter, G. E. (1985). Parity-violating energy differences of chiral minerals and the origin of biomolecular homochirality. *Nature*, *318*(6042), 172-173.

[171] Tranter, G. E. (1987). Parity violation and the origins of biomolecular handedness. *Biosystems*, *20*(1), 37-48.

[172] Salam, A. (1991). The role of chirality in the origin of life. *Journal of Molecular Evolution*, *33*, 105-113.

[173] Zanasi, R., Lazzeretti, P., Ligabue, A., Soncini, A. (1999). Theoretical results which strengthen the hypothesis of electroweak bioenantioselection. *Physical Review E*, *59*(3), 3382.

[174] Mason, S. F., Tranter, G. E. (1985). The electroweak origin of biomolecular handedness. *Proceedings of the Royal Society of London. A. Mathematical and Physical Sciences*, *397*(1812), 45-65.

[175] Buschmann, H., Thede, R., Heller, D. (2000). New developments in the origins of the homochirality of biologically relevant molecules. *Angewandte Chemie International Edition*, *39*(22), 4033-4036.

[176] Quack, M. (1986). On the measurement of the parity violating energy difference between enantiomers. *Chemical physics letters*, *132*(2), 147-153.

[177] MacDermott, A. J., Hegstrom, R. A. (2004). A proposed experiment to measure the parity-violating energy difference between enantiomers from the optical rotation of chiral ammonia-like "cat" molecules. *Chemical physics*, *305*(1-3), 55-68.

[178] Darquié, B., Stoeffler, C., Shelkovnikov, A., Daussy, C., Amy-Klein, A., Chardonnet, C., Zrig, S., Guy, L., Crassous, J., Soulard, P., Asselin, P., Huet, T. R., Schwerdtfeger, P., Bast, R., Saue, T. (2010). Progress toward the first observation of parity violation in chiral molecules by high-resolution laser spectroscopy. *Chirality*, *22*(10), 870-884.

[179] Lahamer, A. S., Mahurin, S. M., Compton, R. N., House, D., Laerdahl, J. K., Lein, M., Schwerdtfeger, P. (2000). Search for a parity-violating energy difference between enantiomers of a chiral iron complex. *Physical review letters*, *85*(21), 4470.

[180] Bargueño, P., Gonzalo, I., de Tudela, R. P. (2009). Detection of parity violation in chiral molecules by external tuning of electroweak optical activity. *Physical Review A*, *80*(1), 012110.

[181] King, G. A. M. (1978). Autocatalysis. *Chemical Society Reviews*, *7*(2), 297-316.

[182] Ostwald, W. (1890). Ueber Autokatalyse. *Berichte über die Verhandlungen der Königlich Sächsischen Gesellschaft der Wissenschaften zu Leipzig*, Mathematisch-Physische Classe, 42, 189–191

[183] Danda, H., Nishikawa, H., Otaka, K. (1991). Enantioselective autoinduction in the asymmetric hydrocyanation of 3-phenoxybenzaldehyde catalyzed by cyclo [(R)-phenylalanyl-(R)-histidyl]. *The Journal of Organic Chemistry*, *56*(24), 6740-6741.

[184] Heller, D. P., Goldberg, D. R., Wulff, W. D. (1997). Positive cooperativity of product mimics in the asymmetric autoinduction of Diels− Alder reactions catalyzed by a VAPOL− aluminum catalyst. *Journal of the American Chemical Society*, *119*(43), 10551-10552.

[185] Storch, G., Trapp, O. (2017). By-design enantioselective self-amplification based on non-covalent product–catalyst interactions. *Nature Chemistry*, *9*(2), 179-187.; 2018

[186] Soai, K., Shibata, T., Morioka, H., Choji, K. (1995). Asymmetric autocatalysis and amplification of enantiomeric excess of a chiral molecule. *Nature*, *378*(6559), 767-768.

[187] Soai, K., Kawasaki, T. (2007). Asymmetric autocatalysis with amplification of chirality. *Amplification of Chirality*, 1-33.

[188] Podlech, J., Gehring, T. (2005). New aspects of Soai's asymmetric autocatalysis. *Angewandte Chemie International Edition*, *44*(36), 5776-5777.

[189] Soai, K., Kawasaki, T. (2006). Discovery of asymmetric autocatalysis with amplification of chirality and its implication in chiral homogeneity of biomolecules. *Chirality: The Pharmacological, Biological, and Chemical Consequences of Molecular Asymmetry*, *18*(7), 469-478.

[190] Gehring, T., Busch, M., Schlageter, M., Weingand, D. (2010). A concise summary of experimental facts about the Soai reaction. *Chirality*, *22*(1E), E173-E182.

[191] Soai, K., Kawasaki, T., Matsumoto, A. (2014). The origins of homochirality examined by using asymmetric autocatalysis. *The Chemical Record*, *14*(1), 70-83.

[192] Geiger, Y. (2022). One Soai reaction, two mechanisms? *Chemical Society Reviews*, *51*(4), 1206-1211.

[193] Shibata, T., Choji, K., Hayase, T., Aizu, Y., Soai, K. (1996). Asymmetric autocatalytic reaction of 3-quinolylalkanol with amplification of enantiomeric excess. *Chemical Communications*, (10), 1235-1236.

[194] Shibata, T., Choji, K., Morioka, H., Hayase, T., Soai, K. (1996). Highly enantioselective synthesis of a chiral 3-quinolylalkanol by an asymmetric autocatalytic reaction. *Chemical Communications*, (6), 751-752.

[195] Soai, K., Shibata, T., Sato, I. (2000). Enantioselective automultiplication of chiral molecules by asymmetric autocatalysis. *Accounts of Chemical Research*, *33*(6), 382-390.

[196] Tanji, S., Kodaka, Y., Ohno, A., Shibata, T., Sato, I., Soai, K. (2000). Asymmetric autocatalysis of 5-carbamoyl-3-pyridyl alkanols with amplification of enantiomeric excess. *Tetrahedron: Asymmetry*, *11*(21), 4249-4253.

[197] Soai, K., Sato, I. (2002). Asymmetric autocatalysis and its application to chiral discrimination. *Chirality: The Pharmacological, Biological, and Chemical Consequences of Molecular Asymmetry*, *14*(7), 548-554.

[198] Soai, K., Matsumoto, A., Kawasaki, T. (2021). Asymmetric autocatalysis as a link between crystal chirality and highly enantioenriched organic compounds. *Israel Journal of Chemistry*, *61*(9-10), 507-516.

[199] Tanji, S., Ohno, A., Sato, I., Soai, K. (2001). Asymmetric autocatalysis of a pyrimidyl alkanol induced by chiral monosubstituted [2.2] paracyclophanes. *Organic letters*, *3*(2), 287-289.

[200] Soai, K., Osanai, S., Kadowaki, K., Yonekubo, S., Shibata, T., Sato, I. (1999). D-and L-quartz-promoted highly enantioselective synthesis of a chiral organic compound. *Journal of the American Chemical Society*, *121*(48), 11235-11236.

[201] Shibata, T., Yamamoti, J., Matsumoto, N., Yonekubo, S., Osanai, S., Soai, K. (1998). Amplification of a slight enantiomeric imbalance in molecules based on asymmetric autocatalysis: the first correlation between high enantiomeric enrichment in a chiral molecule and circularly polarized light. *Journal of the American Chemical Society*, *120*(46), 12157-12158.

[202] Sato, I., Omiya, D., Saito, T., Soai, K. (2000). Highly enantioselective synthesis induced by chiral primary alcohols due to deuterium substitution. *Journal of the American Chemical Society*, *122*(47), 11739-11740.

[203] Soai, K., Sato, I. (2001). Application of asymmetric autocatalysis to the determination of absolute configurations of amino acids with low enantiomeric excesses. *Enantiomer*, *6*(2-3), 189-192.

[204] Sato, I., Yamashima, R., Kadowaki, K., Yamamoto, J., Shibata, T., Soai, K. (2001). Asymmetric induction by helical hydrocarbons:[6]-and [5] helicenes. *Angewandte Chemie*, *113*(6), 1130-1132.

[205] Sato, I., Sugie, R., Matsueda, Y., Furumura, Y., Soai, K. (2004). Asymmetric synthesis utilizing circularly polarized light mediated by the photoequilibrium of chiral olefins in conjunction with asymmetric autocatalysis. *Angewandte Chemie*, *116*(34), 4590-4592.

[206] Kawasaki, T., Sato, M., Ishiguro, S., Saito, T., Morishita, Y., Sato, I., Nishino, H., Inoue, Y., Soai, K. (2005). Enantioselective synthesis of near enantiopure compound by asymmetric autocatalysis triggered by asymmetric photolysis with circularly polarized light. *Journal of the American Chemical Society*, *127*(10), 3274-3275.

[207] Kawasaki, T., Shimizu, M., Nishiyama, D., Ito, M., Ozawa, H., Soai, K. (2009). Asymmetric autocatalysis induced by meteoritic amino acids with hydrogen isotope chirality. *Chemical communications*, (29), 4396-4398.

[208] Kawasaki, T., Matsumura, Y., Tsutsumi, T., Suzuki, K., Ito, M., Soai, K. (2009). Asymmetric autocatalysis triggered by carbon isotope (13C/12C) chirality. *Science*, *324*(5926), 492-495.

[209] Kawasaki, T., Okano, Y., Suzuki, E., Takano, S., Oji, S., Soai, K. (2011). Asymmetric autocatalysis: triggered by chiral isotopomer arising from oxygen isotope substitution. *Angewandte Chemie (International ed. in English)*, *50*(35), 8131-8133.

[210] Matsumoto, A., Oji, S., Takano, S., Tada, K., Kawasaki, T., Soai, K. (2013). Asymmetric autocatalysis triggered by oxygen isotopically chiral glycerin. *Organic & Biomolecular Chemistry*, *11*(18), 2928-2931.

[211] Shindo, H., Shirota, Y., Niki, K., Kawasaki, T., Suzuki, K., Araki, Y., Matsumoto, A., Soai, K. (2013). Asymmetric autocatalysis induced by cinnabar: observation of the enantioselective adsorption of a 5-pyrimidyl alkanol on the crystal surface. *Angewandte Chemie*, *125*(35), 9305-9308.

[212] Matsumoto, A., Ozaki, H., Harada, S., Tada, K., Ayugase, T., Ozawa, H., Kawasaki, T., Soai, K. (2016). Asymmetric induction by a nitrogen 14N/15N isotopomer in conjunction with asymmetric autocatalysis. *Angewandte Chemie*, *128*(49), 15472-15475.

[213] Hawbaker, N. A., Blackmond, D. G. (2018). Rationalization of asymmetric amplification via autocatalysis triggered by isotopically chiral molecules. *ACS Central Science*, *4*(6), 776-780.

[214] Soai, K., Sato, I., Shibata, T., Komiya, S., Hayashi, M., Matsueda, Y., Imamura, H., Hayase, T., Morioka, H., Tabira, H., Yamamoto, J., Kowata, Y. (2003). Asymmetric synthesis of pyrimidyl alkanol without adding chiral substances by the addition of diisopropylzinc to pyrimidine-5-carbaldehyde in conjunction with asymmetric autocatalysis. *Tetrahedron: Asymmetry*, *14*(2), 185-188.

[215] Quaranta, M., Gehring, T., Odell, B., Brown, J. M., Blackmond, D. G. (2010). Unusual inverse temperature dependence on reaction rate in the asymmetric autocatalytic alkylation of pyrimidyl aldehydes. *Journal of the American Chemical Society*, *132*(43), 15104-15107.

[216] Gehring, T., Quaranta, M., Odell, B., Blackmond, D. G., Brown, J. M. (2012). Observation of a transient intermediate in Soai's asymmetric autocatalysis: Insights from 1 H NMR turnover in real time. *Angewandte Chemie*, *38*(124), 9677-9680.

[217] Blackmond, D. G. (2019). Autocatalytic models for the origin of biological homochirality. *Chemical reviews*, *120*(11), 4831-4847.

[218] Athavale, S. V., Simon, A., Houk, K. N., Denmark, S. E. (2020). Demystifying the asymmetry-amplifying, autocatalytic behaviour of the Soai reaction through structural, mechanistic and computational studies. *Nature chemistry*, *12*(4), 412-423.

[219] Athavale, S. V., Simon, A., Houk, K. N., Denmark, S. E. (2020). Structural contributions to autocatalysis and asymmetric amplification in the Soai reaction. *Journal of the American Chemical Society*, *142*(43), 18387-18406.

[220] Trapp, O., Lamour, S., Maier, F., Siegle, A. F., Zawatzky, K., Straub, B. F. (2020). In situ mass spectrometric and kinetic investigations of Soai's asymmetric autocatalysis. *Chemistry–A European Journal*, *26*(68), 15871-15880.

[221] Blackmond, D. G. (2006). Mechanistic study of the Soai autocatalytic reaction informed by kinetic analysis. *Tetrahedron: Asymmetry*, *17*(4), 584-589.

[222] Buono, F. G., Iwamura, H., Blackmond, D. G. (2004). Physical and chemical rationalization for asymmetric amplification in autocatalytic reactions. *Angewandte Chemie International Edition*, *43*(16), 2099-2103.

[223] Blackmond, D. G., McMillan, C. R., Ramdeehul, S., Schorm, A., Brown, J. M. (2001). Origins of asymmetric amplification in autocatalytic alkylzinc additions. *Journal of the American Chemical Society*, *123*(41), 10103-10104.

[224] Schiaffino, L., Ercolani, G. (2008). Unraveling the mechanism of the Soai asymmetric autocatalytic reaction by first-principles calculations: induction and amplification of chirality by self-assembly of hexamolecular complexes. *Angewandte Chemie*, *120*(36), 6938-6941.

[225] Schiaffino, L., Ercolani, G. (2010). Mechanism of the asymmetric autocatalytic Soai reaction studied by density functional theory. *Chemistry–A European Journal*, *16*(10), 3147-3156.

[226] Ercolani, G., Schiaffino, L. (2011). Putting the mechanism of the Soai reaction to the test: DFT study of the role of aldehyde and dialkylzinc structure. *The Journal of Organic Chemistry*, *76*(8), 2619-2626.

[227] Schiaffino, L., Ercolani, G. (2009). Amplification of chirality and enantioselectivity in the asymmetric autocatalytic Soai reaction. *ChemPhysChem*, *10*(14), 2508-2515.

[228] Gridnev, I. D., Vorobiev, A. K. (2012). Quantification of sophisticated equilibria in the reaction pool and amplifying catalytic cycle of the Soai reaction. *ACS Catalysis*, *2*(10), 2137-2149.

[229] Gridnev, I. D., Serafimov, J. M., Brown, J. M. (2004). Solution structure and reagent binding of the zinc alkoxide catalyst in the Soai asymmetric autocatalytic reaction. *Angewandte Chemie*, *116*(37), 4992-4995.

[230] Micheau, J. C., Cruz, J. M., Coudret, C., Buhse, T. (2010). An autocatalytic cycle model of asymmetric amplification and mirror-symmetry breaking in the Soai reaction. *ChemPhysChem*, *11*(16), 3417-3419.

[231] Buhse, T. (2003). A tentative kinetic model for chiral amplification in autocatalytic alkylzinc additions. *Tetrahedron: Asymmetry*, *14*(8), 1055-1061.

[232] Islas, J. R., Lavabre, D., Grevy, J. M., Lamoneda, R. H., Cabrera, H. R., Micheau, J. C., Buhse, T. (2005). Mirror-symmetry breaking in the Soai reaction: A kinetic understanding. *Proceedings of the National Academy of Sciences*, *102*(39), 13743-13748.

[233] Buhse, T., Cruz, J. M., Noble-Teran, M. E., Hochberg, D., Ribó, J. M., Crusats, J., Micheau, J. C. (2021). Spontaneous deracemizations. *Chemical Reviews*, *121*(4), 2147-2229.

[234] Matsumoto, A., Abe, T., Hara, A., Tobita, T., Sasagawa, T., Kawasaki, T., Soai, K. (2015). Crystal structure of the isopropylzinc alkoxide of pyrimidyl alkanol: mechanistic insights for asymmetric autocatalysis with amplification of enantiomeric excess. *Angewandte Chemie*, *127*(50), 15433-15436.

[235] Klankermayer, J., Gridnev, I. D., Brown, J. M. (2007). Role of the isopropyl group in asymmetric autocatalytic zinc alkylations. *Chemical communications*, (30), 3151-3153.

[236] Trapp, O. (2020). Efficient amplification in Soai's asymmetric autocatalysis by a transient stereodynamic catalyst. *Frontiers in Chemistry*, *8*, 615800.

[237] Trapp, O. (2022). Self-amplification of Enantioselectivity in Asymmetric Catalysis by Supramolecular Recognition and Stereodynamics. *Supramolecular Catalysis: New Directions and Developments*, 55-67.

[238] DiRocco, D. A., Ji, Y., Sherer, E. C., Klapars, A., Reibarkh, M., Dropinski, J., Maligres, P., Hyde, A. M., Limanto, J., Brunskill, A., Ruck, R. T., Campeau, L.-C., Davies, I. W. (2017). A multifunctional catalyst that stereoselectively assembles prodrugs. *Science*, *356*(6336), 426-430.

[239] Steinfeld, J. I., Francisco, J. S., Hase, W. L. (1999). *Chemical kinetics and dynamics* (p. 518). Upper Saddle River, NJ: Prentice Hall.

[240] Atkins, P., Atkins, P. W., de Paula, J. (2014). *Atkins' physical chemistry*. Oxford university press.

[241] Donaldson, D. J., Wren, S. N. (2014). Laboratory Kinetics. *Encyclopedia of Atmospheric Sciences*, *1*, 356.

[242] Michaelis, L., Menten, M. L. (1913). Die Kinetik der Invertinwirkung. *Biochem. z*, *49*(333-369), 352.

[243] Gillespie, D. T. (2007). Stochastic simulation of chemical kinetics. *Annu. Rev. Phys. Chem.*, *58*, 35-55.

[244] Lente, G. (2004). Homogeneous chiral autocatalysis: a simple, purely stochastic kinetic model. *The Journal of Physical Chemistry A*, *108*(44), 9475-9478.

[245] Lente, G. (2005). Stochastic kinetic models of chiral autocatalysis: a general tool for the quantitative interpretation of total asymmetric synthesis. *The Journal of Physical Chemistry A*, *109*(48), 11058-11063.

[246] Pross, A., Khodorkovsky, V. (2004). Extending the concept of kinetic stability: toward a paradigm for life. *Journal of physical organic chemistry*, *17*(4), 312-316.

[247] Blackmond, D. G. (2005). Reaction progress kinetic analysis: a powerful methodology for mechanistic studies of complex catalytic reactions. *Angewandte Chemie International Edition*, *44*(28), 4302-4320.

[248] Burés, J. (2016). A simple graphical method to determine the order in catalyst. *Angewandte Chemie International Edition*, *55*(6), 2028-2031.

[249] Burés, J. (2016). Variable time normalization analysis: general graphical elucidation of reaction orders from concentration profiles. *Angewandte Chemie*, *128*(52), 16318-16321.

[250] Burés, J., Larrosa, I. (2023). Organic reaction mechanism classification using machine learning. *Nature*, *613*(7945), 689-695.

[251] Huber, L., Trapp, O. (2022). Symmetry breaking by consecutive amplification: Efficient paths to homochirality. *Origins of Life and Evolution of Biospheres*, *52*(1), 75-91.

[252] Kitamura, M., Okada, S., Suga, S., Noyori, R. (1989). Enantioselective addition of dialkylzincs to aldehydes promoted by chiral amino alcohols. Mechanism and nonlinear effect. *Journal of the American Chemical Society*, *111*(11), 4028-4036.

[253] Noble-Terán, M. E., Buhse, T., Cruz, J. M., Coudret, C., Micheau, J. C. (2016). Nonlinear effects in asymmetric synthesis: a practical tool for the discrimination between monomer and dimer catalysis. *ChemCatChem*, *8*(10), 1836-1845.

[254] Issac, R., Chmielewski, J. (2002). Approaching exponential growth with a self-replicating peptide. *Journal of the American Chemical Society*, *124*(24), 6808-6809.

[255] Li, X., Chmielewski, J. (2003). Peptide self-replication enhanced by a proline kink. *Journal of the American Chemical Society*, *125*(39), 11820-11821.

[256] Varma, S. J., Muchowska, K. B., Chatelain, P., Moran, J. (2018). Native iron reduces $CO2$ to intermediates and end-products of the acetyl-CoA pathway. *Nature Ecology & Evolution*, *2*(6), 1019-1024.

[257] J. Moran (2018), Comment: An acetyl-CoA pathway ahead of enzymes?, Apr 24, 2018, at www.natureecoevocommunity.nature.com (accessed on April 13, 2023).

[258] Pearce, B. K. D., Molaverdikhani, K., Pudritz, R. E., Henning, T., Cerrillo, K. E. (2022). Toward RNA life on early earth: From atmospheric HCN to biomolecule production in warm little ponds. *The Astrophysical Journal*, *932*(1), 9.

[259] Kuramoto, K., Umemoto, T., Ishiwatari, M. (2013). Effective hydrodynamic hydrogen escape from an early Earth atmosphere inferred from high-accuracy numerical simulation. *Earth and Planetary Science Letters*, *375*, 312-318.

[260] Kulikov, Y. N., Lammer, H., Lichtenegger, H. I., Penz, T., Breuer, D., Spohn, T., Lundin, R., Biernat, H. K. (2007). A comparative study of the influence of the active young Sun on the early atmospheres of Earth, Venus, and Mars. *Space Science Reviews*, *129*, 207-243.

[261] Hobbs, R., Shorttle, O., Madhusudhan, N., Rimmer, P. (2019). A chemical kinetics code for modelling exoplanetary atmospheres. *Monthly Notices of the Royal Astronomical Society*, *487*(2), 2242-2261.

[262] Sleep, N. H. (2010). The hadean-archaean environment. *Cold spring harbor perspectives in biology*, *2*(6), a002527.

[263] Bredehöft, J. H., Meierhenrich, U. J. (2008). Amino acid structures from UV irradiation of simulated interstellar ices. *Untersuchungen zum Ursprung der Homochiralität am Beispiel der Aminosäuren*, 19.

[264] Trapp, O. (2020). Soai 7, Compatible With Microsoft Windows 7, 8 and 10. The compiled executable program can be obtained from the author upon request

[265] Beyazay, T., Ochoa-Hernández, C., Song, Y., Belthle, K., Martin, W. F., Tüysüz, H. (2023). Influence of Composition of Nickel-Iron Nanoparticles for Abiotic CO2 Conversion to Early Prebiotic Organics. *Angewandte Chemie*, e202218189.

[266] Peters, S., Semenov, D., Hochleitner, R., Trapp, O. (2022). Synthesis of prebiotic organics from CO2 by catalysis with meteoritic and volcanic particles. *Scientific reports.* doi: 10.1038/s41598-023-33741-8.

[267] Closs, A. C., Fuks, E., Bechtel, M., Trapp, O. (2020). Prebiotically Plausible Organocatalysts Enabling a Selective Photoredox α-Alkylation of Aldehydes on the Early Earth. *Chemistry–A European Journal*, *26*(47), 10702-10706.

[268] Oró, J. (1960). Synthesis of adenine from ammonium cyanide. *Biochem. Biophys. Res. Com., 2*, 407-412.

[269] Oró, J., Kimball, A. P. (1961). Synthesis of purines under possible primitive earth conditions. I. Adenine from hydrogen cyanide. *Arch. Biochem. Biophys., 94*, 217-227.

[270] Zahnle, K. J., Lupu, R., Catling, D. C., Wogan, N. (2020). Creation and evolution of impact-generated reduced atmospheres of early Earth. *The Planetary Science Journal*, *1*(1), 11.

[271] Möhler, P. (2023) Mechanistic and Kinetic Studies on the Soai Reaction. Unpublished Master thesis, LMU, Munich.

[272] United States Committee on Extension to the Standard Atmosphere, United States. Air Force, United States. Weather Bureau, United States. National Oceanic, & Atmospheric Administration. (1962). *US standard atmosphere*. National Oceanic and Atmospheric [sic] Administration, National Aeronautics and Space Administration, US Air Force.